Synthesis, Characterization, and Testing of Self-Lubricating Tetra Hybrid Reinforced Al Matrix Composites via Powder Metallurgy Processing

Demeke Abay Ashebir

A Thesis Submitted to

The Department of Materials Science and Engineering
School of Mechanical, Chemical, and Materials Engineering

Presented in Partial Fulfillment of the Requirement for the Degree of Master's in Materials Science and Engineering

Office of Graduate Studies

Adama Science and Technology University

June-2022

Adama, Ethiopia

Synthesis, Characterization, and Testing of Self-Lubricating Tetra Hybrid Reinforced Al Matrix Composites via Powder Metallurgy processing

Demeke Abay Ashebir

Advisor: Getnet Asrat Mengesha (Ph.D.)

Co-advisor: Devendra Kumar Sinha (Ph.D.)

A Thesis Submitted to

The Department of Materials Science and Engineering
School of Mechanical, Chemical, and Materials Engineering

Presented in Partial Fulfillment of the Requirement for the Degree of Master's in Materials Science and Engineering

Office of Graduate Studies

Adama Science and Technology University

June-2022

Adama, Ethiopia

Declaration

I hereby declare that this Master Thesis entitled "Synthesis, Characterization, and Testing of Self-Lubricating Tetra Hybrid Reinforced Al Matrix Composites via Powder Metallurgy processing" is my original work. That is, it has not been submitted for the award of any academic degree, diploma, or certificate in any other university. All sources of materials that are used for this thesis have been duly acknowledged through citation

Demeke Abay Ashebir	________________________	________________
Name of the student	Signature	Date

Approval Page of M.Sc. Thesis

We, the advisors of the thesis entitled "Synthesis, Characterization, and Testing of Self-Lubricating Tetra Hybrid Reinforced Al Matrix Composites via Powder Metallurgy processing" and developed by Demeke Abay Ashebir, hereby certify that the recommendation and suggestions made by the board of examiners are appropriately incorporated into the final version of the thesis.

Getnet Asrat Mengesha (Ph.D.)	____________________	______________
Major Advisor	Signature	Date
Devendra Kumar Sinha (Ph.D.)	____________________	______________
Co-advisor	Signature	Date

We, the undersigned, members of the Board of Examiners of the thesis by Demeke Abay Ashebir have read and evaluated the thesis entitled "Synthesis, Characterization, and Testing of Self-Lubricating Tetra Hybrid Reinforced Al Matrix Composites via Powder Metallurgy processing" and examined the candidate during the open defense. This is, therefore, to certify that the thesis is accepted for partial fulfillment of the requirement of the degree of Master of Science in Materials Science and Engineering.

____________________	____________________	______________
Chairperson	Signature	Date
____________________	____________________	______________
Internal Examiner	Signature	Date
____________________	____________________	______________
External Examiner	Signature	Date

Finally, approval and acceptance of the thesis are contingent upon the submission of its final copy to the Office of Postgraduate Studies (OPGS) through the Department Graduate Council (DGC) and School Graduate Committee (SGC).

____________________	____________________	______________
Department Head	Signature	Date
____________________	____________________	______________
School Dean	Signature	Date
____________________	____________________	______________
Office of Postgraduate Studies, Dean	Signature	Date

ACKNOWLEDGEMENT

First and foremost, I would like to express my heartfelt gratitude to the almighty God and his mother for providing me with the strength and health I needed to finish my studies with His help and the integration of my best abilities.

I would like to express my heartfelt appreciation to my advisor, Dr. Getinet Asrat Mengesha, and co-advisor, Dr. Devendra Kumar Sinha, for their unwavering support of my M.Sc. studies and research, as well as their patience, motivation, enthusiasm, and deep understanding.

My heartfelt gratitude also goes to the Materials Science and Engineering department's head, Dr. Gebisa Bekele, and the department's whole personnel.

Thank you for your support in conducting wear and friction tests, Anil Kumar, Assistant Professor of Department of Mechanical Engineering, KNIT, Sultanpur, India.

I would like to thank my classmates and lab mates for the insightful talks, the long nights we spent working together on projects before deadlines, and all of the fun we've had over the previous two years. I would like to express my gratitude to ASTU for giving me this scholarship and support by funding my thesis work. I would like to say thanks to Wonji Sugar Factories for their support in providing their solid waste by-products.

Finally, I'd want to express my gratitude to my family: my brothers Hagos and Temesgen Abay, as well as my sister Shiwaga Abay, for always being by my side and spiritually supporting me throughout my life.

.

TABLE OF CONTENTS

LIST OF TABLE

LIST OF FIGURE

LIST OF ACRONYMS

Abbreviation	Description
Al_2O_3	Aluminum oxide
AMC	Aluminum matrix composites
ASTM	American Society for Testing and Materials
BHN	Brinell hardness number
CMC	Ceramic matrix composites
CNT	Carbon nanotube
CTE	Coefficient of Thermal expansion
DTA	Differential Thermal Analysis
EDA	Energy dispersive analysis
EDS	Energy Dispersive X-ray Spectroscopy
EIS	Electrochemical impedance spectroscopy
FA	Fly ash
FSC	Friction stir casting
GNP	Graphene nanoparticle
Gr	Graphite
GRA	Grey relational analysis
HAMC	Hybrid reinforced aluminium matrix composites
HIP	Hot isostatic pressing
HMMC	Hybrid metal matrix composites
HV	Vickers hardness
HVN	Vickers hardness number
IPM	In-situ powder metallurgy
MM	Mechanical milling
MMC	Metal matrix composites
MWCNT	Multi-walled carbon nanotubes
OM	Optical microscopy
OMC	Organic matrix composites
PKSA	Palm Kernel shell ash
PM	Powder metallurgy
PMC	Polymer matrix composites
PRMMC	Particulate reinforced metal matrix composites

RHA	Rice husk ash
SCBA	Sugar cane bagasse ash
SEM	Scanning electron microscopy
SiC	Silicon carbide
TGA	Thermogravimetric analysis
TGRA	Taguchi-based Grey Relational Analysis
UTM	Universal testing machine
VHN	Vickers hardness number
WC	Tungsten carbide
WS	Tungsten sulfide
XRD	X-ray diffraction
$W_{sintered}$	Sintered weight in gram
$W_{submerged}$	Submerged weight in gram
$W_{suspended}$	Suspended weight in gram
Wt%	Weight percentage

ABSTRACT

Hybrid aluminum matrix composites (HAMCs) are a new class of advanced materials that can be customized and engineered to achieve specific properties for specific applications in specific environments. HAMCs find a wide range of popularity in transportation sector because of lower noise and lower fuel consumptions over another material. This research aims to synthesize, characterize, and test the physicomechanical, tribological, and corrosion characteristics of tetra hybrid (SiC, Al_2O_3, Gr, and sugar cane bagasse ash (SCBA)) reinforced HAMCs via powder metallurgy (PM) processing. In the first section, tetra hybrid reinforced HAMCs were synthesized using pure Al matrix with fixed wt% of primary reinforcements (5 wt% SiC and 5 wt% Al_2O_3) and varying wt% of secondary reinforcements such as (0.5, 2.5, 4.5, and 6.5) wt% Gr and (0.5, 2.5, 4.5, and 6.5) wt% SCBA. This section focused on phase purity investigation using XRD, thermal analysis using TGA-DTA, surface area and micropore sizes analysis using BET, morphological study using SEM characterizations, and physicomechanical, tribological, and corrosion tests to explore the materials' behavior of the newly synthesized HAMCs. The second section mainly focused on multi-response optimization with an L_{16} orthogonal array experimental design employing Taguchi-based Grey Relational Analysis (TGRA). This section was intended to explore the influence of hybrid reinforcements containing (5 wt% SiC and 5 wt% Al_2O_3) and the various wt% of Gr and SCBA on physicomechanical properties of HAMCs when milling time, compaction pressure, and sintering temperature were varied. The XRD findings demonstrated that all of the synthesized HAMCs in all proportions contain main peaks that are Al and hybrid reinforcements as miner peaks, with no unwanted peaks. According to BET and SEM analysis, the HAMC (AS4 sample) with 10 wt% (SiC +Al_2O_3) and 9 wt% (Gr +SCBA) showed lower micropore size with dense and uniform microstructure. The increase in wt% of secondary reinforcements decreases both density and porosity, while increasing hardness and compressive strength up to a certain level above which it begins to reverse, because of the increase in wt% of hard particles of SiC, Al_2O_3, and SCBA. The Vickers hardness and compressive strength of the AS4 HAMC were improved by 446.40% and 209.75%, respectively. The wear loss and friction as well as corrosion resistance of the HAMCs increases with increasing of wt% of Gr and SCBA up to certain limit, after which it begins to decrease. The wear loss and coefficient of friction of the AS4 HAMC sample were improved by 54.89 – 60.27% and 50.1 – 55.1%, respectively. The AS4 HAMC sample also shows 99.691% of corrosion inhibition efficiency (IE%) and SEM results also confirm that the morphology of AS4 HAMC sample was not corroded by the NaCl solution, which is due to the uniform distribution of hybrid reinforcements with in the Al matrix. The confirmation test results revealed that the optimal HAMC sample surpasses all 16 experimental tests in all physicomechanical properties, indicating that the TGRA method is a promising technique for developing hybrid reinforced HAMCs via PM processing. The newly synthesized tetra hybrid reinforced HAMCs showed superior physicomechanical, tribological, and corrosion properties as compared to pure Al, and single and double reinforced HAMCs. As a result, the new tetra hybrid reinforced HAMC material is predicted to have potential applications in automotive, aerospace, defense, and various other structural applications.

Keywords: HAMCs; Grey relational analysis; Wear; Corrosion; Powder metallurgy; Sugar cane bagasse ash.

CHAPTER-ONE

1. INTRODUCTION

1.1. Background and Motivation of the Study

Recent engineering applications are concentrating on lightweight, low-cost materials having outstanding mechanical and tribological properties (Menezes et al., 2013). Aluminum matrix composites (AMCs) play a vital role in aerospace, marine, defense, and automotive industries that require materials with high stiffness, high strength, high fatigue resistance, low density, and low wear properties (Singh, 2016). HAMCs containing two or more reinforcements have the prospective to meet the demands of engineering applications (Srivastava et al., 2014).

Composite materials are produced by comprising two or more different materials (Sharma et al., 2014). The basic starting materials have different properties, and their amalgamation gives an entirely new material. It has unique, entirely new, and different properties compared to its constituent components. The aim is to improve the mechanical, structural, tribological, thermal, chemical, wear, and corrosion characteristics of individual materials (Miracle, 2005). The components do not dissolve chemically since two or more phases are clearly distinguished within the composite (Fentahun et al., 2018).

A metal matrix composite (MMCs) can produce via dispersing reinforcement material into a metal matrix, and the developed composites exhibit superior properties (Sharma et al., 2014). AMCs are composites in which aluminum or aluminum alloys serve as a matrix and reinforce with hard ceramic materials such as SiC, Al_2O_3, B_4C, Ti_2B, TiC, ZrO_2, etc., or with other solid wastes such as bagasse ash (Aktar Zahid Sohag et al., 2020; Annigeri et al., 2018; Arun et al., 2015; Bahl, 2021). Aluminum (Al) is certified to be a significant material due to its assuring properties such as lightweight, high strength to weight ratio, corrosion and wear resistance, and workability. The dispersion of hard ceramic materials in an aluminum matrix increases its strength, hardness, wear and corrosion resistance, stiffness, and thermal stability (Arjunan et al., 2018; Chakrapani et al., 2021; Chand et al., 2020; Dhanesh, Kumar, Yohannan, et al., 2021). With the increase in properties such as; lightweight and higher strength to weight ratio, corrosion resistance, wear-resistance, and low thermal coefficient (CTE), there is a lot of interest in AMCs. Aluminum alloys also attain good properties when used as a matrix due to their low density, good corrosion resistance, and excellent mechanical properties (Fentahun et al., 2018). Researchers mainly focused on composites with aluminum and its alloys as a matrix due to their vast applications in manufacturing automobile components (e.g. brake discs, drums, back-plate, engine block, piston, and gearbox parts) (Allison et al., 1993; Chandel et al., 2021b; Ghassemieh, 2011; Koli et al., 2015), aerospace(e.g. fan exit guide vane in gas turbine engine, rotating blade sleeves in helicopters and flight control hydraulic manifolds) (Boyer et al., 2015; Charan Nayak et al., 2020; Pradeep Kumar et al., 2021)**,** and other industries. Traditional fabrication methods such as stir casting, compo casting, squeeze casting, and spray casting was employed to produce the composites (Kammuluri.Baburaja et al., 2016; Umair Zaki et al., 2021).

Stir casting experiences problems such as; porosity, wettability, a chemical reaction between reinforcement and matrix, etc...(Shukla et al., 2018). Powder metallurgy confirms to be one of the best methods to overcome these limitations. Another advantage of this method is that the processing temperature is less than the lower melting point of the constituents and its ability to produce the product at a reasonably low cost. Powder metallurgy is an energy-saving, green technology process that offers complex designs compared to other conventional manufacturing methods such as casting, machining, and forging (M. O. Bodunrin et al., 2015). Powder metallurgy plays a vital role in the mass production of automotive parts. The powder metallurgy process requires powder as the raw material which may be a pure metal, blends, or alloys. These powders produce by using atomization, chemical reduction, electrolysis, etc. Mazen et al. (1998) used a revised powder metallurgy process to produce alumina (Al_2O_3) reinforced Aluminum matrix composites, which involve combining aluminum and alumina powders effectively, supported by hot pressing and hot extrusion operations. Moreover, they compared the tensile and compression properties of Al_2O_3 reinforced Aluminum matrix composites produced using the powder metallurgy process with the usual casting method. They revealed that composites fabricated using their powder metallurgy process possessed higher yield strength, tensile strength, compressive strength, and % elongation than those produced using the casting technique.

The three major processes in the powder metallurgy process are milling, compacting, and sintering. By milling, reinforcement, and matrix powders of different sizes and shapes, homogenous distribution will arrive, and porosity will reduce. Solid lubricants such as Gr are added during blending to decrease friction (Elango M, 2019). The compaction process uses to consolidate the powders into green compacts by punch and die arrangement (Manohar, Pandey, & Ranjan Maity, 2021). The most commonly used compaction processes are cold isostatic and hot isostatic pressing (Kumar et al., 2021). Sintering is a solid phase bonding process where the green compacts will heat in the furnace. Solid-state sintering, liquid phase sintering, activated sintering, microwave sintering, and spark plasma sintering are some types of sintering processes (Kumar et al., 2021; Manohar, Pandey, & Maity, 2021).

1.2. Statement of the Problem

Fuel economy demands, emissions regulations, and the push for energy independence are the crucial factors pushing the automotive, aerospace, marine, defense, and other industries to improve efficiency (Chandel et al., 2021b; Fentahun et al., 2018; Stojanovic et al., 2015). The principal ways of efficiency improvement are powertrain enhancements and mass reduction (Vyas et al., 2013). Due to the increment of new raw material costs and lack of supply, researchers emphasize developing recycling techniques for solid waste products, aiming to protect the environment (Kulkarni et al., 2019). However, few investigations were conducted on agro-industrial solid waste ashes as reinforcement to produce a composite material (Akbar et al., 2020). In Ethiopia, these solid wastes remove by trucks from the factory to the surrounding. On the other side, aluminum or its alloys alone show poor mechanical and tribological properties that led to the development of new materials (Gloria et al., 2019). Most of the research carried out on MMCs, are using single reinforcement such as SiC, Al_2O_3, Gr particles, and solid wastes (such as fly ash, rice husk ash, and sugar cane bagasse ash). Only a few researchers have done on HMMCs using binary or teri reinforcements. No research works that have been carried out on tetra hybrid reinforced aluminum matrix composites to investigate the physical, mechanical, wear, corrosion, microstructural, and thermal properties. Using liquid metallurgy processing methods to fabricate AMC leads to undesirable interfacial bonding reaction, porosity, wettability, and high energy consumption (as the energy of melting the metal and preheating fillers is required) (Kumar et al., 2021). Using these ceramic reinforcements alone to produce AMCs has problems related to property improvement and cost. So, to get HAMCs that have superior and tailorable properties with cost reduction, powder metallurgy process was used and substitute some of the ceramic particulate reinforcements with solid wastes like sugar cane bagasse ash of selecting the proper mixing ratio. In this research work, four reinforcements such as SiC, Al_2O_3 ceramics as primary, Gr, and SCBA as secondary reinforcement with pure Al as the matrix have been employed to synthesize, characterize and, test the physical, mechanical, thermal, chemical, wear, and corrosion behavior of the HAMCs using the powder metallurgy process.

1.3. Objectives of the Study

1.3.1. General objective

The research aims to synthesize, characterize, and test the physical, mechanical, tribological, and corrosion characteristics of a self-lubricating tetra hybrid reinforced (SiC/Al_2O_3/Gr/SCBA) aluminum metal matrix composite using the powder metallurgy process.

1.3.2. Specific objectives

i. To synthesis a self-lubricating tetra hybrid reinforced (SiC/Al_2O_3/ Gr/SCBA) aluminum matrix composites using various wt% of Gr and SCBA via the powder metallurgy (PM) route.

ii. To characterize and test the physicomechanical, tribological, corrosion, and microstructural behaviors of the tetra hybrid reinforced aluminum matrix composites. The sintering temperature was specified after performing the TGA and DTA analysis.

iii. To investigate the effects of the PM process parameters (milling time, compacting pressure, and sintering temperatures) on physicomechanical, tribological, corrosion, and microstructural behaviors of the tetra hybrid reinforced aluminum matrix composites.

iv. To Compare the physicomechanical, tribological, and corrosion behaviors of the tetra hybrid reinforced aluminum matrix composites with a base metal (pure Al).

v. To optimize of input process parameters for the optimum value of output process parameters through Taguchi-based Grey Relational Analysis (TGRA).

1.4. Significance of the Study

The following are the overall significance of this study:

- To progress the understanding of powder metallurgy techniques in developing HAMCs.
- The HAMCs might also provide insight into reducing energy and fuel consumption, weight, and CO_2 emissions in the automotive and aerospace sectors, as well as

recycling and utilizing Ethiopian solid waste sugar cane bagasse ash as secondary reinforcement in the HAMCs development.

- This research could also help the automotive and aerospace sectors focus on the development of HMMCs, especially self-lubricating HAMCs at high temperatures, and the utilization of solid waste sugar cane bagasse ash as secondary reinforcement, intending to reduce both weight and cost.

1.5. Scope of the Study

In terms of scope, this research work consists of an introduction and motivation, a literature survey that covers the essential problems, processing methods, and recently published work in the field of HAMCs with reinforcements SiC, Al_2O_3, SCBA, and Gr particulates. Primarily, this study presents an introduction to composites in general and AMCs in specific. Secondly, a literature survey of recent research into the field of AMCs reinforced with SiC, Al_2O_3 particles, Gr fine powder, and Agro-industrial solid waste such as sugar cane bagasse ash. Thirdly, the techniques and testing procedures include the preparation of composite powders and selected optimal compositional mixtures, details, and parameters of the high energy planetary milling technique, the consolidation of powder composites into solid compacts, the sintering temperature, and then density and porosity measurement, Vickers microhardness, microstructural analysis, compression testing, corrosion measurements, and pin on drum wear and friction testing. Finally, a conclusion and recommendations for future work on the most important improvements and findings of HAMCs are discussed.

1.6. Research methodology

The powder metallurgical HAMCs were synthesized by employing a fixed wt% of SiC and Al_2O_3 reinforcement with changing wt% of Gr and BA, as well as milling time, compaction pressure, and sintering temperature. There are two sections to this research work. In the first section, the role of tetra hybrid reinforcements in the physicomechanical and tribo-corrosion behavior of HAMCs is studied in depth. In this section, only Gr and SCBA contents (wt%) were varied while SiC, and Al_2O_3 content, as well as process parameters, are not changed. Section one's major aims were to select reinforcements and matrix materials for effective HAMC synthesis based on previous research (Ankur et al., 2021). In the second section, the major focus is extended to multi-response optimization of powder metallurgical HAMCs utilizing Taguchi – based Grey Relational Analysis (TGRA) with $L_{16}(4^5)$ orthogonal array experimental design. In this section density, porosity, Vickers microhardness, and compressive strength are the main performance characteristics (factors). The best hybrid composite specimen is chosen after HAMCs with various reinforcement wt% of Gr and SCBA and varying process parameters such as milling duration, compaction pressure, and sintering temperature are created in the second section. The best HAMC specimen with optimal parameter setting was selected based on the multi-response optimization using GRA, and this optimal sample went for further confirmation test and its flexibility and reliability were discussed. The structure shown in figure 1.1 depicts how this research was carried out.

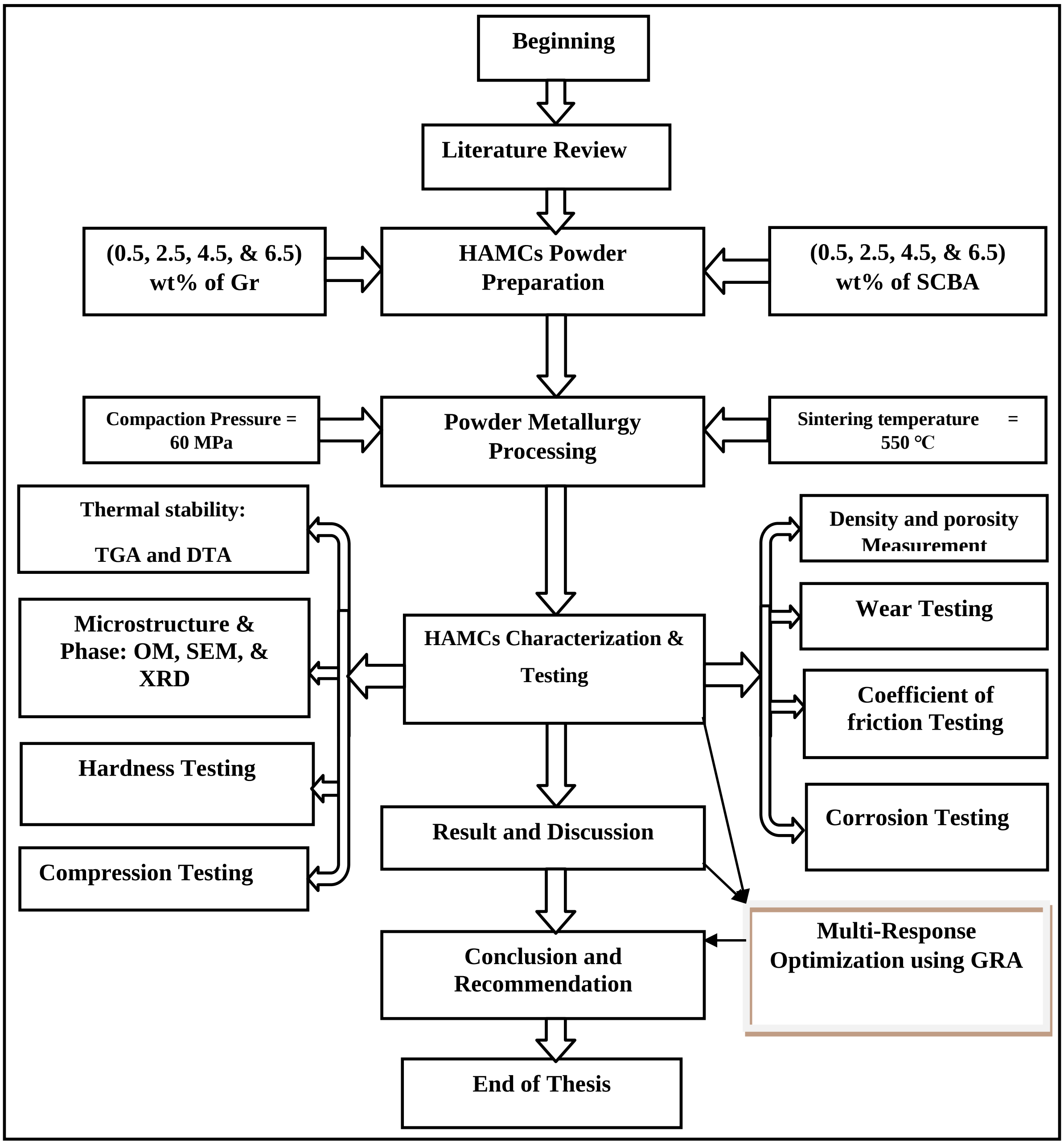

Figure 1.1 Research organization

CHAPTER-TWO

2. LITERATURE REVIEW

2.1. Composite Materials

The composite materials are made of a combination of two or more unsolvable materials that have properties superior to any of the component materials (Mondal, 2021). Composites comprise one or more discontinuous phases surrounded by a continual phase. Composites are composed of two or more materially distinct phases whose blending produces enhanced properties different from those of their constituents (M. O. Bodunrin et al., 2015). In certain respects, composites are the foremost interesting engineering materials because their structure is more complex than the opposite three types (metals, ceramics, and polymers) (Mavhungu et al., 2017; Miracle, 2005). The technological and industrial investment in composite materials derives from the fact that their characteristics are not merely different from their parts but are often incomparably superior (Sharma et al., 2014).

As investigated by Raju et al. (2014), hybrid Composite materials are comparatively new and found by combining two or more different reinforcement materials in a matrix. Hybrids have an improved all-around combination of properties than composites containing only a single reinforcement phase. The synthesis of HAMCs has recently received a lot of attention due to its applications in industrial and scientific research in the fabrication of value-added materials with significantly improved physical, mechanical, and tribological properties. In comparison to traditional single and binary reinforced metal matrix composites, the fabricated hybrid reinforced aluminum matrix composites have shown significant improvement in terms of physical and mechanical properties.

According to Singh et al. (2016), HAMCs are the next generation of amalgams that have the potential to replace single reinforced composites due to improved and superior properties in specific application areas. They concluded that hybrid MMCs provide additional flexibility and reliability in the desired possible parts based on the reinforcement's combination and form.

Sharma et al. (2014) investigated the various manufacturing processes of AMCs and discovered that the mechanical and tribological properties of single reinforcement composites outperform pure aluminum and its alloys regardless of the manufacturing process. Furthermore, HAMCs have better physical, mechanical, and tribological properties than single reinforcement AMCs. The mechanical and tribological properties of HAMCs were superior to those of the pure aluminum matrix. When second reinforcement is combined with single reinforced composites, the tribological properties of the majority of HAMCs improve.

2.2. Classification of Composite Materials

Composites can be broadly categorized based on their type of matrix, reinforcement, size, form, composition, temper state, etc. (Chandra Kandpal et al., 2018). The wide-ranging composite material categories based on matrix include; Organic Matrix Composites (OMCs), Metal Matrix Composites (MMCs), and Ceramic Matrix Composites (CMCs). The term organic matrix composite is generally assumed to involve two subclasses of composites, namely Polymer Matrix Composites (PMCs) and carbon matrix composites referred to as carbon-carbon composites.

A polymer matrix composite (PMC) is a composite material made up of various short or continuous fibers that are held together by an organic polymer matrix (Sajan et al., 2021). The purpose of PMCs is to transfer loads between fibers and the matrix. They can be found in almost every aspect of modern life, from electronic components to a wide range of automotive accessories. PMCs are made up of a matrix of thermoplastic or thermosetting polymers and one or more reinforcements such as carbon, glass, metal, and natural fibers (Mallick, 2021). Polymers are well-known for their lightweight properties. PMCs have a wide range of characteristics. High strength, excellent impact, compression, and fatigue characteristics, cost-effective manufacturing and tooling methods, excellent chemical and corrosion resistance, chemical inertness at a low cost, and excellent mechanical characteristics are among them. PMCs are commonly used in rockets, aircraft, and sports equipment (Sharma et al., 2020).

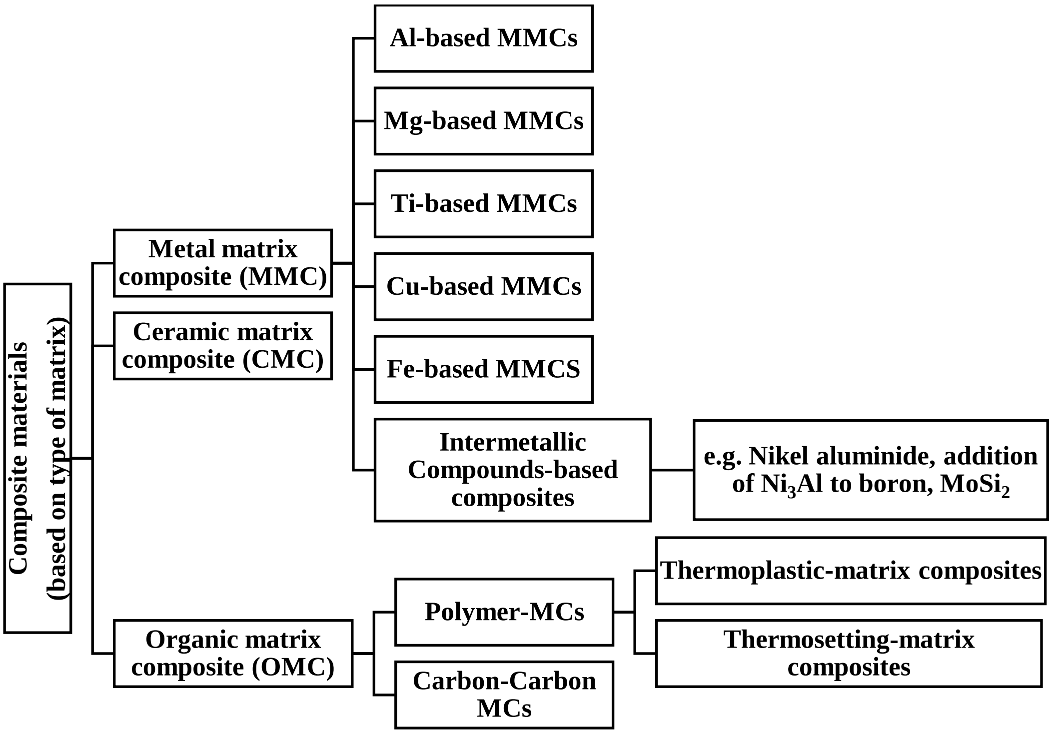

Figure 2.1 Classification of composite materials based on matrix type (Khanna et al., 2021).

Table 2.1 Metallic matrix and their drawbacks (Dhanesh, Kumar, Fayiz, et al., 2021)

Matrix Materials	**Density (g/cm^3)**	**Major drawbacks to be filled by reinforcements**
Al	2.70	⇒ Temperature range is restricting its potential application in high temperatures ⇒ Low hardness and strength
Mg	1.74	⇒ Low wear and corrosion resistance, rapid creep rate, and chemical reactivity
Cu	8.92	⇒ Low tensile and compressive strength, as well as low creep resistance, low hardness
Fe	7.87	⇒ Low tensile yield strength, low hardness, and poor wear and corrosion resistance

MMCs are classified into four categories based on their reinforcing type: nanocomposites, structural composites, fiber-reinforced composites, and particulate-reinforced composites (Callister et al., 2018; Mistry et al., 2018).

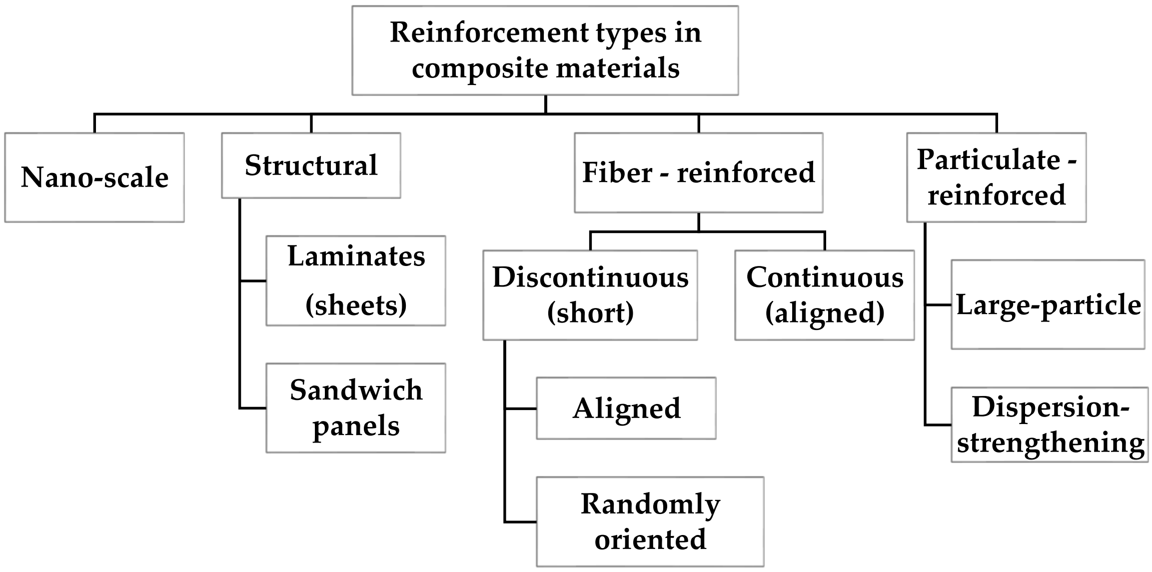

Figure 2.2 MMC classification based on reinforcement type(Callister et al., 2018)

Table 2.2 MMCs and potential applications in automotive and aerospace (Chandel et al., 2021a)

Type of MMCs	Possible Reinforcements	Potential Application	Possible Advantages	Fabrication Techniques
Al-MMCs	SiC particles and fibers Al_2O_3 particulates and fibers	Pistons & connecting rods Thermal management Aero engines Space applications Engine parts and driveshaft	Customizable CTE Low density Relatively cheap High specific rigidity Good fatigue and wear resistance	Powder metallurgy Casting/Hot Isostatic Pressing Additive manufacturing
Mg-MMCs	Gr, Al_2O_3 particulates	Tubes used in truss construction applications	Good thermal conductivity, Better dimensional stability, Reduced CTE	Vacuum assist casting Powder metallurgy
Cu-MMCs	Al_2O_3 fibers Gr-particulates	Compressed air turbopump, rocket propulsion housing Thermal regulation	Dimensional stability, High thermal conductivity, High-temperature capability,	Pressure infiltration PVD Additive manufacturing Friction stir consolidation
Ti-MMCs	Monofilament and fibers made of SiC	Exhaust valves Aeroengine components such as blades and vanes, compressor bling, casings, shafts, struts, and links	Increased rigidity, Max hardness, Reduced weight and Resilience to high temperatures	Hot isostatic pressing Plasma spray technique Extrusion and forging
Fe-MMCs	Titanium diboride	Piston, cylinder, and engine parts of automobile	Reduction in weight, high elastic modulus, high mechanical and fatigue features	Powder extrusion and machining

2.3. Ceramic Particulate Reinforced AMCs and HAMCs

According to Etemadi (2014), MMCs have higher temperature capacity, stronger stiffness and strength, and a lower coefficient of thermal expansion when compared to matrix alloys. In addition, many particulates and whisker-reinforced MMCs are fabricable with conventional processes. However, incorporating ceramic phases may result in lower ductility, fracture toughness, and thermal conductivity. Compared to particulate reinforced metal matrix composites, higher cost, complex fabrication methods, and recyclability problems are among the disadvantages of fiber-reinforced composites. Moreover, particulate reinforcement has the main advantage over other forms such as fiber, and whisker reinforcement, being reasonably compatible with most conventional processing routes such as casting, spray deposition, and is particularly compatible with the powder metallurgy processing route (Evans et al., 2003). Although particulate is less than that of continuous fiber, short fiber, or whisker reinforcement, substantial improvement in material properties can achieve by incorporating this particulate type reinforcement within a matrix compared to the unreinforced matrix material. An advantage of particulate reinforced metal matrix composites (PRMMCs) over the other forms of MMCs is the isotropy of their material property. Particulate reinforced aluminum matrix composites (PRAMCs) have the following advantages over unreinforced materials (Ononiwu et al., 2020):

- Superior strength
- Improved stiffness
- Reduced density (weight)
- Improved high-temperature properties
- Controlled thermal expansion coefficient
- Thermal/heat management
- Enhanced and tailored electrical performance
- Improved abrasion and wear resistance
- Control of mass (especially in reciprocating applications)
- Improved damping capabilities
- Compared to whiskers, particulate reinforcement can be handled easily and safely without the need for specialized equipment.

Due mainly to the property enhancements obtainable, the low cost and availability of particulate materials, and the processing adaptability of particulate reinforced materials to conventional technology, PRMMCs are currently the most widely investigated and utilized MMC type. The most regularly used particulate reinforcing materials are SiC, Al_2O_3, Si_3N_4, TiC, and B_4C (Chandel et al., 2021b). Among individually reinforced particles in

AMCs, SiC exhibits the unique combination of extremely high hardness, low specific gravity, high elastic modulus, high melting point, high thermal conductivity, good wear resistance, excellent chemical resistance, and high capability for neutron absorption (Chandradass et al., 2021). In recent years, hybrid aluminum matrix composites (HAMCs) are attracting increasing attention because of their superior performance. They are considered a new generation of composite materials and can potentially be used as substitutes for single-reinforced AMCs (Muley et al., 2015). As shown in Figure 2.3, the individual percentage contributions of SiC, Al_2O_3, and Gr are more than others; further, in recent studies, the contribution of hybrid reinforcements is substantial in the HAMCs.

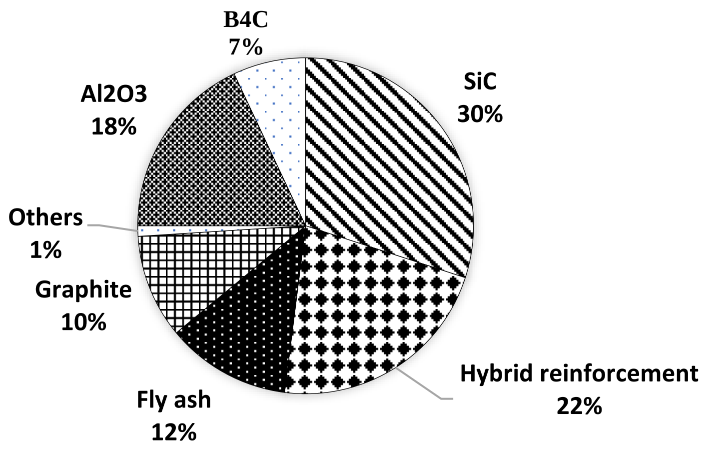

Figure 2.3 Percentage contribution of research on reinforcements (Srivastava et al., 2018).

Table 2.3 Comparision of monolithic and single and hybrid reinforced aluminium matrix composites (Sharma et al., 2014; Singh, 2016)

Properties for Comparision	Materials type		
	Monolithic (pure Al or its Alloys	Single reinforced aluminium composite	Hybrid reinforced aluminium composites
Physical	Insufficient	Good	Best
Mechanical	Low-to-medium	Medium-to-high	Very high or superior to the others
Wear	Wearable	Depends on the percentage of reinforcement, still insufficient	Excellent wear resistance
Corrosion	Moderate	Depends on the type of reinforcement, still not enough	Excellent corrosion resistance
CTE	High	Low	Very low CTE

In comparison to single reinforced composites, hybrid composites consolidate two or more types of dispersed phases (e.g., SiC + Al_2O_3, Al_2O_3 + Gr, SiC + Gr, and SiC + Al_2O_3 + Gr) within the same matrix. Hybridization increases synergies between the adopted dispersed phase materials. Thus, hybrid reinforcements can exhibit new structural properties. HMMCs can show excellent properties compared to those composites comprising individual reinforcements at the same loading. That is due to a robust synergistic outcome on the composite properties by the practice of hybrid reinforcements. Therefore, hybrid composites; are investigated for devices such as; wear resistance, lightweight, chemical stability, and combining advantages of the dispersed phases based upon the requirements of the application. This type of composite material can find usage in numerous applications such as aviation, defense, aerospace, and automobile. As with single element reinforcement, strategies are required to reduce their losses and improve their advantages (Gaohui Wu, 2020; Mussatto et al., 2021).

Natrayan et al. (2019) used powder metallurgy to produce Al/SiC/Al_2O_3 HAMCs with 7.5, 15 wt.% SiC and 7.5, 15 wt.% Al_2O_3 to compare mechanically and wear characteristics. The results showed that incorporating SiC and Al_2O_3 into the Al matrix improves its mechanical and wear behavior by up to 25% and 40%, respectively. In comparison to Al_2O_3, the addition of SiC resulted in higher wear resistance.

Hadzima et al. (2018) investigated the tribological properties of Al/SiC/Gr hybrid composites in terms of reinforcement content and load level. The difficulties in the fabrication process and machining of those hybrid composites were caused by the use of a larger volume share of SiC particles in composites fabrication in previous years. The reason for this was due to the increased hardness of those composites, which was primarily determined by SiC particles. The content of SiC particles then gradually decreased to a range of 3 – 10 wt%. This improved the production as well as the processing (machining) of hybrid composites with the Al matrix. The shape and distribution of hard or soft particles reinforced in the matrix also influence the friction and wear properties of composites. Hard particles increase the strength and wear resistance of composites while decreasing their ductility, whereas soft particles act as reinforcement.

Viswanatha et al. (2013) investigated the microstructure and mechanical properties of HAMCs with A356 alloy as the matrix reinforced with 0, 3, 6, and 9 wt% of SiC and 3wt% of Gr particulates using a stir casting process. The processed composites were investigated for microstructure to understand the particle distribution in the matrix material. The result revealed that the increase in wt% of SiC particles leads to a meaningful enhancement in hardness and tensile properties and a reduction in percentage elongation, and maximum hardness and tensile strength had obtained at 9 wt% of SiC particles.

Singh (2016) discussed the various properties of Al/SiC/Gr hybrid composites that can be used in a variety of tribological applications. According to the findings, the processing route plays a significant role in achieving a homogeneous structure for these hybrid composites. The size of the matrix and reinforcement powders is critical in powder metallurgy, whereas wettability between the reinforcement particles and the molten alloy is a major challenge in liquid metallurgy. The addition of SiC particles improves the mechanical strength and wear resistance of Al composites. However, under extreme conditions, the ejection of these particles can reduce the wear performance of Al composites. Gr particles aid in the formation of a thick and extensive tribolayer on the wear surface. Under certain conditions, this layer reduces direct contact between the rubbing surfaces, lowering the wear rate. Morphological examination of worn surfaces confirmed that the hybrid composites exhibit.

Rathika (2013) investigated the fundamental tribological properties of Al 2024/5 wt% SiC/(0, 5, and 10) wt% Gr HAMCs using powder metallurgy and pin-on-disc equipment. The friction and wear properties of HAMCs were evaluated in terms of applied load, sliding speed, and sliding distance. Three types of combinations of composites were developed in this study: Al reinforced with 5 wt% SiC AMC, Al reinforced with 5 wt% SiC and 5 wt% Gr HAMCs and Al reinforced with 5 wt% SiC and 10 wt% Gr HAMCs. The findings revealed that as the sliding velocity and applied load grew, so did the wear loss and friction coefficient; however, increasing the graphite wt% reduced the wear loss. Due to Gr's self-lubricating action, the composite with 5 wt% Gr had the lowest wear loss and friction coefficient. Wear loss and friction coefficient in composites containing 10 wt% Gr increased significantly due to the softening characteristic of graphite. The hardness and density of the HMCs decreased as the Gr content rose. Wear resistance and friction coefficients were both good in the HAMCs having 5 wt% Gr. The addition of solid lubricant particulates to the aluminum matrix as a secondary reinforcing phase improves wear and friction characteristics significantly (Prasad et al., 2004). The Al–5 wt% SiC composites' wear process was oxidative wearing with substantial plastic deformation, as per SEM evaluations of worn surfaces and wear debris. The Al–5 wt% SiC–10 wt%

HAMCs showed oxidative wearing with delamination wearing as the wear mechanism. In the Al/5 wt% SiC/5 wt% Gr HAMCs, delamination wearing was the most popular method of wearing. Both wear loss and friction coefficient were reduced by applying a homogenous Gr coating on top of the worn surface. As a result, the Al/5 wt% SiC/5 wt% Gr HAMCs did not suffer from excessive wear.

Iacob et al. (2015) investigated the impact of the reinforcements wt% and milling time on the wear rate and micro-hardness of Al/Al_2O_3/Gr hybrid composites fabricated via powder metallurgy and revealed that increasing Al_2O_3 and Gr particle wt% and prolonging the milling time have a potential influence on the structural development of the AMCs. The rate of wear in optimum condition was decreased due to the mechanically homogenized zone formed between the composites specimens and the surface of the steel ball. The bearing of Gr particles reduces the wear rate and acts as a solid lubricant. Vickers microhardness was raised by prolonging the mechanical milling time and also by increasing the reinforcement wt%. The increase in micro-hardness was due to the addition of hard particles of Al_2O_3 embedded in the Al matrix.

Sudindra et al. (2013) synthesized 10 wt% Al_2O_3 and (3, 6, and 9) wt% Gr particulates hybrid reinforced Al6061 matrix composite using stir casting technique to study the hardness, tensile strength, and wear resistance properties. The results revealed that the addition of Al_2O_3 improved the hardness and tensile strength compared to base matrix Al6061; such an increment in hardness and tensile strength of composites could be attributed to the behavior of the stiffer and harder Al_2O_3, which resists deformation occurring in higher pressure surviving ability. Even though the addition of Gr particulate makes the material ductile, the hardness and tensile strength don’t vary the hardness and tensile strength much to Al_2O_3 added composition and below the base material. Moreover, the addition of Al_2O_3/Gr particulates decreases the wear rate, so these hybrid reinforced Al matrix composites could be used for automotive and antennas in aircraft.

2.4. Solid-Waste Particulate Reinforced AMCs and HAMCs

The use of agro-industrial solid wastes in AMCs is becoming more popular because the ashes of these wastes can be used as reinforcing particles in metal matrices to improve their strength properties. Furthermore, using agro-industrial solid wastes as reinforcement of AMCs can reduce product manufacturing costs while also reducing pollution to the environment. Many solid waste materials can be used as reinforcement for MMCs, and they are generally classified into three types: industrial solid wastes, agricultural solid wastes, and post-consumer solid wastes. We only focused on the agro-industrial solid wastes because they are excellent candidates for secondary reinforcement in AMCs. Several studies have recently been conducted on AMCs that use Rice husk ash, Bamboo leaf ash, Coconut shell ash, Palm oil fuel ash, and bagasse ash. Large amounts of sugar cane are processed in Ethiopia, resulting in a large amount of solid waste (Mosisa et al., 2019). A portion of these solid wastes is used to feed animals, while others are disposed of and burned in public landfills, both of which hurt the environment.

Gupta et al. (2017) investigated alloy 7075-based matrix hybrid composites produced by stir casting with reinforcing particulates of sugarcane bagasse-ash varying in wt% (3, 6, and 9) wt% and SiC 3 wt%. They conducted hardness, dry sliding wear, and tensile strength tests on single SiC-reinforced alloy 7075-based matrix composites and binary (SiC and SCBA)-reinforced hybrid composites. The results showed that the hybrid composite (Al7075 + 3 wt% SiC + 3 wt% SCBA) was more efficient, economical, and superior to single SiC reinforced alloy 7075 based matrix composites and unreinforced matrix. Based on the findings, we can conclude that, rather than using single-reinforced Al-SiC composites, Al-SiC-SCBA binary hybrid composites could be an excellent advanced material in areas where lightweight and enhanced mechanical properties are important.

Naim Shaikh (2018) statistically analyzed the wear behavior of aluminum hybrid composites reinforced with flay ash and SiC particles via the powder metallurgy technique. They investigated the wear characteristics of aluminium hybrid composites reinforced with SiC (10 wt%) and Fly ash (0, 5, 10, and 15 wt%). The wear loss for Al/SiC/FA hybrid composite was lower than for Al/SiC composite. Figure 2.4 revealed that 10 wt% of FA was the minimum wear loss at load 20N, sliding speed 2m/s, and 600m sliding distance. The wear resistance of the composite was superior compared to the base matrix. The unreinforced aluminium was softer than Al/SiC/FA hybrid composite. This enhancement in the wear resistance was because of the following reasons: the large hardness declared by Fly ash particulates, which restricts plastic flow during the sliding condition, and powerful interfacial bonding between reinforcement particle and matrix phase. The wear resistance of the composites increased with the addition of the fly ash particle content. The wear rate was at 10 wt% FA reinforced Al/SiC had decreased by 28% of the wear rate for the Al/SiC composite material. The wear behavior increases with increasing velocity, sliding distance, and load during sliding.

2.5. Solid-Lubricant Particulates Reinforced AMCs and HAMCs

Gr is a low-density, solid-lubricant 3D carbon material (Alaneme et al., 2015; M. Bodunrin et al., 2015; Wu et al., 2020). In the cases of ceramic (such as SiC, Al_2O_3) and solid waste (such as rice husk ash, bagasse ash, and fly ash), hybrid reinforced AMC encouraging levels of ductility and fracture toughness equivalent to that of single alumina reinforced composites were examined (M. Bodunrin et al., 2015; Gupta, 2013). But, potential enhancements in mechanical properties and wear and corrosion performance are yet uncertain and rewarding subjects for further research (Alaneme et al., 2015; Sydow et al., 2021). Within AMCs, Gr attends as a solid lubricant between the composite and rubbing surface to assist in the reduction of composite wear without the need for conventional solid and liquid lubrication (Srivyas et al., 2018). In addition, Gr has also been used as a hybrid reinforcement with Al_2O_3 and SiC in AMCs with characteristic enhancements in strength and wear characteristics (Sydow et al., 2021).

Menezes et al. (2013) investigated the effect of Gr content, particle size, normal pressure, sliding speed, sliding distance, surface texture, temperature, current density, environment, and counterpart materials on the friction coefficient and wear rate of metal and ceramic matrix composites reinforced with Gr particles. They discovered that as the amount of Gr released on the worn surface produced a thin transfer film on the contacting surfaces, the overall friction coefficient and wear rate decreased. The proper material selection is critical to (1) ensuring that the solid lubricant areas are not sheltered by wear debris and (2) allowing the development of lubricating transfer films at the tribo-interface. Finally, the advantage of self-lubricating composites over thin solid lubricating films deposition on ceramic substrates is the ability to have an infinite source of solid lubricant, which has been sustained as the matrix material wears (Suresha et al., 2010). When compared to the material deposited by solid lubricant films, which fail after the film has worn away, self-lubricating matrix composites reduce the possibility of failure (M. O. Bodunrin et al., 2015). Self-lubricating composite materials can withstand low friction and wear without the need for external lubricants. The incorporation of Gr particles reduces the coefficient of friction and wear rate of Gr particle reinforced metal and ceramic matrix composites compared to similarly unreinforced material. With increasing Gr particle wt.%, the matrix composite's friction and wear rate decrease. The Gr particles were discovered to be superior to other lubricant particles, and they provided efficient lubrication when used at high temperatures (Zeren, 2015).

Alaneme et al. (2015) investigated the microstructural characteristics, and mechanical and wear behaviors of tri (Al_2O_3, RHA, and Gr) reinforced HAMCs via a two-step stir casting process. Al_2O_3 with an average particle size of 30 mm, RHA, and Gr with particle sizes (<50 mm) were combined in different weight percentages to produce 10 wt% tris reinforced AA6063-based composites. The rice husk ash, Gr, and alumina particles were preheated individually at a temperature of 250 ℃ to remove humidity and increase wettability within the molten AA 6063. And then charged into the semi-solid melt at this temperature (600 ℃) and stirred manually for 10 min. The semi-solid hybrid composite was then super-heated to 780 ± 30 ℃ and stirred employing an automated mechanical stirrer. Hardness, tensile properties, and wear behaviors of the hybrid reinforced composites had characterized, and the results revealed hardness decreased with an increase in the weight percentages of RHA and Gr in the hybrid composites and with RHA content greater than 50 wt%, the effect of Gr on the hardness becomes less significant. The hybrid reinforced composites without Gr showed greater wear sensitivity compared to the hybrid reinforced composite comprising Gr. But the wear resistance decreased with an addition in the Gr content from 0.5 to 1.5 wt%.

Table 2.4 Solid lubricants (Gr, MoS_2 and soft metals such as Pb, Ag, Au, Cu) properties and application area (Miyoshi, 2007; Reeves et al., 2013).

Requirements	**Characteristics**	**Application Area**	**Draw Backs**
⇒ Avoid abrasion in dirt-filled conditions. ⇒ Do not contaminate the product or the environment. ⇒ Offer long-term storage or a fixed service. ⇒ Fretting corrosion and wear	⇒ Low friction coefficient, ⇒ Exceptional thermal stability, ⇒ Shear strength, very low	⇒ Locations where liquid lubricants are prohibited. ⇒ In spacecraft and rovers with limited weight ⇒ Farm and mining equipment, as well as off-road trucks and equipment ⇒ In extreme freezing ⇒ Ineffectiveness of fluid lubricants in some areas ⇒ When the temperature is exceedingly high	Due to oxidation, the use of Gr in high-temperature applications is limited.

2.6. Tribological and Corrosion Behavior of AMCs and HAMCs

Because of their low-density aluminum and its alloys have a high wear rate, while these materials have more potential applications in the areas of automobile and aerospace (Omrani et al., 2016; Shanmughasundaram et al., 2013). In addition, owing to its superior lubricating effect Gr during dry sliding Al/Gr composites have been used as self-lubricating materials (Rathika, 2013).

M. M. Ravikumar et al. (2021) experimented on the fabrication of Al_2O_3 and SiC particulates reinforced HAMCs via stir casting method to study the effect of reinforcement and heat treatment on the corrosion properties of Al matrix and HAMCs investigated by polarization, impedance (EIS), and weight loss methods. The result showed that the rate of corrosion decreases with increasing the content of Al_2O_3 and SiC particulates in the HAMCs. The SEM micrograph examination showed the minor formation of pits due to corrosion upon increasing Al_2O_3 content, which can utilize for future corrosive applications in various sectors. The unreinforced metal has a corroded surface compared to the Al/ Al_2O_3/SiC composite because the material loss due to corrosion had decreased by the presence of Al_2O_3. Additionally, pitting and grain boundary corrosions had seen on the pure Al matrix and the Al/ Al_2O_3/SiC composites. The combined impact of inclusions and defects generated at the time of AMC fabrication decrease the sensitivity of Al/ Al_2O_3/SiC composites to pitting by decreasing the needed driving force.

Radhika, Ramanathan, et al. (2012) used the stir casting method to create Al_2O_3 and Gr hybrid Al matrix composites to improve dry sliding wear resistance and to investigate the effects of sliding speed, load, and reinforcement content on wear properties and contact friction. The reinforcements were alumina particles with average sizes of 15-20 m and wt% of 3, 6, and 9, as well as 3 wt% Gr particles with average sizes of 50-70 m. Mechanical properties of HAMCs, such as hardness and tensile strength, had significantly improved. The wear rate and coefficient of friction for Al matrix and composites decreased with increasing sliding speed and increased with decreasing sliding speed (Ahamad et al., 2020). They used SEM to investigate the worn surfaces of the hybrid composites, and the results revealed that the damage was greater in Al than in the hybrid composites. As the sliding speed and load increase, so do the depth and number of grooves. The layer of materials discarded as trash was smaller in Al/9 wt% Al_2O_3/3 wt% Gr, and it could be seen in the comparatively smooth worn surface. Because of the addition of Gr particles, the friction and wear rate in MMC are significantly reduced when compared to those in the Al matrix (Radhika, Subramanian, Venkat Prasat, et al., 2012).

2.7. AMCs and HAMCs Fabrication Processes

Mussatto et al. (2021) reviewed advanced production routes and potential applications for AMCs. Powder metallurgy and casting routes are still extensively used for the production of AMCs. As shown in Figure 2.4, the PM process is a more beneficial route than other manufacturing processes because it eliminates the possibility of undesirable intermetallic reactions, and this improves the porosity of composite materials.

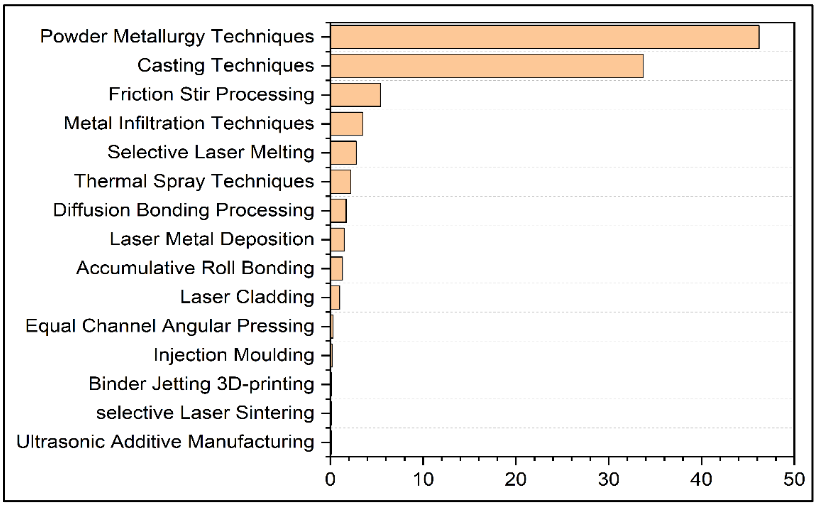

Figure 2.4 Comparision of MMCs Processing techniques (Mussatto et al., 2021)

Guttikonda et al. (2018) reviewed the effect of powder metallurgy processing in a homogeneous distribution of reinforcement in the matrix by ball milling or mechanical milling and how powder metallurgy enhances the mechanical properties of the composites. From earlier investigations, the main difficulty met by the MMCs is wettability and the interfacial bonding formed between the interface of the reinforcements and the matrix materials as they are fabricated via conventional methods like stir casting, squeeze casting, and other techniques that use liquid molten metals. And the main difficulty met by the traditional methods is the uniform distribution of the reinforcement particles in the Al matrix. Many researchers studied to get the uniform distribution of reinforcements in the matrix but get it difficult via traditional methods, and among each, they get powder metallurgy processing is efficient. The type, application, and purpose of different MMC fabrication techniques have been discussed in detail in Table 2.5 below.

2.8. Powder Metallurgy Processing

The PM route for the production of AMCs had introduced to reduce the problems of wettability or interfacial reactions often encountered with liquid processing, with an added benefit of the improved spatial distribution of particulates in dis-continuously reinforced AMCs (Liu et al., 1994).

2.8.1.1. Milling or blending of feedstock powders

Powder blending is one of the main steps in PM in which powder of different materials having a wide range of mechanical and chemical properties are blended into a single form with the help of a ball mill. The key purposes of the milling process are particle size reduction (breaking down the material), mixing or blending, and particle shaping (Parveen et al., 2021). Blending leads to uniformity in shape and the homogenous mixing of powder particles, which will impart a wide range of mechanical properties having homogenous characteristics throughout the material. The particles are broking into fine particles by compressing operation in compression force type (Hayajneh et al., 2009). The fine powders are blended or mixed with a solid lubricant; the lubricants serve adequate fluidity to the particles. The powder particles are loaded with the grinding medium in a container and subjected to high deformation in the planetary ball mill operation (Kho et al., 2014).

2.8.1.2. Uniaxial pressing (compaction) process

Powder compaction is performed with the help of a die and punches assembly, which applies high pressure on the particles to form a cohesive bond between them(Dixit et al.). The compaction processes are performed at room temperature (cold compaction). The strength that originates throughout compaction is known as green strength. Compaction directs to a decline in the voids between the powder particles. It also creates adhesion and bonding between the particles. Compacting can also promote the plastic deformation between the particles thereby leading, to an increase in the density of the consolidated powder. Increasing the compaction pressure increases the green density of the specimen. In general, this cold compaction has four main functions: (1) to create the desired shape, (2) to control the dimensions, (3) to control porosity, and (4) to impart adequate strength for handling (Ankur et al., 2021). Figure 2.7 shows the detailed process during cold uniaxial compaction pressing (CUP).

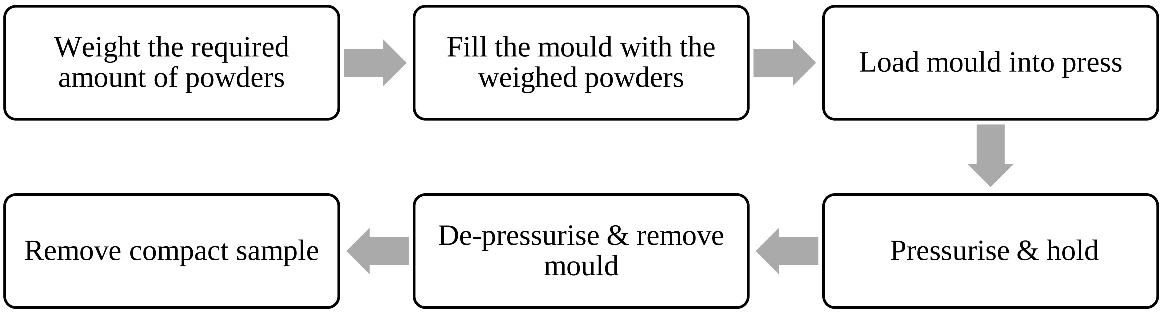

Figure 2.5 Uniaxial cold compaction processing steps (Ankur et al., 2021)

2.8.1.3. Sintering

Sintering is the technique of condensing a loose powder aggregate or a green compact of the required composition under controlled temperature and time conditions. It is usually done at atmospheric pressure and an elevated temperature. The sintering temperature for the material must be below the melting temperature of the principal material. But the temperature would be up to (0.7 – to – 09) T_m of its constituents (having low T_m) as it will allow the diffusion between the neighboring particles (Ankur et al., 2021). The heating process is carried out in a controlled manner and in an inert atmosphere to prevent oxidation. The sintering process intensifies the mechanical properties, such as the density of the final part by reinforcing the incipient holes and improving the area of contact between the powder particles.

2.9. Potential Application of AMCs and HAMCs

AMCs and HAMCs are attractive for applications comprising high mechanical properties, low densities, tailorable properties, design and manufacturing flexibility, excellent corrosion resistance, and cost-effective product development (Arunachalam et al., 2019; Dev Srivyas et al., 2019; Garg et al., 2019). Composites have emerged as the preferred material for decreasing weight and fuel consumption while improving powertrain performance in vehicles. As shown in Figure 2.6, Hybrid composite materials are used in a wide range of engineering applications due to their diversified properties such as lightweight, strength-to-weight ratio, low cost, ease of structure shipbuilding, and high strength.

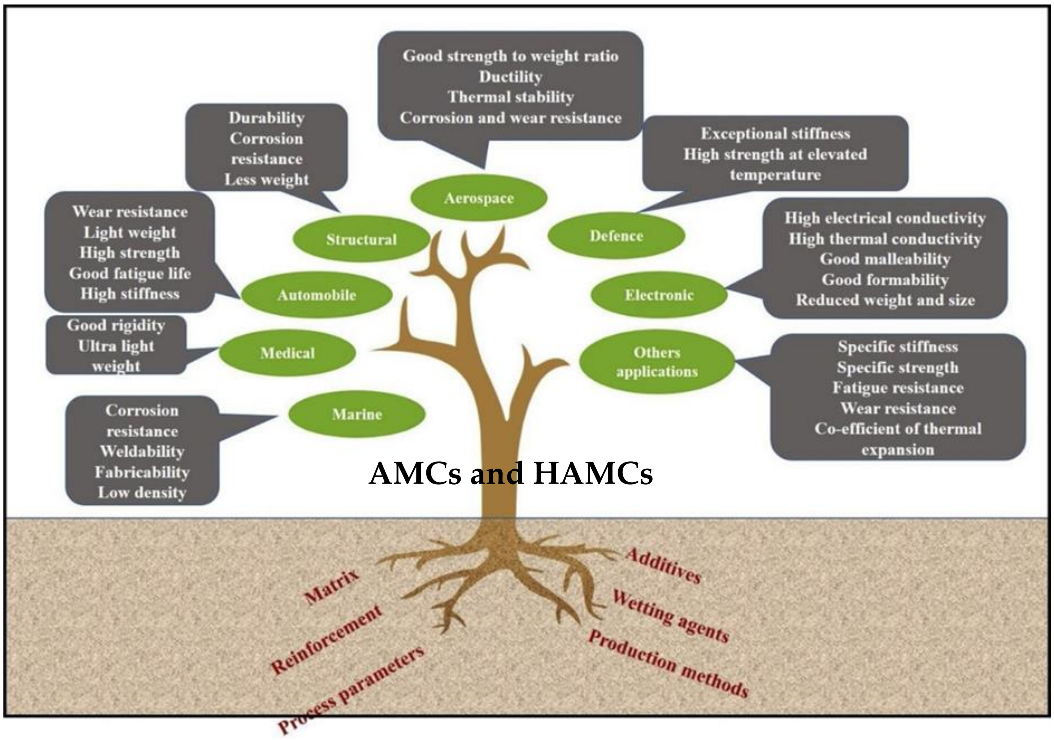

Figure 2.6 Applications of AMCs and HAMCs in various fields (Arunachalam et al., 2019)

2.10. Summary and Research Gaps

According to previous research, reinforcement materials such as ceramic particles, SiC, Al_2O_3, Gr, and agro-industrial solid wastes such as fly ash, rice husk ash, and sugar cane bagasse ash influence the physicomechanical, and tribological, corrosion properties of AMCs and HAMCs. According to the studies cited above, AMCs and HAMCs reinforced with ceramic particles (SiC, Al_2O_3), solid wastes (such as SCBA, RHA, FA), and solid lubricants (Gr, MoS_2) have the potential for excellent wear and corrosion resistance and tailorable properties suitable for tribological applications. To date, no research has been conducted to investigate the behavior of SCBA, Al_2O_3, and SiC fine particles as tetra hybrid reinforcement or Gr, Al_2O_3, and SiC fine particles as tri-hybrid reinforcement with the pure aluminum matrix material. Furthermore, the use of Gr as part of a tri and tetra hybrid reinforcing practice for HAMCs has not been reported in previous studies. This study looked at the effects of different wt% of reinforcing materials such as SiC, Al_2O_3, Gr, and SCBA on the microstructure, physicomechanical, tribological, corrosion, and thermal stability behavior of the Al matrix. There is also no research on the fabrication of either of the aforementioned HAMCs using powder metallurgy. There is also a scarcity of research on the application of modern characterization techniques in HAMCs characterization investigations. The current work is concentrated on the powder metallurgy fabrication of tetra hybrid reinforced aluminium matrix composites with pure Al as matrix material and SiC, Al_2O_3, Gr, and SCBA fine particles as hybrid reinforcements.

CHAPTER -THREE

3. MATERIALS AND METHODS

3.1. Role of Tetra Hybrid Reinforcements on Materials' Behavior of HAMCs

3.1.1. Particulate reinforcements used to synthesis HAMCs

In this research work, four different particulates namely; SiC, Al_2O_3, Gr, and SCBA are used as reinforcement materials.

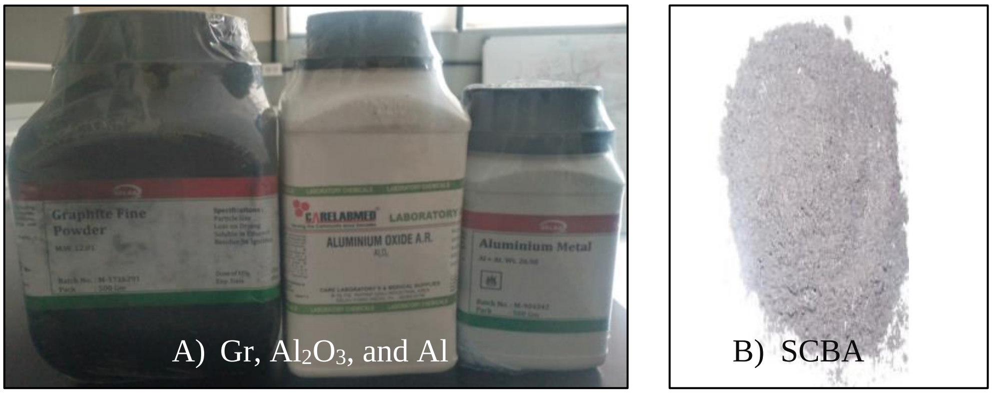

Figure 3.1 Raw materials used throughout the research work

Table 3.1 Raw materials and reasons selecting for HAMCs production

№	Raw materials		Reasons for the selection to use in HAMCs	Ref.
1.	**Matrix**	Pure Al	• Lightweight, and low density, but the low melting point hinders its use in the high-temperature application. • High ductility, malleability, and toughness with Low strength, soft, and low wear and friction resistance	(Miracle, 2005)
2.	**Reinforcements**	SiC	• High hardness and mechanical stability at high temperatures because of its very high melting point • Excellent thermal conductivity and low coefficient of thermal expansion, • Excellent resistance to chemical, wear, thermal shock, corrosion, and oxidation	(Miracle, 2005)
3.		Al_2O_3	• High hardness and mechanical stability at high temperatures because of its very high melting point • Excellent thermal conductivity and low coefficient of thermal expansion,	(Miracle, 2005)

			• Excellent resistance to chemical, wear, thermal shock, corrosion, and oxidation	
4.		Gr	• Lightweight, low density • Superior solid-lubricating material • High friction resistance • Low cost	(Guttikonda et al., 2021; Miloradović et al., 2020; Miracle, 2005)
5.		SCBA	• Lightweight, low density, porous • Easily available as it is a solid waste material • A promising alternative for MMCs	(Dawoud et al.; Sultana et al., 2013)

The physicomechanical characteristics of Al, SiC, Al_2O_3, Gr, and SCBA are superior to those of the base metal (pure Al). The general physicomechanical properties of Al, SiC, Al_2O_3, Gr, and SCBA are depicted in Table 3.2.

Table 3.2 Physicomechanical properties of the raw materials (Chawla, 2012; Miracle, 2005)

Materials	Al (pure)	SiC	Al_2O_3	Gr	SCBA
Appearance (form)	White powder	Dark gray powder	White powder	Black powder	Black-gray
Density (g/cm^3)	2.7	3.2	3.96	1.8	0.8 - 1.477
M.W.	26.98	40.096	101.96	12.01	NA
Melting pt. (°C)	660	2730	2054	3652 - 3697	1350
Particle grain size (μm)	≤ 50	≤50	≤ 50	≤50	≤ 50
Vickers hardness (MPa)	167	20000-27000	11000-17000	67	NA
Compressive Strength (MPa)	110	2800	2500	20-200	NA
Tensile Strength (MPa)	130-195	310	221	3 – 33	NA
Young's Modulus (GPa)	70	410	379	380 – 470	NA
Purity (%)	99.5	97	97	98	NA

NA indicates Not applicable (or, No accessible information)

3.1.2. Pre-treatment and characterization of sugar cane bagasse ash

Sugarcane bagasse ash (SCBA) was collected from the Wonji Shoa sugar factory. The recently constructed and modernized Wonji Shoa Sugar Factory has a total output of crushing 6,250 tons of cane a day, manufacturing 174,946 tons of sugar annually, which is then increased to 12,500 tons of sugar per year with future development work (Yemane, 2020). Bagasse is defined as the dry pulpy residue left after the extraction of juice from sugar cane. The sugar extracted from sugarcane left behind sugarcane bagasse, when grid powdered to ash, is called sugarcane bagasse ash (SCBA). SCBA is an agro-industrial waste material composed mainly of silicon dioxide. SCBA is one of the most inexpensive and low-density reinforcements available in large quantities as an agro-industrial waste by-product during the combustion of waste sugarcane. Equipment used in the preparation of SCBA are Crucible, 45 μm size Sieve, Becker, sample holder, drying oven, and muffle furnace. The synthesis of SCBA is shown in figure 3.2 below.

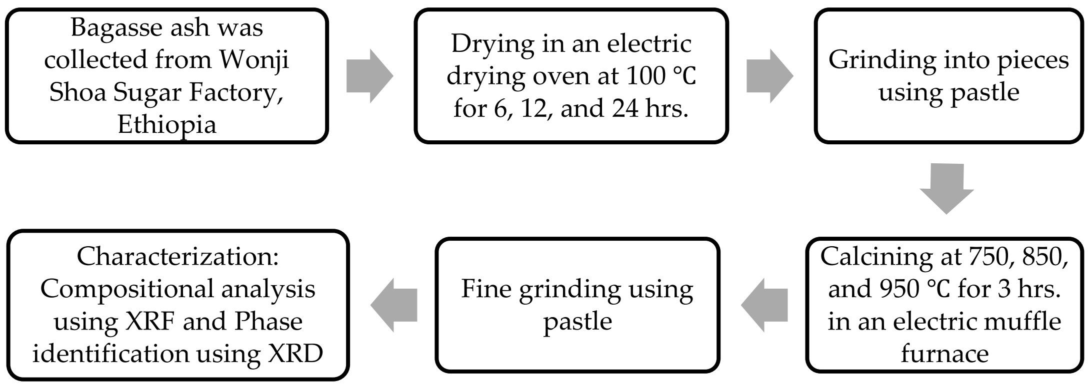

Figure 3.2 Synthesis of SCBA fine powder particulates (Yashpal et al., 2020)

3.1.3. Synthesis of HAMCs using PM process

3.1.3.1. Chemical composition and sample designation in the synthesis of HAMCs

In this study, Al fine powder with particle size (≤ 50 μm) and reinforcement fine powders with particle sizes (≤ 50 μm), namely SiC, Al_2O_3, Gr, and SCBA, are employed. Following the selection of matrix and reinforcement materials, the next critical duty was to blend or mix them with the optimal composition. The powder metallurgy technique was used for the synthesis of HAMCs from the Al matrix and using SiC and Al_2O_3 as primary reinforcements, and Gr and SCBA as secondary reinforcements. Using SiC and Al_2O_3 as primary reinforcements within the range of 3 – 10 wt% yields superior physical, mechanical, and tribological properties (Bhoi et al., 2020; Veličković Gajević et al., 2018).

Table 3.3 Chemical composition and sample designation used in the HAMCs

Sample designation	**Al (wt%)**	**SiC (wt%)**	**Al_2O_3 (wt%)**	**Gr (wt%)**	**BA (wt%)**
Pure Al	100	0	0	0	0
AS1	90	5	5	0	0
AS2	89	5	5	0.5	0.5
AS3	85	5	5	2.5	2.5
AS4	81	5	5	4.5	4.5
AS5	77	5	5	6.5	6.5

Table 3.4 Powder metallurgical process parameters for this study (Mahdi et al., 2021)

Samples	Chemical Composition	PM processing parameters
Pure Al	Al	1. Milling time = 2 hrs. 2. Compaction pressure = 60 MPa 3. Sintering temperature = 550 °C 4. Sintering time = 3 hrs.
AS1	$Al/5SiC/5Al_2O_3$	
AS2	$Al/5SiC/5Al_2O_3/0.5Gr/0.5SCBA$	
AS3	$Al/5SiC/5Al_2O_3/2.5Gr/2.5SCBA$	
AS4	$Al/5SiC/5Al_2O_3/4.5Gr/4.5SCBA$	
AS5	$Al/5SiC/5Al_2O_3/6.5Gr/6.5SCBA$	

The dimension of the die and punch and all specimens are described in Table 3.5 and Figure 3.4, respectively.

Table 3.5 The die and punch dimensions

No.	Parameters of die and punch	Dimension (mm)
1.	Outer diameter of die	50
2	Inner diameter of die	20
3	Length of the die	50
4	Diameter of the punch	20-clearance
5	Length of the punch	50

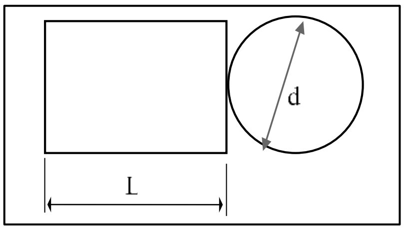

Figure 3.3 Dimension for all specimen

The pre-designed die and punch were used to manufacture the required number of specimens based on the following types of tests to be conducted;

⇒ All the specimens for hardness, corrosion, and microstructural tests were prepared in a cylindrical shape having 20 mm in diameter and 8 mm in height.

⇒ The wear test specimen length and diameter were 12 mm and 6 mm, respectively.

⇒ The amount of material removed by grinding (machining and grinding allowance) of 2 mm is considered. The volume of the cylindrical specimen is calculated using Equation 3.1;

$$V = \pi \times L \times r^2 \text{ -------------------------- } 3.1$$

Where, V is volume of specimen in mm^3, L is length = 8 mm, and d is diameter = 20mm (r=10 mm)

$$V = \pi \times L \times r^2 = \pi \times 8mm \times (10mm)^2 = 2{,}512\ mm^3 = 2.512\ cm^3$$

The weight of Al matrix and SiC, Al_2O_3, Gr, and SCBA hybrid reinforcements in each specimen for the given compositions are estimated using Equation 3.2.

$$m_x = V_{total} \times \rho_x \times y ---------------------- 3.2$$

Where m_x is weight, x is matrix/reinforcement and y the wt% of matrix or reinforcement x.

3.1.3.2. Steps in PM process

PM process is one of the most economical processes for fabricating the near-net particulate reinforced MMCs and thereby allowing greater flexibility, a significant reduction in manufacturing costs due to minimizing machining process, and minimized scrap losses(Liu et al., 1994; Mussatto et al., 2021). Since the powder metallurgy fabrication method offers more uniformity in the distribution of the reinforcement material it eliminates the clustering problem to some extent thereby increasing the mechanical properties as studied by Mazen et al. (1998) and Dubey et al. (2016). The steps of the powder metallurgy technique are shown as follows (Hussain et al., 2016). The basic steps in powder metallurgy (PM) processes are powder mixing, powder compaction, and sintering process.

1. **Blending (or mixing):** The HAMCs were mixed using a high energy planetary blending machine with 10 wt% of primary reinforcements (i.e., 5 wt% SiC and 5 wt% Al_2O_3) and different wt% of secondary reinforcement (0.5, 2.5, 4.5, and 6.5 wt% for each of Gr and SCBA) (Bahrami et al., 2016).
2. **Compaction.** The blended HAMCs were compacted in a uniaxial hydraulic press machine to obtain a cylindrical shape of the solid green sample at room temperature. The test samples were compacted using a 60 MPa compaction pressure. As shown in Figure 3.5 a self-prepared die and punch assembly with a maximum die diameter of 20 mm was employed during bulk HAMCs fabrication.

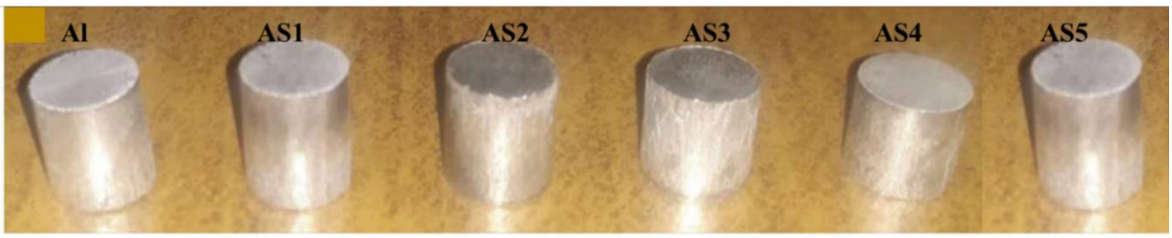

Figure 3.4 Green compacted Al and HAMC samples

3. **Sintering.** The samples were sintered from room temperature to 550 °C at a rate of 10 °C/min for 55 mins, then maintained at that temperature for 3 hrs. To reduce oxidation during heating, the samples were sealed with Al foil. The samples were then allowed to cool to room temperature within the furnace before being exposed to the environment. Figure 3.7 depicts the full experimental setup of the HAMCs synthesis.

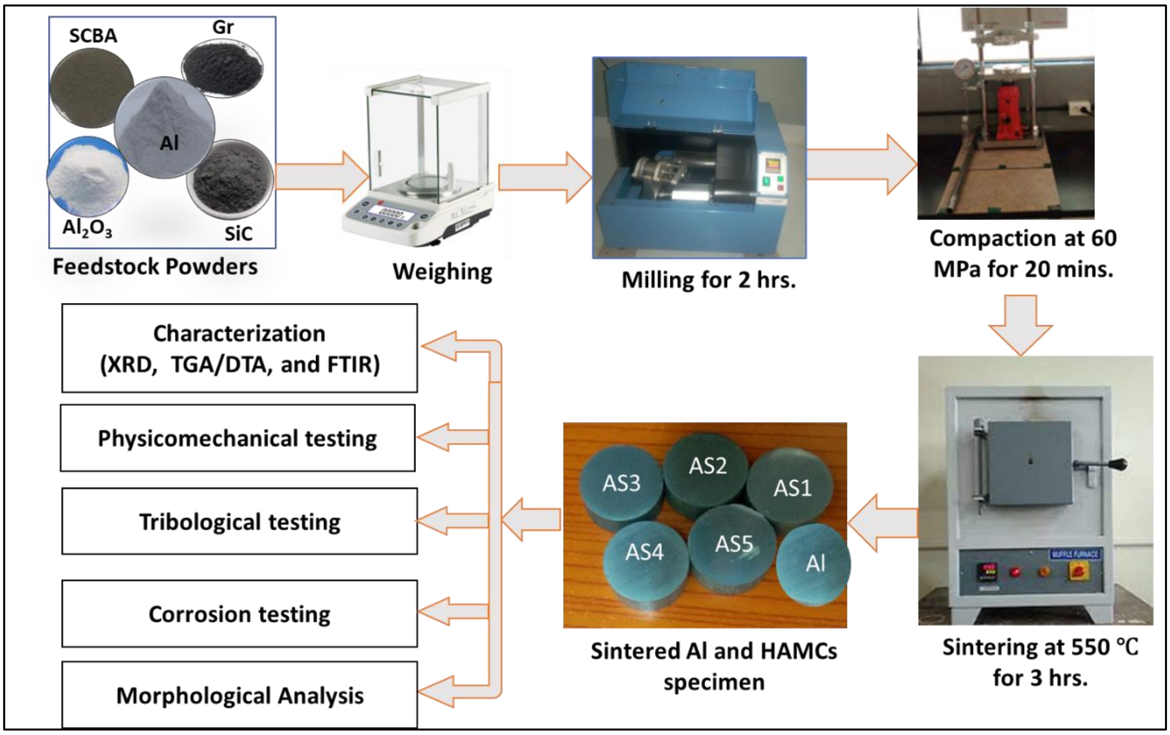

Figure 3.5 Experimental setup for the synthesis of HAMCs using powder metallurgy process (Aynalem, 2020)

3.1.4. Material characterization techniques and equipment

Table 3.6 Type and purpose of the equipment used throughout the research work

No	Equipment	Purpose
1.	High energy ball milling	• Blending or mixing and grinding into very fine powders of the Al matrix and the SiC, Al_2O_3, Gr, and SCBA multiple particulate reinforcements
2.	Hydraulic pressing machine	• Consolidating into a green compact body the mixed Al-(SiC +Al_2O_3 + Gr +SCBA) hybrid composite powder
3.	Electrical muffle furnace	• Sintering the green-compacted hybrid composite specimens at a given temperature to further strength increment. • Sinter SCBA to get fine powder and use as reinforcement in the hybrid composite production.
4.	Grinder/Polisher	• Used to obtain a flat mirror-like surface free from excessive

		deformation and to get a better surface finish.
5.	Chemical (Killer's etchant) solution.	• To avoid any particles, dust, debris…. etc., from the sintered hybrid composite specimens for microstructural characterization
Materials characterization techniques used in this research work		
6.	Optical microscope (OM)	• For examining the structural characteristics of the Al matrix and Al/ (SiC +Gr +SCBA), Al/ (Al_2O_3 +Gr + SCBA), and Al/ (SiC + Al_2O_3 + Gr + SCBA) hybrid composite specimens
7.	Scanning Electron Microscope (SEM)	• For morphological characterization of the surfaces of the hybrid composite in general. • To understand the wear mechanism of unreinforced Al matrix and hybrid composite specimens. • To study the effect of Corrosion on the surfaces.
8.	Thermogravimetric Analysis (TGA)	• Thermal analysis of HAMCs samples was performed to determine the exact sintering temperature in the temperature range of 23–1000 °C at a heating rate of 25°C/min(Lal et al., 2018). • This technique also provides the upper use temperature of the material and above this temperature, the material began to degrade. Hence to identify our samples' working temperature as lubricant thermogravimetric analysis was performed.
9.	Fourier Transform Infrared spectroscopy (FTIR)	• For interfacial reaction and functional group study of the HAMC materials.
10.	X-ray diffraction (XRD)	• Phase composition of a sample: quantitative phase analysis: determine the relative amounts of phases in a mixture by referencing the relative peak intensities • Crystallite Size and Macrostrain
11.	Vickers hardness machine	• To test the hardness of the matrix and composite
12.	Universal testing machine (UTM)	• To test the compressive strength or capacity of Al matrix and Al/ (SiC +Gr +SCBA), Al/ (Al_2O_3 +Gr + SCBA), and Al/ (SiC + Al_2O_3 + Gr + SCBA) hybrid composite specimens to withstand loads tending to reduce size.
13.	Pin-on-disc test apparatus	• Used to investigate the wear rate and coefficient of friction of the hybrid composite specimens
14.	Electronic weighing machine	• For measuring the weight loss of the specimens during the wear test.
15.	Electrical vacuum oven	• For drying the SCBA sample after proper washing.

3.2. Multi-Response Optimization of HAMCs using Taguchi-Based Grey Relational Analysis

3.2.1. Design of experiment using Taguchi method

A design of experiments (DOE) is the process of arranging experiments, collecting data, and analyzing the results while making near-optimal use of available resources (Tosun, 2006; Tsao, 2009). It is an experimental approach for determining the impact of process factors on performance attributes that was conceived and developed. It establishes the process levels and trends of process parameters, which have an impact on response variables.

An orthogonal array (OA) is a fractional factorial matrix that assures a balanced comparison of levels of any factor or interaction of factors (Haq et al., 2008). The array is called orthogonal because all columns can be evaluated independently of one another. Experiments are conducted with five factors each at four levels and hence a four-level OA is chosen. The Taguchi approach is one of the most powerful and successful ways for developing high-quality HAMC systems using L_{16} OAs (Agboola, 2021). L_{16} (or 4^5) orthogonal arrays indicate that there are five parameters such as milling time, compaction pressure, sintering temperature, wt% of Gr, and wt% of SCBA, and there are four levels for each of the five factors, resulting in 16 experiments. Taguchi's experimental design focuses on minimizing the number of iterations. It also allows for the best results in a short time. This powerful tool analysis was performed using the Minitab Statistical Software (version 20.3) to simulate experimental runs.

Table 3.7 Process and reinforcement factors and their levels

Parameters	**Symbol**	**Unit**	**Levels**			
			L_1	**L_2**	**L_3**	**L_4**
Milling Time	MT	Hrs.	2	3	4	5
Compaction Pressure	CP	MPa	45	50	55	60
Sintering Temperature	ST	℃	400	450	500	550
Wt% of Gr	Gr	wt%	0.5	2.5	4.5	6.5
Wt% of SCBA	SCBA	wt%	0.5	2.5	4.5	6.5

Degree of Freedom (DoF) is defined as the number of comparisons made between process parameters that are made to determine a better level. That is used to compute the minimum number of experiments that will be conducted to investigate the observed factors. The DoF value is given by equation 3.3, and Table 3.8 shows the overall DoF of experimental factors in this investigation.

$$\text{Degree of Freedom} = \text{number of levels} - 1 \quad ----------------3.3$$

Table 3.8 DoF of Experimental factors

Experimental factors	DoF (Level – 1)	Sub Total
MT	4 – 1	3
CP	4 – 1	3
ST	4 – 1	3
Gr	4 – 1	3
SCBA	4 – 1	3
Total DoF		**15**

Table 3.9 shows an L_{16}(4^5) OA, where, L_{16} is the maximum number of rows (experiments), 4 is the number of levels, and 5 is the number of columns (factors).

Table 3.9 L_{16} (4^5) orthogonal array Experimental Design

Exp. No.	MT	CP	ST	Gr	SCBA
1.	2	45	400	0.5	0.5
2.	2	50	450	2.5	2.5
3.	2	55	500	4.5	4.5
4.	2	60	550	6.5	6.5
5.	3	45	450	4.5	6.5
6.	3	50	400	6.5	4.5
7.	3	55	550	0.5	2.5
8.	3	60	500	2.5	0.5
9.	4	45	500	6.5	2.5
10.	4	50	550	4.5	0.5
11.	4	55	400	2.5	6.5
12.	4	60	450	0.5	4.5
13.	5	45	550	2.5	4.5
14.	5	50	500	0.5	6.5
15.	5	55	450	6.5	0.5
16.	5	60	400	4.5	2.5

Signal to noise (S/N) is a quality in the communication and engineering field, where is the ratio between the power of the signal (μ^2) and the power of the noise (σ^2) which expresses in decibels (dB) (Haq et al., 2008). S/N ratio has been used as the quality characteristic, which is available depending on the type of character such as smaller the better, larger the better, or nominal is the best.

Table 3.10 Types of problems and respective signal-to-ratio function

S/N function	S/N formula	Usage when the goal is to…
Smaller the better	$S/N = -10\log\left[\frac{1}{3}\sum_{i=1}^{3} y_i^2\right]$	Minimizing the response: for instance, in this study, minimizing the response of ➢ Exp. density ➢ Porosity
Nominal the better	$S/N = 10\log\frac{\mu^2}{\sigma^2}$	Target the response and you want to base the S/N ratio on means and standard deviations
Larger the better	$S/N = -10\log\left[\frac{1}{n}\sum_{i=1}^{n}\frac{1}{y_i^2}\right]$	Maximize the response: for instance, in this study, maximizing the response of ➢ Vickers' microhardness, and ➢ Compressive strength

3.2.2. Grey Relational Analysis

This study attempts to determine and optimize physicomechanical parameters with the following two goals in mind: (1) to minimize density, and porosity, and (2) to maximize the micro-Vickers hardness, compressive, and ultimate tensile strength of a new HAMC material fabricated using a powder metallurgical process. As a result, it's an instance of multi-response optimization, as opposed to single-performance characteristic optimization (Prakash et al., 2021). When one performance feature has a greater S/N ratio, another could have a lower S/N ratio. As a result, for the optimization of numerous performance aspects, an overall evaluation of the S/N ratio is necessary. Grey Relational Analysis (GRA) is an efficient tool for such multi-response analysis. GRA is a measurement of the absolute value of the data difference between sequences, and it could be used to measure the approximate correlation between sequences

The GRA is a method of determining the absolute value of a data difference between two sequences, as well as an estimated correlation between them. It's a good way to look at the relationship between sequences with a small amount of data and it can look at a lot of different things.

Taguchi-based Grey relational analysis (TGRA) is familiar for treating problems having inter-functional relationships among multiple input parameters and response variables. Multiple input parameters considered are the wt% of SCBA and Gr, milling time, compaction pressure, and sintering temperature. Sixteen different sets of experiments are carried out in this study which is further optimized using GRA. The responses considered during this study are density, porosity, hardness, compressive strength, and ultimate tensile strength. These physicomechanical property performances were transformed into a single common dataset by estimating Grey Relational Grade (GRG). The highest value of GRG is assumed to be the most influential combination and is assigned with rank accordingly. GRG was estimated for all sets of data values and it is used to identify the most significant levels of input parameters at which improved results are obtained. The GRG is an average sum of the grey relational coefficient. The following diagram shows the major steps of GRA. Details of the GRA have been discussed in the result and discussion section by applying the response during optimization.

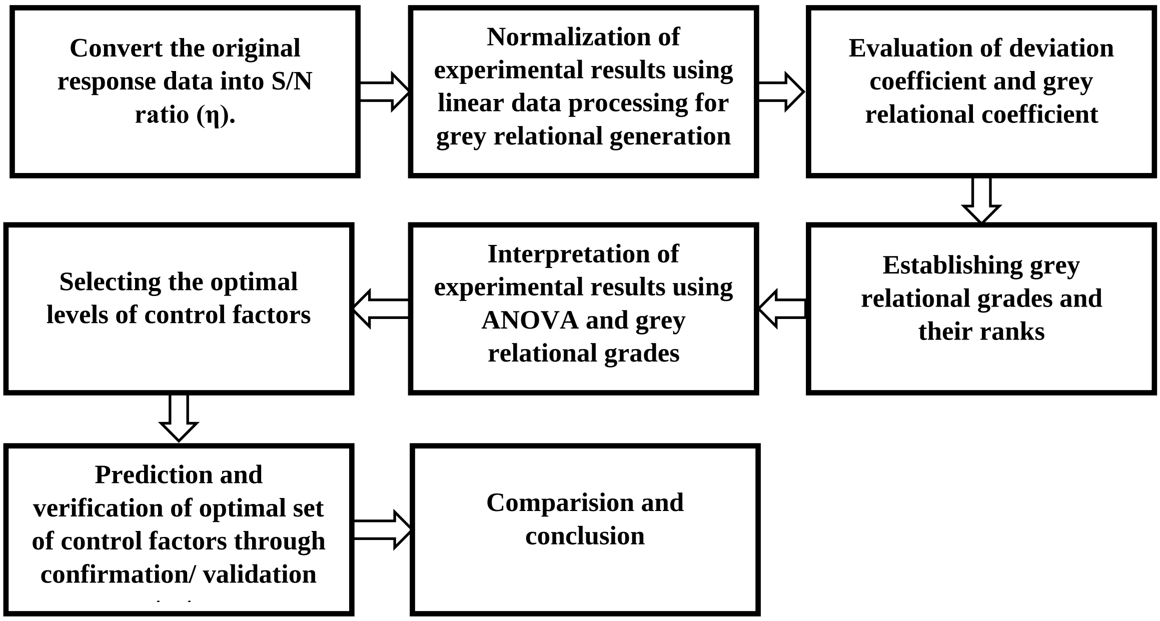

Figure 3.6 Major steps involved in TGRA (Yunus et al., 2016)

CHAPTER-FOUR

4. RESULTS AND DISCUSSIONS

4.1. Compositional and Phase Analysis of SCBA Fine Particulates

Table 4.1 XRF analysis of SCBA

Composition	SiO_2	Al_2O_3	Fe_2O_3	CaO	MgO	Na_2O	K_2O	MnO	P_2O_5	TiO_2	H_2O	LOI
SCBA (%)	65.50	16.52	4.08	0.01	0.01	0.01	1.5	0.1	0.5	0.24	0.66	10.87

The largest proportion of the primary components (SiO_2 + Al_2O_3 + Fe_2O_3) in the solid waste SCBA is 86.2 %, making it a suitable secondary reinforcement for the creation of innovative MMC materials. Furthermore, XRD measurements of SCBA calcined at 850 °C verified the existence of SiO_2 and Al_2O_3, with strong SiO_2 peaks and low Al_2O_3 peaks. Figure 4.1 depicts the phase identification of SCBA using XRD. As a result, the obtained SCBA fine powder can be used as an effective secondary reinforcing material in the fabrication of tetra hybrid reinforced HAMC materials.

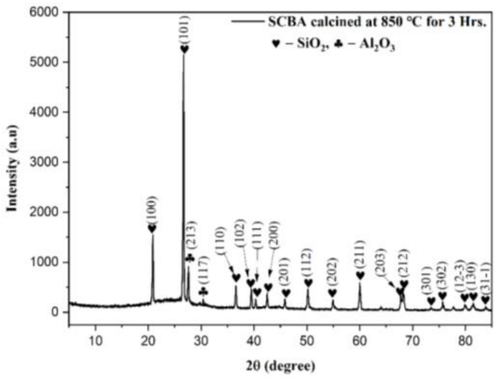

Figure 4.1 XRD graph of SCBA calcined at 850 ℃ for 3 hrs.

4.2. Role of Tetra Hybrid Reinforcements on Behavior of HAMCs

4.2.1. Phase Analysis of the HAMCs

The XRD patterns of the HAMC specimens were analyzed using Origin and High score Plus software (Alam et al., 2021).

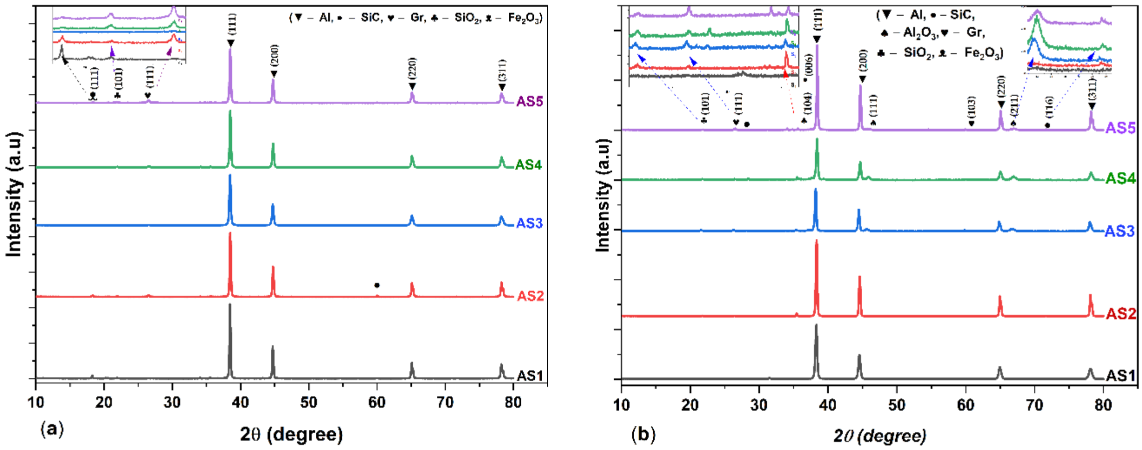

Figure 4.2 XRD results of HAMCs of (a) before sintering (b) after sintering

Figure 4.2 (a) depicts the XRD plot of the HAMCs powders following milling before compaction and sintering were performed. The graph shows that there is a dominancy of the Al matrix and other reinforcements' significant peaks are not shown, which ascribes that in the milling process there was no undesirable interfacial chemical reaction between the hybrid reinforcements and the matrix (Ravindran, Manisekar, Vinoth Kumar, et al., 2013). As shown in Figure 4.2, Al with a cubic crystal structure with a = b = c = 4.0500 Å and ∝= β = γ = 90° with an experimental density of 2.675 g/cm^3 can be detected in the HAMCs samples, regardless of whether it is before or after sintering. However, in the composite shown in Figure 4.2 (b), peaks corresponding to distinct phases are recognized as Al, SiC, Gr, Al_2O_3, SiO_2, and Fe_2O_3. The presence of SiO_2, Al_2O_3, and Fe_2O_3 in the HAMCs is highly correlated with the presence of SiO_2, Al_2O_3, and Fe_2O_3 in the SCBA (Ikubanni et al., 2021b; Suresha et al., 2012), this is strongly associated with XRF results depicted in Table 4.1.

The minor peak of Fe_2O_3 (JCPDS card number: 046-1212) was shown at AS2 and AS3 at 2θ =18.062˚ corresponding to the (111) crystallographic plane, but in other samples, this oxide is not further shown as it is dominated by the other oxides such as Al_2O_3 and SiO_2, which comes from SCBA (Venkatesh et al., 2021). The minor peak of Gr was shown at angles 2θ =26.603˚ corresponds to the (111), (JCPDS *card number: 025-0284*), and 21.895˚corresponds to the (101) crystallographic plane of SiO_2 (JCPDS *card number*: 046-1045), The minor peaks at angles 2θ = 36.651˚, 60.034˚, and 71.772˚ correspond to the (006), (103), and (116) crystallographic planes, indicates the presence of SiC (JCPDS card number: 073-0603). The minor peaks Al_2O_3 were also shown at angles of 35.324˚, 45.790˚, and 66.763˚ (see AS3, AS4, and AS5) corresponding to (104), (111), and (211) crystallographic planes (JCPDS card number: 046-1212). The presence of more Al_2O_3 and SiO_2 ascribes to the presence of SCBA, which confirms that SCBA could be a promising material for the development of the tetra hybrid reinforced HAMC materials with Al as a matrix for the application of Aerospace and Automotive components (Gupta et al., 2019; Ikubanni et al., 2021a; Ravindran, Manisekar, Vinoth Kumar, et al., 2013).

4.2.2. TGA - DTA Thermal Behavior of HAMCs

Figure 4.3 (A) depicts the TGA-DTA curves for the AS1 HAMC sample. At 25 °C, the TG curve represents 100 wt% weight. When the heating temperature of the material increases the mass of the material remains as the initial, though there was an increase in mass of the material at the temperature from 80 °C to 220 °C about 0.01 – 0.02% increase and this might be due to the impurity introduced by the inert nitrogen environment. Heating from 220 °C to 560 °C begins slight loss in mass is due to decomposition of material on increase in temperature, but from 600 °C to 1000 °C, the pattern reveals a gradual increase in weight, with a total of 1.00% weight gain at 1000 °C. As can be observed from Figure 4.3 (A), the weights of all powders rapidly increased with increasing temperature, from approximately 860.10 to 1000 ℃. The formation of oxides which were generated due to the exothermic reactions between Al and oxygen was assumed to have caused the increase in weight (Park et al., 2019). In addition, due to the heat involved in the TGA process, Al and oxygen reacted to form Al_2O_3, and their presence in the composites was confirmed using the XRD patterns. A wide variety of alumina ceramics has been studied for reactions and wettability with different metals (Leon-Patino, 2001). It is generally recognized that alumina cannot be wetted by pure Al below about 800 ℃. However, as wetting transitions are very sensitive to the nature of the substrate, quality of the atmosphere, and other factors, the temperature for wetting transition is seldom universal and well defined. The stationary contact angle of Al on single-crystal alumina decreases linearly in the 800-1000 ℃ temperature range, a typical wetting behavior in a non-reactive metal/alumina system (Leon-Patino, 2001). Therefore, the formation of Al_2O_3 will not hurt the behavior of HAMC.

One endothermic peak of 664.10 ℃ was observed in the DTA plot as revealed in figure 4.3 (A), which indicates the point of phase transformation occurs. Both SiC and Al_2O_3 particles have lower thermal conductivity and heat of diffusivity than Al, allowing them to store rather than transfer heat. As a result, the temperature of these reinforcing particles in Al (SiC +Al_2O_3) HAMCs is always somewhat higher than that of Al. The HAMCs' total softening/melting was delayed by the SiC and Al_2O_3 particles. The more SiC and Al_2O_3 particles are added, the greater the softening/melting resistance. Because of this, there is more thermal stability in these HAMCs as compared to a more reactive base material. The DTA curve also shows an exothermic peak at 650.01 ℃. This could signify there was some weight gain at this instant of temperature (Fayomi et al., 2019).

Figure 4.3 (B)-(E) represent the TGA -DTA plots for AS2, AS3, AS4, and AS5 with the addition of secondary reinforcements (Gr and SCBA) into AS1 HAMC. Figure 4.3 (B) plot evaluates the TGA and DTA of the AS2 HAMC sample. These plots were employed to see the effect of secondary reinforcements on the thermal stability and phase change of the AS1 HAMC. There is no more change in the weight gain ranges though some slight variations have happened in TGA curves. As can be observed in figure 4.3 (B), in the first stage, the material loses moisture and impurities. From 285 to 485 the thermal stability is more than that of AS1, which is one of the positive impacts of secondary reinforcements on the HAMCs. The endothermic peaks were shown at 662.10 ℃ which shows the phase transformation temperature, As the temperature increases, the mass of the composite decreases gradually with a total mass loss of 0.03% and stabilizes between 540.56 to 590.69 ℃ before the material started gaining mass from 601.16 to 1000 ℃ due to the hygroscopic nature of the secondary reinforcement materials (SCBA) (Fayomi et al., 2019). As shown in figure 4.3 (B), the DTA plot indicated one endothermic peak of 662.10 °C, indicating the site of phase change. Due to the addition of secondary reinforcements, there is an exothermic peak at 707.62 °C. This exothermic peak in AS2 is a higher temperature than AS1 HAMC (see Figures 4.3 (A) and (B)). Furthermore, the weight gain in AS2 is more than in AS1, it is because of the SCBA, which has more oxides that can form Al_2O_3 with pure Al(V. Singh et al., 2014). After 985 ℃ the HAMC starts thermal stability, which shows that AS2 is more thermal performance than Al (V. Singh et al., 2014).

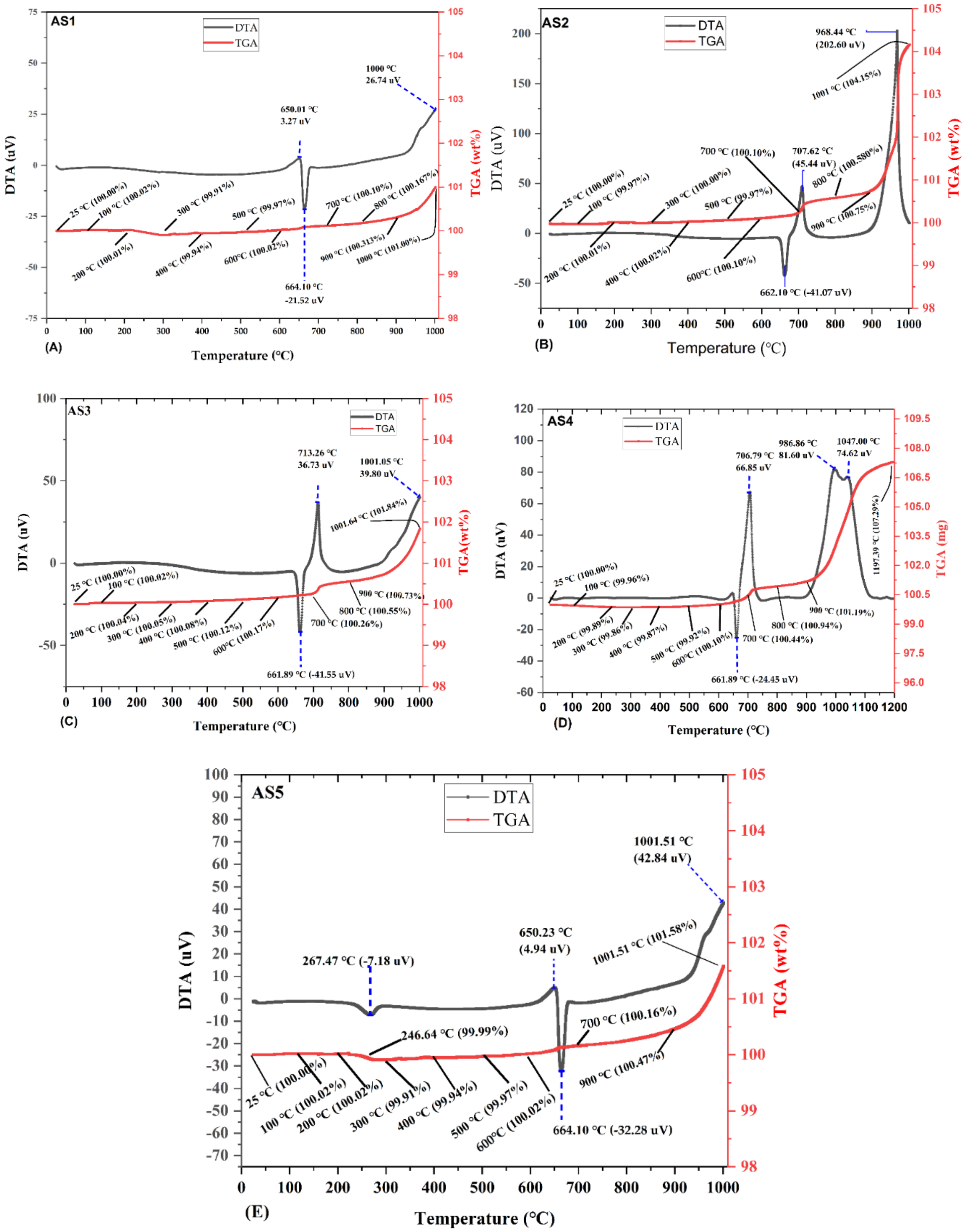

Figure 4.3 TGA and DTA graph of (A) AS1, (B) AS2, (C) AS3, (D) AS4, and (E) AS5 of HAMCs samples

As can be observed in figure 4.3 (C), the endothermic and exothermic peaks of AS3 are increased relative to AS2. A slight increase in weight is observed between the temperatures of 60 °C to 700 °C due to the removal of impurities and moistures at the beginning and oxidation in the latter. Comparatively, a sudden increase in weight gain is observed from the temperature of 700 °C to 1000 °C. In this test, noticeable weight loss or gain did not happen which indicates the thermal stability of the material. Moreover, stability in heat flow is also seen through little fluctuation between the temperatures up to 630 °C.

As can be shown in Figure 4.3 (D), from 40 ℃ to 580 ℃ there is a slight weight loss. The weight loss at low temperatures up to 100 °C may be due to escape of the moisture which transforms to vapor on heating, and at high temperatures some of the impurities available in the secondary reinforcement material (SCBA) may burn off, thus resulting in loss of mass(Lal et al., 2018). It demonstrates that the weight gain is started at around 600 ℃ and continues up to 1200 ℃. The warm strength of hybrid reinforcements is higher than that of Al. Hence, as the wt% of these hybrid reinforcements in the HAMCs expands its introduction of start temperature increments or gets fortified. Al may respond with the barometrical oxygen to frame an Al_2O_3 film which is stable, definitely following, and dense.

The TGA -DTA plots in Figure 4.3 (E) (AS5) are almost the same as in Figure 4.3 (B) and (C) up to 600 ℃. The DTA curve in figure 4.3 (E) includes two endothermic peaks at 267.11 °C, and 664.10 °C, indicating that phase change occurs at these temperatures. The first endothermic peak could be because of the phase change of some volatile impurities on the surface of the sample and the inert gas environment. the phase change on the second peak could be because of the melting temperature of base metal (pure) Al.

To summarize the TGA-DTA analysis results the following key points are generalized Figure 4.3 (A – E) represents the TGA -DTA curves for HAMCs. These curves provide the thermal behavior of HAMCs during heating. The initial decrease in mass of every sample up to 100 °C is due to loss of moisture. While the further slight loss in mass is due to decomposition of material on increase in temperature. Somewhere increase in mass can be seen which is due oxidation of composite. The peak on the DTA in the curves depicts phase transition during the heating or cooling cycle. The tetra hybrid reinforcements (SiC, Al_2O_3, Gr, and SCBA) have lower thermal conductivity and heat of diffusivity than aluminum, allowing them to store heat rather than transfer it (V. Singh et al., 2014). As a result, the temperature of these reinforcing particles in HAMCs is always somewhat higher than that of Al. The HAMCs' total softening/melting was delayed by the SiC, Al_2O_3, and SCBA particles. The more SiC, Al_2O_3, and SCBA particles are added, the greater the softening/melting resistance.

The DTA shows endothermic peaks between 661.89 °C to 64.10 °C and represents phase transformation from solid to liquid (melting). There is not much change in the melting point because both phases (matrix and reinforcements) have their own identity in the material and exist as a free state. As the melting point of aluminum (660 °C) is reached during heating, matrix material starts softening and then proceeds to melt leaving the tetra hybrid reinforcements (SiC, Al_2O_3, Gr, and SCBA) in the melt. A small change in heat of fusion can be seen, due to the presence of tetra hybrid reinforcements (SiC, Al_2O_3, Gr, and SCBA). Composites do not melt at a single temperature; rather they melt on a range of tempera small changes in heat of fusion can be seen, due to the presence of tetra hybrid reinforcements (SiC, Al_2O_3, Gr, and SCBA) as shown in Table 4.2. Composite starts melting at solidus temperature while melting completely at liquidus temperature. The details of the thermal behavior of the developed HAMCs which comprises the weight loss/gain, the range of material thermal stability obtained from TGA, and the phase transformation by DTA are presented in Table 4.2 below.

Table 4.2 Summary of the Thermal Behaviour of the HAMCs.

Samples	Total weight gain (%)	TGA (Range of material thermal Stability (°C))	DTA (Phase transformation) (°C)
AS1	1.00	300 -620	664.10
AS2	4.15	300 -620	662.10
AS3	1.84	300 -620	661.89
AS4	7.29	300 -620	661.89
AS5	1.58	300 -620	664.10

The oxidation of AS4 is higher than that of all others, and at a higher temperature, it shows more thermal stability, while AS1 has lower weight loss as the primary reinforcements are more chemical, and thermal stable than secondary reinforcements.

The range of thermal stability increases with the addition of hybrid reinforcement particulates, for example; 10% of primary reinforcements and 1% of secondary reinforcements reinforced HAMCs were stable at the temperature range of 300 to 620 ℃ above the range of material stability for the base metal (pure Al). All HAMCs display excellent thermal resistance and material stability at a higher temperature ranging from 300.560C to 610.00 ℃ compared to base metals (Al with melting temperature = 660 ℃). According to Table 4.2, the phase transition temperature is between 660 and 670 °C. Based on this information, the new tetra hybrid reinforced HAMCs' sintering temperature must be less than 0.7 to 0.9 % of the phase transformation temperature (melting point) of the given material. These TGA and DTA analyses were well supported by previous research (Ankur et al., 2021; Wolla et al., 2014). Based on the results, the sintering temperatures of the tetra hybrid reinforced HAMCs was determined to be 400, 450, 500, and 550 °C, which are all within the specified domain.

4.2.3. FTIR Characterization of HAMCs

In the region of 1000-500 cm^{-1}, the vibration of the main functional groups of Si-O and Al-O was observed. The peak observed around 550 cm^{-1} is characteristic of Fe-O vibrations The HAMCs exhibit peaks at 510 and 1082 cm^{-1} that corresponds to the Al-O bonds. The band at around 1100 – 1010 cm^{-1} is assigned to Si-O stretching vibrations and the absorption bands at 914, 540, and 470 cm^{-1} are attributed to Si-O-Si bending vibration. These bands are assigned to the symmetric and asymmetric vibrations of valence bonds Si–O–Si (Gadsden, 1975; Merabtene et al., 2019). The doublet at 780 – 798 cm^{-1} is due to Si-

O-Si inter tetrahedral bridging bonds in SiO_2 (Hospodarova et al., 2018; Merabtene et al., 2019). The drop in IR transmittance in the wavenumber interval between 400 and 900 cm^{-1} is due to the absorption produced from Al–O stretching. The weak IR band around 1,177 cm^{-1} is from the Si–O–Si stretching of silica species. The peaks at 1702, 1594, and 1408 cm^{-1} are due to the presence of the sp^2 bond of graphite (Kúdela et al., 2008). The FTIR spectrum peaks 883, 2353, and 2374 corresponds of Si-C group (Vaziri et al., 2020). As seen in Figure 4.4's FTIR spectra of all HAMCs, a broad absorption peak at 3353 cm^{-1} corresponds to the stretching vibration absorption peak of Al–OH (Feng et al., 2018). Large bands around 3400, 3700, and 3856 cm^{-1} are also observed, due to the -OH groups adsorbed on the HAMCs surface (Feng et al., 2018).

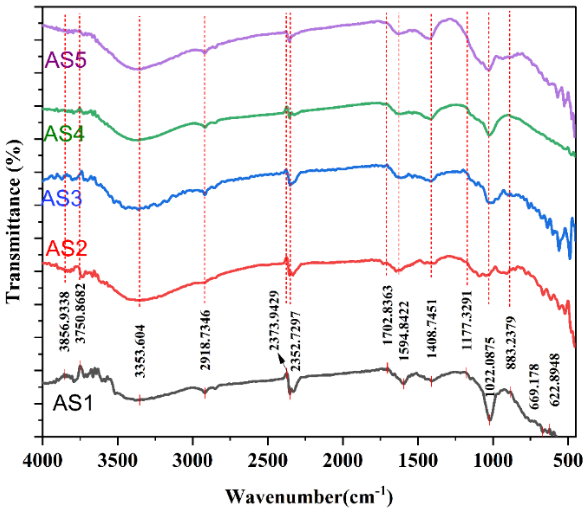

Figure 4.4 FTIR spectra of the HAMC samples

4.2.4. Brunauer-Emmett-Teller (BET)

Table 4.3 BET results of AS1 and AS4 HAMC powder samples

Sample	Surface area (m^2/g)	Pore volume (cm^3/g)	Pore size (nm)
AS1	581.542	0.03815	0.1684
AS4	290.866	0.01316	0.1324

As seen in Table 4.3, the AS1 HAMCs have a greater surface area, pore-volume, and pore size than the AS4 HAMCs. The AS1 HAMC sample's large specific surface area might be attributable to the inclusion of hard particles such as SiC and Al_2O_3 in the AS1 HAMC sample. The HAMC materials also contain the Dubinin-Radushkevich (DR) Method micropore with sizes and volumes of 0.1684 nm and 0.03815 cm^3/g for AS1 and 0.1324 nm and 0.01316 cm^3/g for AS4, according to the data in Table 4.3. The AS4 HAMC sample has a smaller surface area and micropores due to the inclusion of 4.5 wt% Gr and

4.5 wt % SCBA secondary reinforcements. This is due to an increase in particulate uniform distribution within the matrix. And Gr aids in the rearrangement and movement of hard particles inside the base materials, resulting in increased hardness and decreased porosity (Singh et al., 2021).

4.2.5. Physicomechanical Behavior of HAMCs

4.2.5.1. Density and Porosity Measurement

Figure 4.5 shows the variation of experimental density, theoretical density, and % void content with the different compositions of the HAMC specimen. AS1 HAMC sample has greater theoretical and experimental densities than base metal due to the inclusion of SiC and Al_2O_3, which are harder and stronger particles than Al. With the addition of secondary reinforcements, both 0.5 wt% Gr and 0.5 wt% SCBA particulates into AS1 start decreasing in density and porosity of HAMC samples, due to the lower density of Gr (2.28 g/cm^3) and SCBA (1.48 g/cm^3) compared to the primary reinforcements, SiC (3.20 g/cm^3), Al_2O_3 (3.96 g/cm^3), and base matrix, Al (2.70 g/cm^3). According to Figure 4.5, both the experimental and theoretical density of the HAMC are in accordance with each other, indicating the applicability of the PM process, and this is closely associated with prior studies (Prasad et al., 2014). Because of the lower density of SCBA and Gr secondary reinforcements, the density of the HAMC samples from AS1 to AS5 decreases as the SCBA and Gr particulate content increases. However, porosity exhibits slight perturbation, with AS4 having the lowest porosity of all samples; this result is significantly associated with XRD and BET results. This is also seen in the developed HAMCs material's enhanced hardness, strength, corrosion, and wear resistance, and with previous findings (Singh, 2016). The increased wt % of secondary reinforcements caused increased porosity due to the increase in SCBA content, which could initiate cracking in the HAMCs, and the Gr content above the optimal range could also cause more porosity because of its light weight and inability to easily rearrange and move with the Al, instead accumulating in some portions, causing partial distribution of hybrid reinforcements in the Al matrix.

Table 4.4 Density and porosity results of the developed HAMCs

Sample	Chemical Composition	Theo. Density (g/cm^3)	Exp. Density (g/cm^3)	Porosity (%)
Al	Pure Al metal	2.700	2.675	0.926
AS1	Al/5SiC/5Al_2O_3	2.766	2.726	1.446

AS2	Al/5SiC/5Al_2O_3/0.5Gr/0.5SCBA	2.751	2.713	1.381
AS3	Al/5SiC/5Al_2O_3/2.5Gr/2.5SCBA	2.696	2.659	1.372
AS4	Al/5SiC/5Al_2O_3/4.5Gr/4.5SCBA	2.643	2.629	0.530
AS5	Al/5SiC/5Al_2O_3/6.5Gr/6.5SCBA	2.592	2.549	1.659

Higher void content in HAMCs is undesirable and represents poor quality. High void content HAMCs material affects various properties and performance when in use. Therefore, it can be said that a basic criterion with which to evaluate their quality is the density of HAMCs.

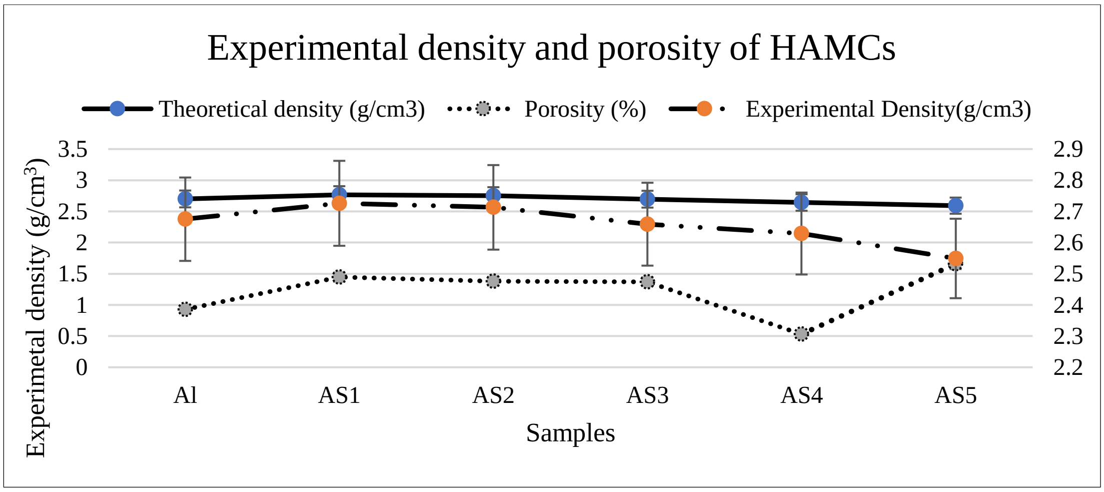

Figure 4.5 HAMC Experimental Density Variation with reinforcement type and wt%

4.2.5.2. Vickers Microhardness (HV)

The five trials and average Vickers microhardness values of the six sintered HAMCs samples are shown in Table 4.5, and the average HV values are shown in Figure 4.6. The addition of 10 wt% (5 wt% SiC + 5 wt% Al_2O_3) hard particles base metal (Al) enhances the hardness by 2.34 times, with a 134.49% of improvement, as indicated in the Figure 4.6. Because of the hard SCBA fine particulates, there is an increasing trend in hardness from AS1 to AS4 with the addition of secondary reinforcements up to 9.0 wt% (4.5 wt% of Gr and 4.5 wt% of SCBA) of fine particulates, confirming that SCBA is a promising material capable of substituting hard particles (ceramic particulates) to be used as reinforcement. This is a huge advance since agro-industrial solid wastes such as SCBA are light in weight, low in density, and widely available, while still ensuring a safe and clean environment. The greatest hardness value observed in the AS4 HAMC sample is 358.66, which is 5.464 times greater than the average hardness value of base metal Al, or it is 446.40% enhanced for an increase to 9 wt% (4.5 wt% Gr + 4.5 wt% SCBA), after which the hardness trend begins to decline. The decrease in hardness may be attributed to the presence of softer reinforcement (Gr) particles. This finding is well associated with earlier research (Singla et al., 2009; Suresha et al., 2012). The size, volume, and type of reinforcement particulates are the most important factors influencing hardness (Fanani et al., 2021). The average HV improvement is depicted in Figure 4.6 (B). Table 4.5 displays the average HV values of five trials of HAMCs with fixed amounts (5 wt%) of SiC and Al_2O_3 and changing wt% of SCBA and Gr fine particles.

Table 4.5 Five trial and average micro hardness values of the sintered HAMCs sample

Sample	Chemical Composition	HV_1	HV_2	HV_3	HV_4	HV_5	$HV_{Average}$
Al	Pure Al metal	63.90	66.10	66.00	65.70	66.50	65.64
AS_1	$Al/5SiC/5Al_2O_3$	153.00	159.40	153.20	150.00	154.00	153.92
AS_2	$Al/5SiC/5Al_2O_3/0.5Gr/0.5SCBA$	201.10	199.00	193.80	200.10	194.80	197.76
AS_3	$Al/5SiC/5Al_2O_3/2.5Gr/2.5SCBA$	197.90	204.40	199.00	204.40	206.60	202.46
AS_4	$Al/5SiC/5Al_2O_3/4.5Gr/4.5SCBA$	380.60	402.60	332.60	348.00	329.50	358.66
AS_5	$Al/5SiC/5Al_2O_3/6.5Gr/6.5SCBA$	167.40	177.60	192.30	170.20	176.30	176.76

The greater microhardness of the SiC, Al_2O_3, and SCBA (that comprises SiO_2, Al_2O_3, and Fe_2O_3) can be ascribed to the improvement in the hardness of the HAMCs with increasing reinforcing content. This is strongly correlated with previous research (Radhika et al., 2013; Radhika, Subramanian, Prasat, et al., 2012) Because of the inclusion of higher modulus powders, smaller grain sizes, and numerous reinforcements, the hardness of the hybrid composites was greater than that of the single and double reinforced composites, which was higher than that of the base metal. Moreover, the high cost and limited supply of conventional ceramic reinforcing materials especially in developing countries have remained a major problem associated with the development of HAMCs. Using two or more reinforcing materials gives room for the possible reduction of cost coupled with property optimization in HAMCs (J. Singh et al., 2014).

4.2.5.3. Compressive Strength Testing

According to Table 4.6 and Figures 4.6 (A) and (B), incorporating tetra hybrid reinforcements into the base metal during HAMC manufacture boosted their compressive strength. This might be because the microstructure acts as a barrier to grain dislocation(G et al., 2019). The use of hybrid reinforcements was shown to boost compression strength. When additional Gr and SCBA particles were introduced, the inter-particulate space between them shrank, causing the dislocation pack to rise. Moreover, compression improved from 134.49 % (for AS1) to 209.75 % (for AS4). The compressive strength tests follow the same pattern as the Vickers hardness results; such results are unique in tetra hybrid reinforced HAMCs due to the customizability behavior of hybrid reinforcements used in the fabrication of HAMCs.

Table 4.6 Three trial and average CS values of the sintered HAMCs

Sample	Chemical Composition	CS_1	CS_2	CS_3	$CS_{Average}$
Al	Pure Al metal	110.00	108.00	112.00	110.00
AS_1	$Al/5SiC/5Al_2O_3$	262.38	245.03	252.56	253.32
AS_2	$Al/5SiC/5Al_2O_3/0.5Gr/0.5SCBA$	273.00	255.65	263.18	263.94
AS_3	$Al/5SiC/5Al_2O_3/2.5Gr/2.5SCBA$	312.34	294.99	302.52	303.28
AS_4	$Al/5SiC/5Al_2O_3/4.5Gr/4.5SCBA$	349.78	332.44	339.96	340.73
AS_5	$Al/5SiC/5Al_2O_3/6.5Gr/6.5SCBA$	225.92	208.58	216.10	216.87

Moreover, the testing findings revealed that AS4 with 10% primary reinforcements (SiC and Al_2O_3) and 9% secondary reinforcements (Gr and SCBA) of HAMCs had the highest potential in terms of decreased porosity and better compressive strength. It can be stated that 10% of the primary reinforcements (SiC and Al_2O_3) and 9% of the secondary reinforcements (Gr and SCBA) of HAMCs had superior physicomechanical characteristics when compared to other compositions. Particulate reinforced AMCs outperform conventional materials in terms of hardness, tensile and compressive strength, and tribological properties (Sahu et al., 2020). Because of its ease of use and the ideal combination of configurable tribological and mechanical properties, high strength-to-weight ratio, and environmental friendliness, HAMCs have become a popular choice for the aerospace, automotive, sporting, and electronics industries (Sahu et al., 2020).

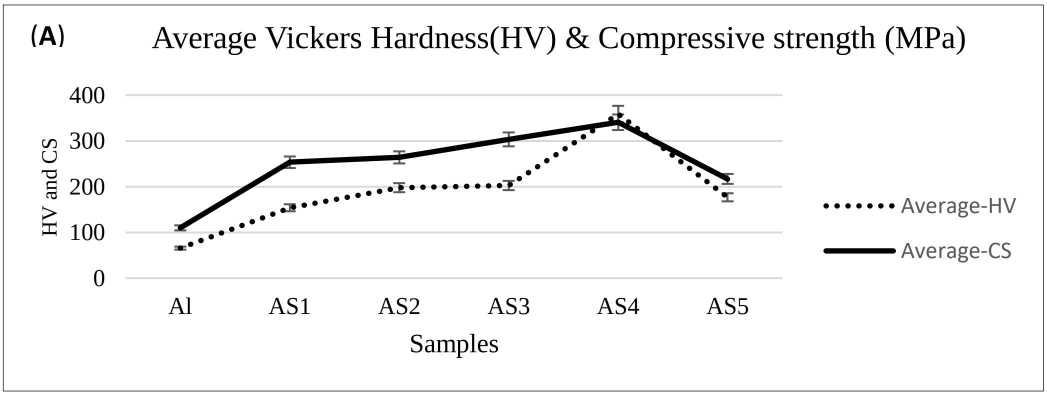

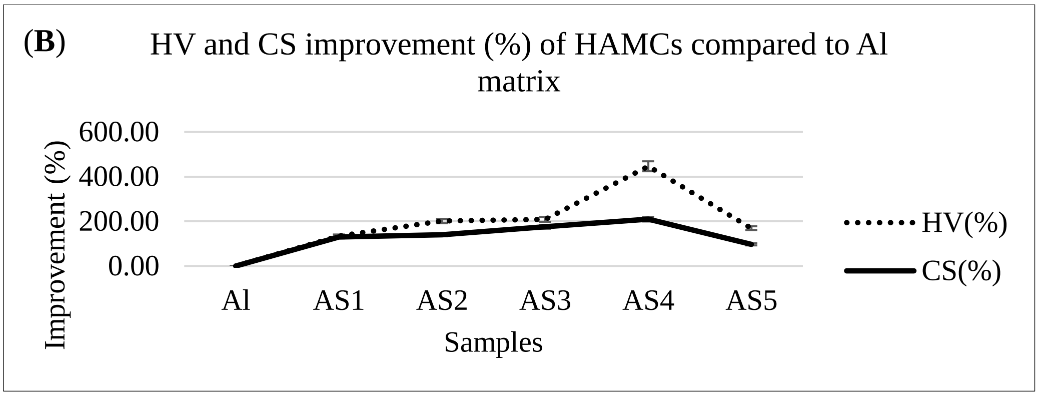

Figure 4.6 (A) Graph of average HV and CS values of HAMC samples, (B) improvement (%)

The percentage of improvement in material properties was calculated using the following equation;

$$Improvement(\%) = \frac{\text{New}(X_i) - \text{Original}(X_i)}{\text{Original}(X_i)} \times 100 - - - - - - - - - - - -4.1$$

Where, the original (X_i) is the average value of base metal Al and X_i is the test (HV, CS)

New (Xi) is the average value of the HAMC samples. All improvement percentages in this research are based on this equation. Based on this, improvement (%) of HV and CS for each HAMC sample is the plot in Figure 4.6 (B).

4.2.6. Tribological Behavior of HAMCs

4.2.6.1. Dry Sliding Wear Behavior of HAMCs

Figure 4.7 (A) shows the wear loss plotted against load for a base metal (pure Al) and five Al/SiC/Al_2O_3/Gr/SCBA HAMC samples with different wt% of Gr and SCBA particulates. The applied load is the most important factor influencing HAMC wear during sliding. The wear loss of both base metal and HAMCs rises with increasing applied load, as shown in Figure 4.7 (A). Several studies have found that there is a critical transition load beyond which the wear rate rapidly rises (Manivannan et al., 2018). In reality, when applied loads are less than this threshold value, mild or oxidative wear occurs, and at larger loads, severe or metallic wear occurs, followed by increasing plastic deformation. As shown in Figure 4.7 (A), the wear loss of Al increases as the load is raised from 10 to 30 N. The rise in wear loss is caused by wear deteriorating at increasing loads. During sliding wear, the temperature of Al rises, causing significant damage to surface asperities and lowering the material's hardness. The hardness, as well as the sharpness of a material's surface, influence its wear resistance. Both SiC and Al_2O_3, as well as SCBA particulates in $Al/SiC/Al_2O_3/Gr/SCBA$ HAMCs (see in sections 4.2.5.2 and 3) behave as load-bearing elements, increasing the HAMC's hardness and compressive strength (Rao et al., 2010; Zhan et al., 2003). These improved properties boost the HMAC's resistance to plastic deformation at the subsurface and its wear resistance. As a result, the wear surface of the $Al/SiC/Al_2O_3/$ hybrid composite forms very little wear debris (AS1). Furthermore, the SiC and Al_2O_3 particles protrude beyond the wear surface and help build a stable tribolayer on the hybrid composite surface. Wear loss in HAMCs reduces with the addition of secondary reinforcements such as Gr and SCBA up to a point, beyond which it begins to grow with more Gr and SCBA addition (Figure 4.6 (A), and Figure 4.7 (A) and (B)). For example, the incorporation of secondary reinforcements (Gr and SCBA) into Al/ (5% SiC+5%Al_2O_3) binary reinforced HAMCs (the change in composition from AS1 to AS2) improves the wear resistance of the base metal by 34.33 – 41.54%. This is due to the fact that SCBA contains high levels of ceramic oxides (SiO_2, Al_2O_3, and Fe_2O_3), that assist the composite (1) preserve the role of Al_2O_3 in the hybrid composite, and (2) SiO_2 and Fe_2O_3 offer additional qualities to the wear resistance behavior of the HAMCs developed (Imran et al., 2016). The inclusion of tetra hybrid reinforcing components, which aid in the creation of a stable surface film on the wear surface, contributes to the decrease in the wear rate of hybrid composites up to a certain reinforcement addition (Reddy et al., 2020). The ceramic phases increase the HAMC's hardness and other mechanical properties, whereas Gr particles aid in the creation of a stable tribolayer.

Regardless of loading variation, the direction in which wear loss behavior varies as a result of hybrid reinforcements content into the base metal is similar. Wear decreased from 0.0112 (pure Al) to 0.0088 for AS1, 0.0066 for AS2, 0.0060 for AS3, and 0.0051 for AS4 HAMC samples with the addition of tetra hybrid reinforcement particles up to certain limits, and as the wt % of the tetra hybrid reinforcements increased above this optimal limit, the wear loss increased. However, given the same type of reinforcements and their contents, increasing loading causes wearing. Higher loads accelerate abrasive wear due to increased local tension, resulting in deeper grooves. The dislocation density is increased by the work hardening effect when there is a thermal mismatch between the particle and the base material. Dislocations travel through the particle's pileup dislocation at the grain boundary as the load rises, and stress concentration causes the delamination crack at the particle or matrix material owing to shear deformation at the subsurface (Suresh, 2020).

The percentage of improvement in wear behavior of the HAMCs is shown in Figure 4.7 (B). According to Figure 4.7, the wear loss of AS1 is lower than the wear loss of Al at all applied loads due to its higher hardness (Table 4.4). Material wear resistance improves as hardness increases. The increased wear resistance against plastic flow reduces HAMC wear loss. The addition of hard SiC and Al_2O_3 particles, as well as SCBA particles, to HAMCs, enhances hardness and strength while also compensating for Gr's weakening effect.

The hard particles (SiC, Al_2O_3, and SCBA) properties that improve the hardness of the HAMCs (as discussed in section 4.2.5.2), impede dislocation movement, and wear deformation are effectively hindered. Furthermore, Gr, the most common solid lubricant, has the highest contribution in the wear improvement (Singh, 2016).

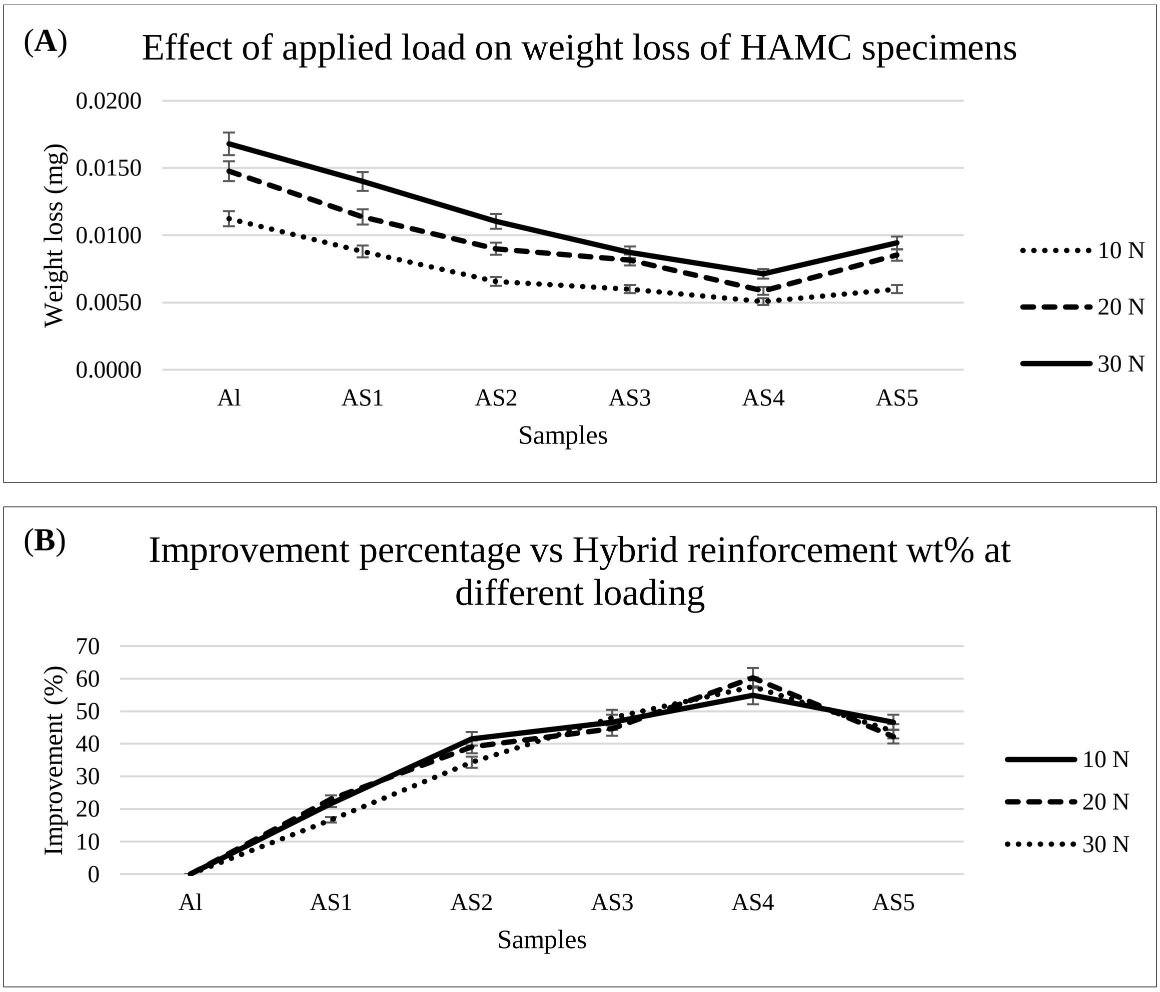

Figure 4.7 Wear loss of HAMCs (A) at different applied load and (B) improvement (%)

The addition of 10 wt% (SiC and Al_2O_3) into the base metal, both of which have increased hardness, results in a 21.66 -32.02% improvement in wear resistance in the AS1 HAMC sample. A further reduction in wear can be ascribed to Gr's lubricating action, which prevents direct contact between pin (HAMC samples) and disc (counterpart material) during sliding wear. Unlike the other four HAMC samples, the wear loss of AS5 does not decrease with the increase of load due to the agglomeration of hard SCBA particles. However, the wear resistance of AS5 is high compared to base metal (pure Al). These trends are consistent with the results of previous studies (Manivannan et al., 2018; Singh, 2016).

Effect of sliding distance and sliding velocity on the wear behavior of HAMCs

The variation in wear loss concerning the type and weight % of tetra hybrid reinforcements for 600, 1200, and 1800 m of sliding distance and 1.5, 2.5, and 3.5 m/s of sliding velocity are shown in Figures 4.8 (A) and (B). The wear loss pattern of both base metal and HAMCs depicted in Figures 4.8 (A) and (B) is nearly the same as Figure 4.7 (A). The solid lubricating characteristic of Gr reduces wear loss in HAMCs containing Gr particles. The Gr particles smeared from contact surface during sliding surface and forms mixed layer which avoids metal to metal contact. Because of its hexagonal closed cell structure, Al_2O_3 has been found to have a solid lubricating action, making it a suitable solid lubricant like Gr (Singh, 2016). Wear loss is reduced in HAMCs due to the creation of a tribo-layer between the sliding surfaces. This layer prevents micro-cutting and scratching, particularly at higher loads. For all HAMCs, wear loss rises with increasing sliding distance from 600 m to 1800 m. The thermal softening localized melting and evaporation will cause a high wear rate during sliding at 1200 m. This is similar to the material removal rate during machining to time duration (Vijayakumar et al., 2013). HAMCs have a slower wear rate than base materials (Al). According to Figures 4.8 (A) and (B), increasing the percentage of secondary reinforcements (Gr and SCBA) in the HAMCs from 1 to 9 wt% (from AS1 to AS4) reduces wear loss owing to an increase in hardness of (AS4 > AS3 > AS2 > AS1) for all sliding distances and sliding speeds. When compared to other HAMC samples, the wear loss of AS4 is much lower. On the contrary, increasing the percentage of secondary reinforcements (Gr and SCBA) from 9 to 13 wt% increases the wear loss. Unlike the other four HAMC samples, the wear loss of AS5 does not decrease with the increase of sliding distances, this may be due to the agglomeration of hard SCBA particles. However, the wear resistance of AS5 is high compared to base metal (pure Al). These trends are consistent with the previous research results of previous researches (Manivannan et al., 2018; Singh, 2016). Figure 4.8 (B) depicts the influence of sliding speed on wear loss. The wear loss lowers as the sliding speed is increased from 1.5 to 3.5 m/s. Material removal through fracture of the reinforcement and matrix due to high frictional force and transferring material layer is also seen at lower sliding speeds (1.5 m/s). The oxide-like transferred layer has been seen at moderate (2.5 m/s) and higher (3.5 m/s) speeds, reducing direct interaction with the hard counter surface. At low and moderate speeds, adhesion and abrasion wear predominate, while localizing melting wear at high speeds.

Based on the wear test findings, it is feasible to deduce that using secondary reinforcement such as a solid lubricant (Gr) and a solid waste (SCBA) can improve the wear performance of the HAMCs. Furthermore, agro-industrial solid waste reinforcements for HAMCs with an aluminum matrix can be used to improve their tribological performances.

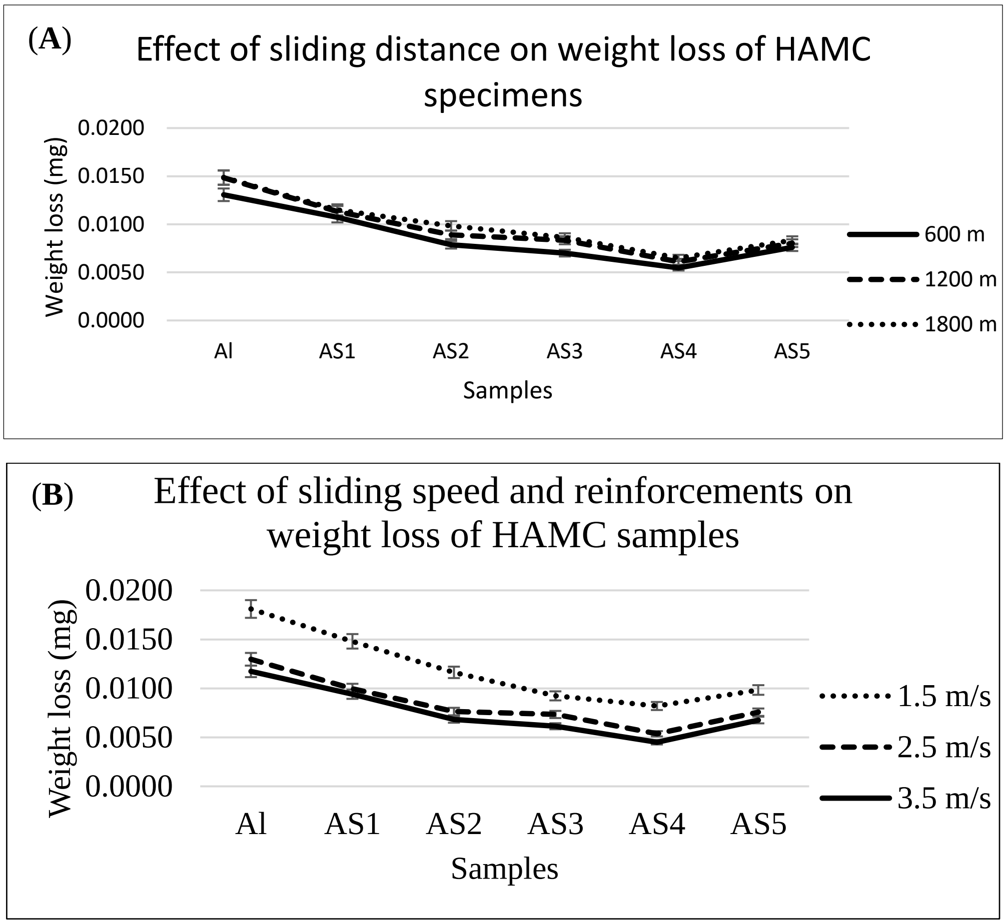

Figure 4.8 Wear loss of HAMCs at different (A) sliding distance and (B) sliding speed

The incorporation of Gr as secondary reinforcement increases the wear resistance of composites by forming a protective layer between pin and counter face and the inclusion of SCBA as a secondary reinforcement also has a significant effect on the wear behavior. However, an increase in the Gr content beyond a limiting value can deteriorate the tribological properties of these composites. Therefore, true optimization of a tribosystem (of the hybrid composite and counter phase) can be achieved by selecting appropriate reinforcement contents (Singh, 2016). A decrease in wear loss with an increase in sliding velocity is mainly caused by the solid lubrication of Gr particles, which are released during sliding and form a tribolayer at the contact surfaces (Baradeswaran et al., 2014). With greater than 9 wt% of secondary (4.5 wt% Gr + 4.5 wt% SCBA) reinforcements, the wear loss tends to increase. This tendency may be attributed to a decrease in the fracture toughness of the HAMCs. Under all studied sliding velocities, the AS4 (Al/ 5SiC/5Al_2O_3/4.5Gr/4.5SCBA) HAMCs demonstrated the lowest wear loss (Ravindran, Manisekar, Narayanasamy, et al., 2013).

4.2.6.2. Coefficient of Friction Behavior of HAMCs

As shown in Figure 4.9, the coefficient of friction increases with increasing load. The increase in the applied load significantly increased the coefficient of friction of the HAMCs because, at lower loads, the graphite film was found to be more stable than at higher loads, as the film was destroyed at a faster rate with an increase in the load (Ravindran, Manisekar, Narayanasamy, et al., 2013). The coefficient of friction decreased as the wt% of secondary reinforcements increased up to 9 wt% (4.5 wt% Gr + 4.5 wt% SCBA) and further increased with increasing wt%. This result is due to the presence of Gr in the Al matrix, which acts as a solid lubricant material on the surface and results in the formation of a solid lubricant-rich film on the tribosurface, thereby reducing the friction by preventing metal-to-metal contact on the sliding surface (Ravindran, Manisekar, Narayanasamy, et al., 2013). When the percentage of Gr was above 4.5 wt%, the friction showed an increasing trend due to fracturing of the oxide layer within the surface, which weakens worn surfaces. Abrasion through the decohesion of sliding surfaces causes contact between the HAMCs and counterface. As a result, the coefficient of friction increased.

Figures 4.9 point out that an increase in the coefficient of friction with an increase in load has been attributed to the maximum speeds at different wt% of the hybrid reinforcements. It has been experiential that, the value of the coefficient of friction has been low at initial loads for the base matrix and its HAMCs. However, the AS4 HAMCs possess the lowest friction coefficient at any particular load. Thus, the coefficient of friction increases with an increase in applied load. With a further increase in secondary reinforcements, the coefficient of friction starts to increase. It has also been apparent that as the sliding speed and wt% of hybrid reinforcement increases, the coefficient of friction decreases due to less frictional force, whereas it has been the reverse for the applied load.

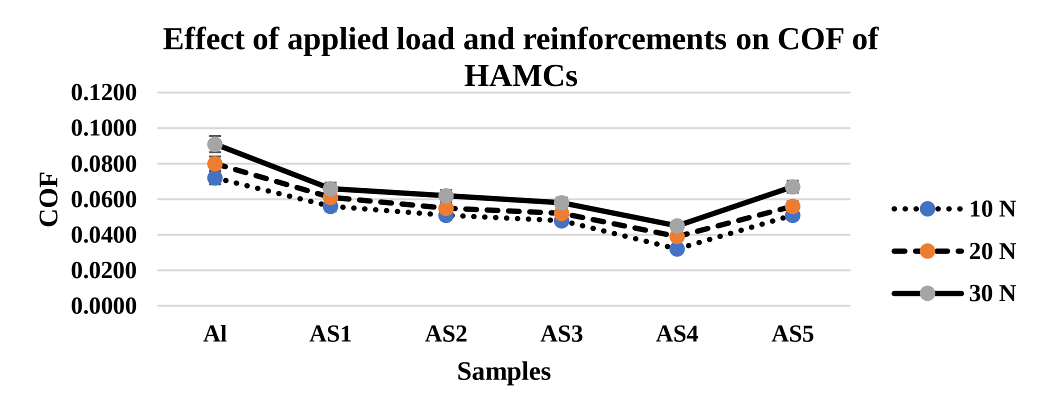

Figure 4.9 Effect of applied load and wt% of hybrid reinforcements on coefficient of friction of HMACs

Figures 4.10 (A) demonstrate the influence of sliding speed on the coefficient of friction. When the sliding speed is increased from 1.5 - 3.5 m/s, the coefficient of friction reduces. Material removal via fracture of the reinforcement and matrix due to high frictional force and transferred material layer is also observed at low sliding speeds (1.5 m/s). The oxide-like transferred layer has been seen at moderate (2.5 m/s) and high speed (2.5 m/s) speeds, which decreases direct contact with the hard counter surface (Vijayakumar et al., 2013).

The friction coefficient of HAMCs increases with increasing sliding distance. This condition can be attributed to the increase in surface temperature caused by increasing contact between the rubbing surfaces. Figure 4.10 (B) shows that the friction coefficient of AS2 HMACs is lower than those of AS1 HMACs and base metal (pure Al). The AS4 HAMC reinforced with10 wt% of primary and 9 wt% of secondary reinforcements (4.5 wt% Gr and 4.5 wt% SCBA) possesses the lowest friction coefficient of all other specimens (pure Al, AS1, AS2, AS3, and AS5) under all operating conditions. Gr is a solid lubricant that smears the contact surfaces. This ability reduces metal-to-metal contact between the rubbing surfaces and helps in the formation of a surface layer at the interface. Therefore, HAMCs reinforced with optimal wt% of Gr exhibit lower friction coefficient and lower wear rate (Hadzima et al., 2018; Ravindran, Manisekar, Narayanasamy, et al., 2013; Singh, 2016).

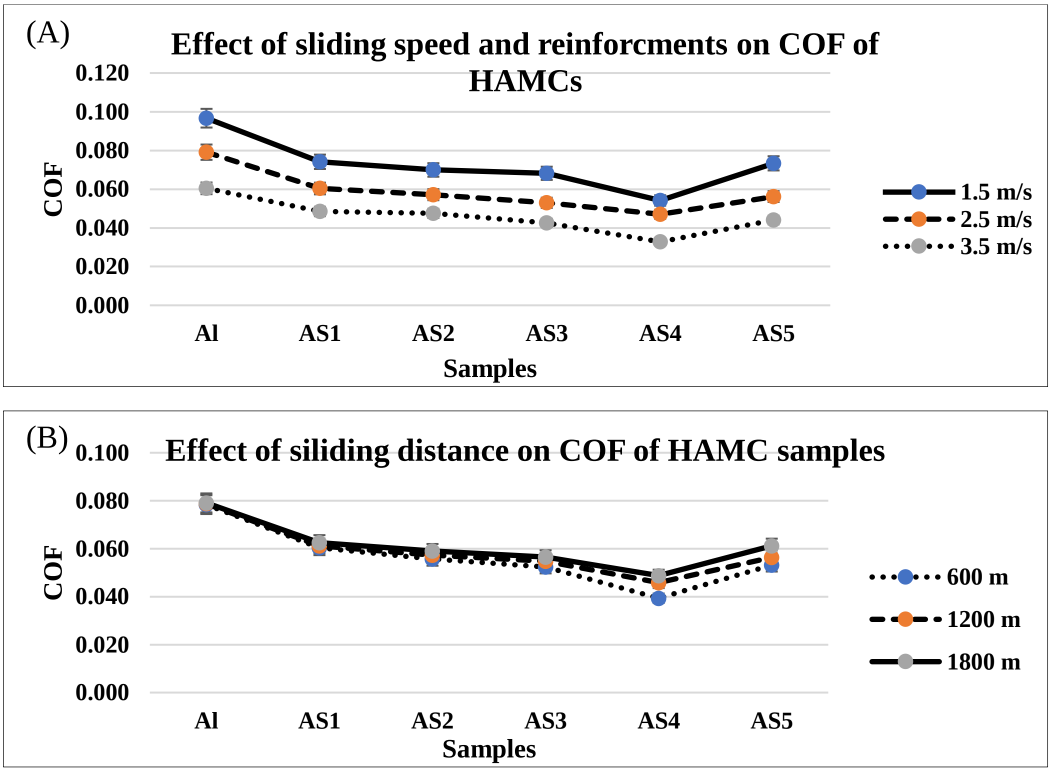

Figure 4.10 Effect of sliding speed, sliding distance, and wt% of hybrid reinforcements on coefficient of friction of HMACs

The properly prepared waste material may be used as a filler or reinforcement for metal-based composites aimed at use in various applications, e.g., as tribological materials directly related to the wear processes due to friction. With increased Gr and SCBA percentages in HMACs, the coefficient of friction declines. This pattern may be explained by the fact that when the reinforcing content of lubricating particles increases, so does the thickness of the surface film (Ravindran, Manisekar, Narayanasamy, et al., 2013). In particular, adding a little percentage of Gr to hybrid composites reduces the friction coefficient between the rubbing surfaces significantly. This decrease might be related to a shift in the wear process from adhesive to delaminating. Furthermore, when the Gr content increases, the surface area of these films grows across the HAMCs surface. As a result, metal-to-metal contact between the rubbing surfaces decreases, as does surface adhesion (Singh, 2016).

4.2.7. Corrosion Behavior of HAMCs

4.2.7.1. Potentiodynamic Polarization Technique

The potentiodynamic polarization test was carried out to study the corrosion behavior of different HAMC samples in 3.5% NaCl solution at room temperature. Figure 4.11 represents the Tafel polarization curves obtained from the potentiodynamic polarization test. The corrosion potential (E_{corr}) and corrosion current density (I_{corr}), polarization resistance (R_P), and corrosion rate (C_R) extracted from the plots are reported in Table 4.7. Also, the polarization resistance (R_P) of samples was determined by the Stern–Geary equation 4.2 (Verma et al., 2015):

$$R_p = \frac{\beta_a \beta_c}{2.303 I_{corr}(\beta_a + \beta_c)} ------------------------ 4.2$$

Where, β_a and β_c are anodic and cathodic slopes of polarization curves, and improved corrosion resistance can be estimated by increasing the potential of corrosion, while the current density is reduced. High E_{corr} and low I_{corr} indicate a low corrosion rate besides more uniform corrosion and high corrosion resistance function. The HAMC's inhibition efficiency (IE%) was calculated by the following equation:

$$Inhibitor\ Efficiency\ (IE\%) = \frac{I^0_{corr} - I_{corr}}{I^0_{corr}} \times 100 ------------ 4.3$$

Where, where I^0_{corr} and I_{corr} represents the corrosion current density values of pure Al and HAMCs, respectively.

As shown in Figure 4.11 and Table 4.7, the I_{corr} value of the base metal (Al) is the highest among the six samples, while the E_{corr} value is the lowest of all. This is due to the dissolution of the Al ions from the lattice into the solution and leads to thinning of the passive layer on the metal surface and ultimately increasing the corrosion rate in the base material (Sunitha et al., 2019). A potentiodynamic polarization test in an aerated 3.5% NaCl solution revealed that incorporating hybrid reinforcement particles into the base material (pure Al) caused the E_{corr} to move in the positive direction and the I_{corr} to decrease, as shown in Figure 4.11. The SiC and Al_2O_3 resist the severity of corrosion attack to some extent. The interface between aluminum and SiC can also influence the corrosion rate and weight loss. The SiC particles play a significant role as a physical barrier (Mahdi et al., 2021). Al_2O_3 is believed to form a stable inner oxide layer that acts as a shield to prevent corrosion (Kanayo Alaneme et al., 2013). Furthermore, unlike liquid metallurgy, there is no formation of undesirable intermetallic compounds such as Al_4C_3, (which initiates more corrosion sites) during the fabrication of HAMCs. Moreover, as shown in Table 4.7, the inhibition efficiency (IE%) of Al and HAMCs is in the order of AS4 >AS3 > AS5>AS2 >AS1 >Al. AS4 shows the highest inhibition efficiency of 99.691%. This is one of the advantages of powder metallurgy. These findings are also in line with XRD, Vickers hardness, compressive strength, and wear and friction measurements, as well as earlier studies (Suresh Kumar et al., 2022). With further addition in wt% of secondary reinforcement (Gr and SCBA) particles, the E_{corr} of the HAMCs (AS2, AS3, and AS4) have shifted in the noble direction, while the I_{corr} has decreased. According to Figure 4.9 and Table 4.7, AS4 has the highest potential and polarization resistance of all samples, which could be attributed to the uniform distribution of hybrid reinforcements, high hardness, and compressive strength of HAMC at the given proportion (Al /10 wt% (SiC +Al_2O_3)/4.5 wt% Gr/4.5 wt% SCBA). The mixed potential theory by Katkar et al. (2011) predicts that when the reinforcement content in the HAMC increases, the potential of the HAMC shifts in the noble direction. However, increasing the wt% of secondary reinforcements in the HAMCs causes the protective surface oxide layers to become more discontinuous, making the AS5 HAMC sample more sensitive to chloride ions and producing a less noble potential. This is because the incorporation of high content of the reinforcing phase may induce discontinuities in the protective film, thereby increasing the number of corrosion sites (Mahdi et al., 2021). In the case of hybrid composites, the slight increase in corrosion rate might be due to galvanic coupling in presence of Gr (M. Ravikumar et al., 2021). And corrosion rate increases as polarization curves are shifted to a high corrosion current.

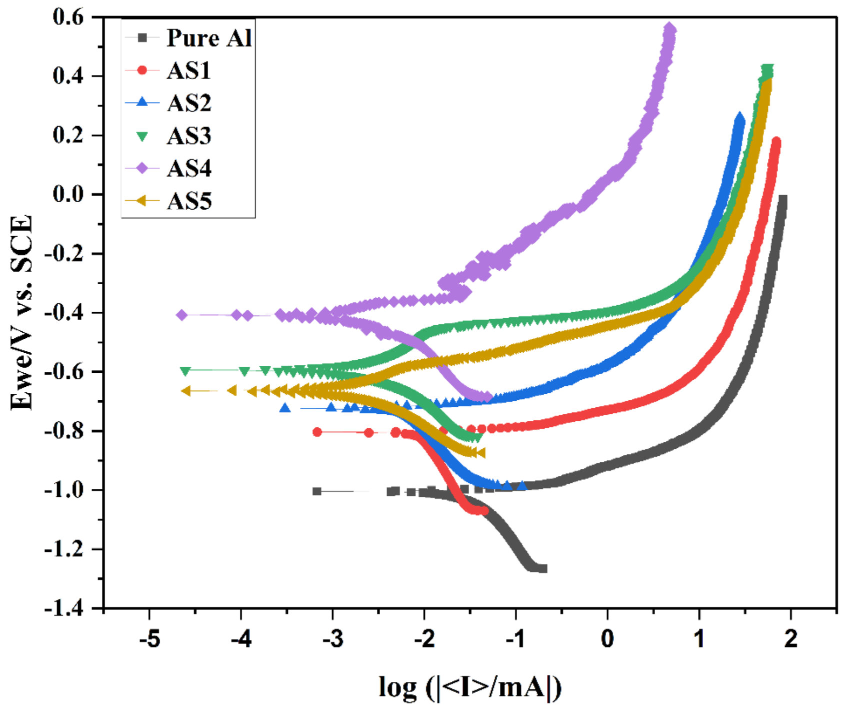

Figure 4.11 Polarization curves of base materials (pure Al) and HAMCs

Table 4.7 Corrosion extrapolation from Figure 4.8 of HAMC Specimens

Samples	E_{cor} (mV)	I_{corr} (μA/cm^2)	$β_c$ (mV)	$β_a$ (mV)	R_P (Ω)	C_R (mmpy)	(IE%)
Al	-1006.780	4.847	314.800	112.700	7.434	1.860	0.000
AS1	-804.075	1.792	294.420	107.000	19.015	0.268	63.029
AS2	-727.108	0.695	232.200	235.350	73.034	0.194	85.661
AS3	-590.153	0.216	223.400	283.500	251.414	0.090	95.544
AS4	-409.055	0.015	171.900	245.200	2977.541	0.023	99.691
AS5	-664.856	0.318	269.790	278.780	187.036	0.124	93.439

4.2.7.2. Electrochemical Impedance Spectroscopy Techniques

Figure 4.12 shows the Nyquist plots produced for Al and HAMC sample electrodes at their open-circuit potential after 1 hour of immersion in 3.5% NaCl solutions. The spectra represented in Figure 4.12 were analyzed by best fitting to the equivalent circuit model shown in Figure 4.13. Impedance spectra show HAMCs exhibit better resistance towards corrosion as the diameter of the semicircle is large for HAMCs followed by the base metal. Increasing the secondary reinforcement content in the HAMCs (from AS1 to AS4) in the 3.5% NaCl solution causes the Nyquist plot to have larger diametric semicircles and less corrosion current. The parameters of the equivalent circuit model shown in Figure 4.13 can be defined according to the usual convention as follows; R_S represents the solution resistance, Q_1 and Q_2 are the constant phase elements (CPEs), and R_{p1} and R_{p2} are the polarization resistances. It is seen from Figure 4.12 that both pure Al and HAMCs showed only one semicircle and the diameter is wider for HAMCs than it is for pure Al. This indicates that the resistance against corrosion for HAMCs is higher than for pure Al. As can be observed in Table 4.8, the R_S, $R_{p1,}$ and R_{p2} values for HAMCs are greater than those for pure Al due to the increased corrosion resistance of the HAMCs surface over the Al surface. The constant phase elements (Q, CPEs) with α values close to 1.0 for all samples represent double-layer capacitors with little porosities (Abbas shafqat et al., 2019; Alaneme et al., 2014; Han et al., 2015). This is because depending on the value of α, CPE can represent resistance (Z(CPE) = R, α = 0), capacitance (Z(CPE) = Cdl, α = 1) or Warburg impedance for (α = 0.5) (Sherif, 2014). Therefore, the CPE for Al and HAMCs is substituted for the capacitor to fit the semicircle more accurately. The admittance and the impedance of a CPE can be defined according to the following equations, respectively.

$$Y_{CPE} = Y_0(j\omega)^{\alpha} ------------------------ 4.4$$

$$Z_{CPE} = \left({}^{1}/_{Y_0}\right)(j\omega)^{-\alpha} ------------------------ 4.5$$

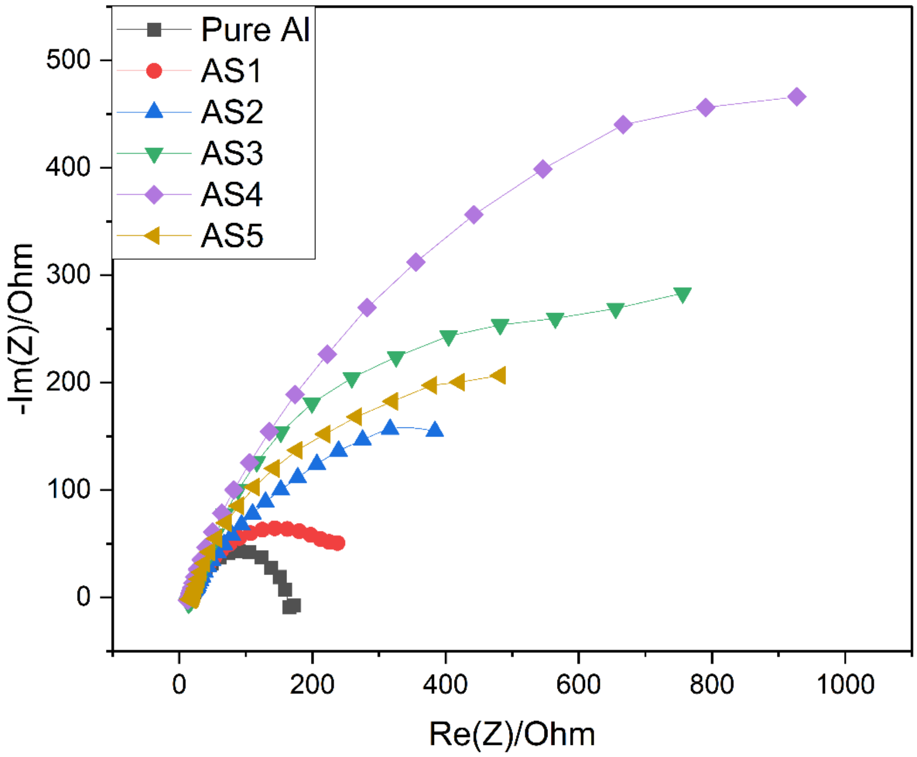

Figure 4.12 EIS Nyquist plots for pure Al and HAMCs after 1 hr. immersion in 3.5% NaCl solution

Where; Y_0 is the modulus, ω is the angular frequency, and α is the phase. As can be observed in Figure 4.13, increasing the hybrid reinforcement content, increased the size of the diameter of the semicircle of the HAMCs, and AS4 HAMC's curve has a wider diameter as compared to other HAMCs and Al. It is also seen from Figure 4.12 that the diameter of the semicircle plotted for all HAMCs was much wider than that drawn for Al. The parameters listed in Table 4.8 showed that the values of the resistances, R_S, R_{p1}, and R_{p2} obtained for HAMCs recorded higher values compared to the ones obtained for Al and their values with AS4 were highest compared to others under the same conditions. Furthermore, the CPEs with HAMCs were lower than those with Al, and additional reductions were achieved by increasing the wt% of secondary reinforcements up to a certain point, after which it increased again. Two main reasons are responsible for enhancing the anti-corrosion performance of HAMCs. Firstly, primary reinforcements of (SiC and Al_2O_3) into the Al matrix not only refine the grain, and make the HAMC smooth and uniform, but also act as a physical barrier layer and hinder the process of corrosion (M. Ravikumar et al., 2021). Secondly, the uniform dispersion of secondary reinforcement (Gr and SCBA) particles improves the strength of the HAMC and inhibits the matrix dissolution, significantly enhancing the HAMC corrosion resistance.

The EIS measurements thus confirm that the AS4 HAMC sample showed superior corrosion resistance and higher surface passivation compared to other HAMCs and Al. The EIS data are in good agreement with the results obtained by potentiodynamic polarization, measurements. All data confirmed that the base material (pure Al) is more susceptible to uniform and pitting corrosion compared to the hybrid reinforced HAMCs in 3.5% NaCl solutions and the increase in wt% of hybrid reinforcements, decreases the severity of the chloride ions against corrosion due to the oxide film and corrosion product thickening on the surface of the Al and HAMCs.

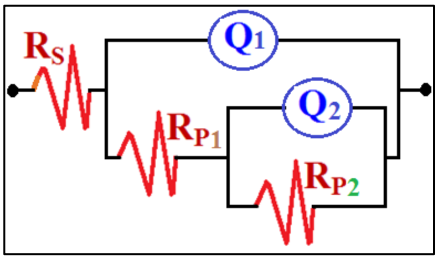

Figure 4.13 The equivalent circuit model used to fit the EIS experimental data (Sherif, 2014)

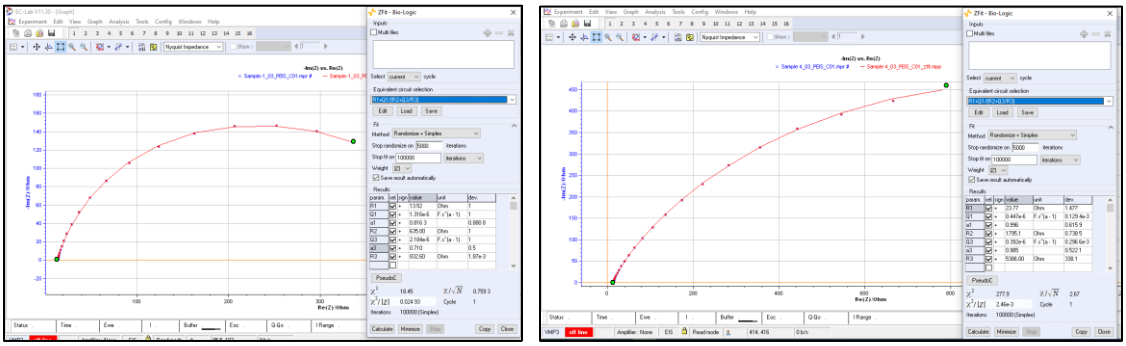

Figure 4.14 Z-fitting to the EIS Nyquist plot for AS1(left) and AS4(right) HAMCs

Symbols represent the measured data and the solid line represents the best fit using the equivalent circuit shown in Figure 4.13.

Table 4.8 EIS data combined with the equivalent circuit diagram in Figure 4.13

Sample	**R_s (Ω cm^2)**	**Q_1 (µF/cm^2)**	α_1	**R_{p1}(Ω cm^2)**	**Q_3 (µF/cm^2)**	α_3	**R_{p2} (Ω cm^2)**
Al	6.470	7.440	0.730	295.000	6.170	0.700	467.000
AS1	13.520	1.316	0.816	635.000	2.184	0.710	832.600
AS2	16.750	1.300	0.880	1102.000	1.690	0.720	1524.000
AS3	18.870	1.040	0.930	1223.000	1.340	0.800	2415.000

AS4	23.77	0.447	0.996	1795.1	0.392	0.985	5386.000
AS5	18.693	1.121	0.911	1198.540	3.815	0.784	2366.700

The potentiodynamic polarization and impedance studies of the corrosion behavior of Al and its HAMCs showed that the corrosion resistance of the HAMCs is greater than that of the base metal. Tafel curves show I_{corr} decreased with an increase in hybrid reinforcement content in the HAMCs up to a certain limit, above which it starts to increase, owing to the hard particle (SiC, Al_2O_3, and SCBA) that leads to the formation corrosion sites.

4.2.7.3. Morphological Characterization of after Corrosion HAMCs

Metallurgical optical microscopic study of corroded HAMCs samples

Typical optical micrographs of HAMCs with different wt% of secondary reinforcements (Gr and SCBA) after 1 hr. immersion at ambient temperature are shown in Figure 4.15. After corrosion testing, the Al surface shows delamination, and pitting corrosion is also shown with the addition of primary reinforcements, as shown in AS1, AS2 and AS3. In general, the HAMCs outperformed when compared to pure Al matrix in corrosion resistance. The corrosion resistance of HAMCs improved when the wt% of secondary reinforcement particles increased in the matrix. Among the tested HAMC samples, AS4 does not show either uniform or pitting corrosion, as can be seen in Figure 4.15. AS4 has higher corrosion resistance due to its high hardness and homogeneous distribution of hybrid reinforcements, which inhibits the formation of corrosion sites and hence minimizes pitting corrosion.

Al	Al	Al
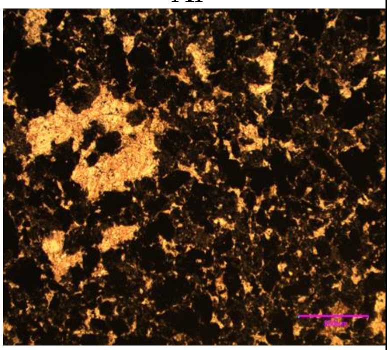	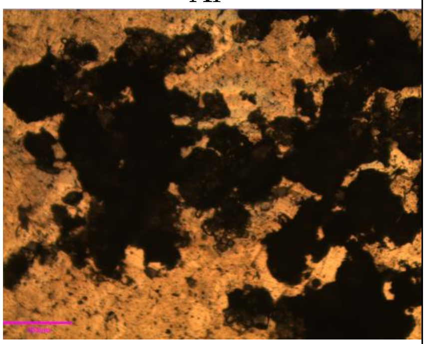	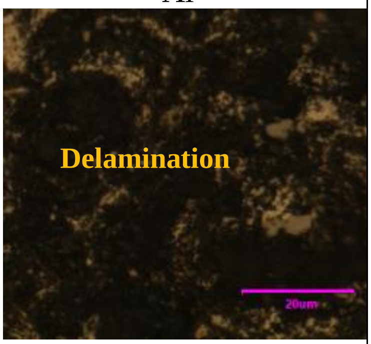
100 µm	50 µm	20 µm

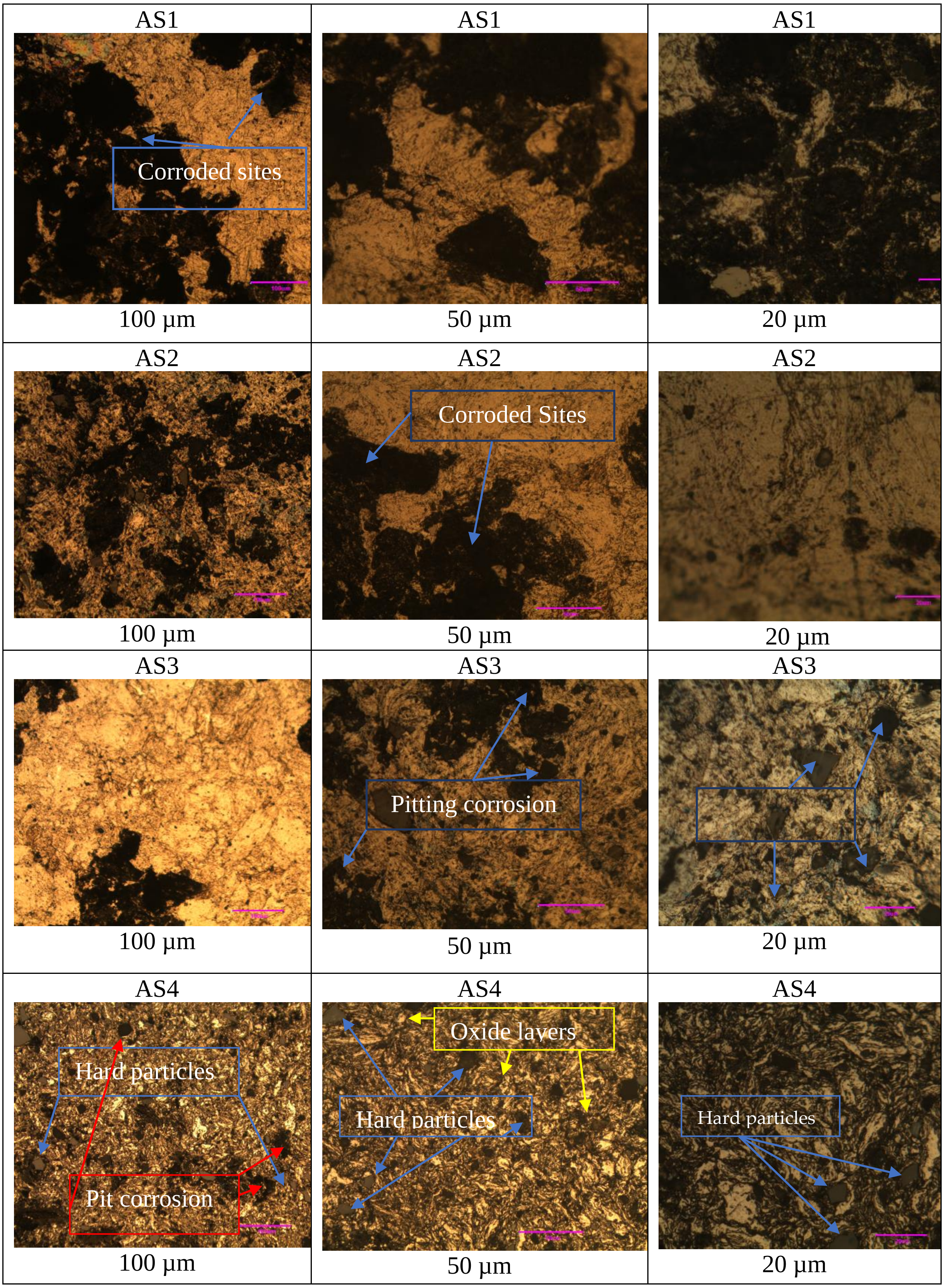
AS1
AS1
AS1
Corroded sites
100 µm
50 µm
20 µm
AS2
AS2
AS2
Corroded Sites
100 µm
50 µm
20 µm
AS3
AS3
AS3
Pitting corrosion
100 µm
50 µm
20 µm
AS4
AS4
AS4
Hard particles
Pit corrosion
Oxide layers
Hard particles
Hard particles
100 µm
50 µm
20 µm

AS5	AS5	AS5
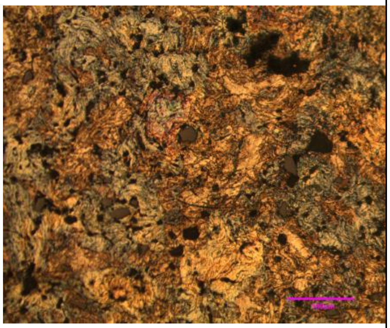	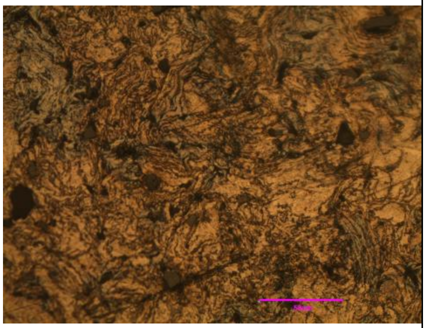	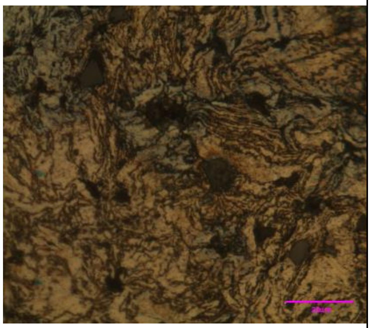
100 µm	50 µm	20 µm

Figure 4.15 OM micrograph of corroded HAMC samples

Scanning electron microscopic study of pre-and-post-corrosion HAMC samples

The SEM photographs of the surfaces of the AS1 and AS4 HAMCs before and after immersion in 3.5% NaCl solution are given in Figure 4.16 below.

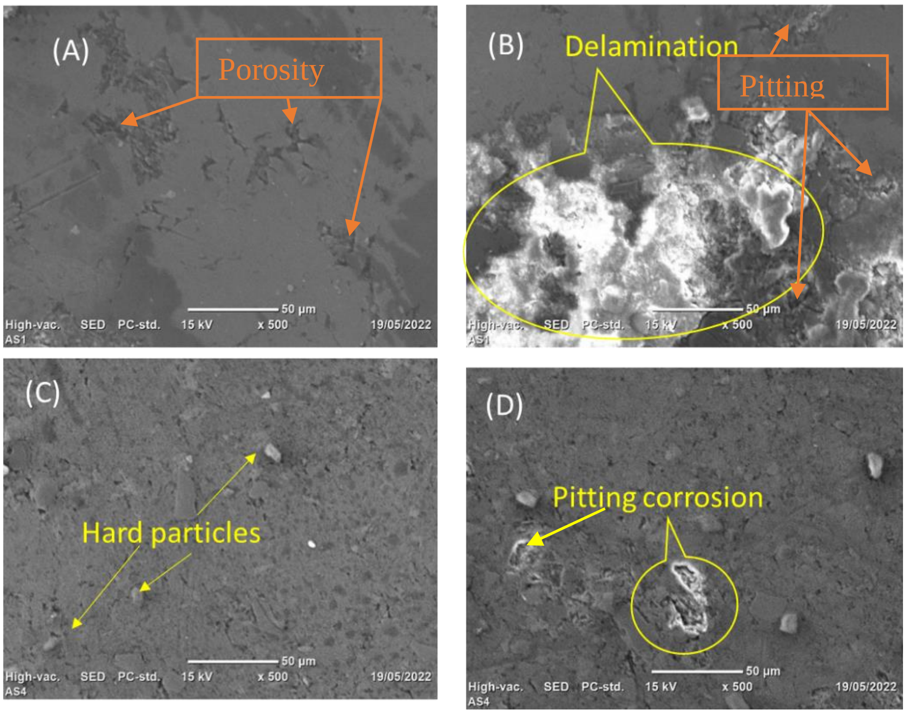

Figure 4.16 SEM micrograph of AS1 and AS4 HAMC samples

Figure 4.16 (A) and (B) depict SEM micrographs of the AS1 HAMC sample's uncorroded and corroded surfaces, respectively, showing metallurgically strong reinforcement bonding of Al_2O_3 and SiC with the matrix. It is porous like nature on the uncorroded surface, which agrees with the density and porosity findings (as discussed in section 4.2.5.1). Figures 4.16 (C) and (D) depict SEM micrographs of uncorroded and corroded surfaces with metallurgically strong reinforcement bonding of main reinforcements including Al_2O_3 and SiC, as well as secondary reinforcements comprising Gr and SCBA with the matrix. When comparing the un-corroded HAMC surfaces in Figures 4.16 (A) and (C), AS1 displayed a more porous appearance, whereas AS4 revealed hard particles, indicating the introduction of SCBA hard particulates. Unlike AS1, which has a porous nature, AS4 has hard particles on the uncorroded surface, indicating that hard particles (4.5 wt% SCBA) were added, resulting in decreased porosity and increased hardness, which coincides with the physicomechanical property findings (as discussed in sections from 4.2.5.1 to 4.2.5.3). The corroded HAMC micrographs confirm the fact that the material loss due to corrosion was lowered by the presence of secondary reinforcements in addition to SiC and Al_2O_3. This is due to the reduction in salt deposition owing to an increase in the wt% secondary reinforcement up to a certain limit, above which it may form agglomeration that makes undesirable corrosion sites (Alaneme et al., 2011; Bolboacă et al., 2007). As can be observed in Figures 4.16 (B) and (D), the surface of the AS4 HAMC sample has been less damaged compared with AS1. The addition of optimum wt% of secondary reinforcements particulates (4.5 wt% of Gr and 4.5 wt% of SCBA) into AS1(Al/ 5SiC /5Al_2O_3) HAMC resulted in lesser surface degradation (compare Figure 4.16 (B), and (D)). In addition, pitting corrosion was observed on the AS1 as well as on the AS4 HAMCs. The combined influence of tetra hybrid reinforcement produced at the time of HAMC fabrication decrease the susceptibility of Al/Al_2O_3/SiC/Gr/SCBA HAMCs to pitting by reducing the required driving force. The morphological analysis by SEM micrographs revealed the lesser damage for HAMCs than for the Al matrix.

Finally, it can be concluded that the tetra hybrid reinforcement particulates have enhanced the corrosion resistance of the HAMCs which can be utilized for future applications in various sectors.

4.3. Multi-Response Optimization of HAMCs using TGRA

4.3.1. XRD Characterization for Phase Identification

The XRD patterns of the HAMC powder samples were determined using Origin Pro and High Score Plus Software (Alam et al., 2021). The diffraction angle (2 theta) has been maintained between 10° and 80°. JCPDS was used to index the peaks of Al and tetra hybrid reinforcements. Figure 4.17 shows XRD results of milled Al/SiC/Al_2O_3/Gr/SCBA HAMC powder samples. The presence of major peaks indicates Al and the minor peaks represent the SiC, Al_2O_3, Gr, and SCBA particulates. Because the wt% of SiC, Al_2O_3, SiO_2, Gr, and SCBA is lower than that of Al when mechanically combined, the peaks of tetra hybrid reinforcements in HAMCs seem weaker. According to the XRD patterns, the tetra hybrid reinforcement particles are equally dispersed in the Al matrix (Ravindran, Manisekar, Vinoth Kumar, et al., 2013). The diffraction peaks of SiO_2 (JCPDS card number: 046-1045) and Fe_2O_3 (JCPDS card number: 046-1212) were found in samples S_1 and S_2 HAMCs in addition to Al, SiC, Al_2O_3, and Gr diffraction peaks (Venkatesh et al., 2021). It indicated that the presence of the SCBA, and similar results were reported by Jinfeng et al. (2009). Hence, the iron oxide and Gr commonly acted as solid lubrication to reduce the friction coefficient between the contact surfaces and the wear of the tribo-system (Seshappa et al., 2021; Singh, 2016). As shown in Figure 4.16, only aluminum with a cubic crystal structure with a = b = c = 4.0500 Å and $\propto = \beta = \gamma = 90°$ with the experimental density of 2.689 g/cm^3 can be detected in the HAMCs samples. Figure 4.17 (a) depicts the XRD graph of the HAMCs powders following milling before compaction and sintering were performed. The graph in S_1 shows that there is a dominancy of the Al matrix and other reinforcements are shown smaller, which ascribes that during the milling process there was no unwanted interfacial chemical reaction between the hybrid reinforcements and the matrix. Among the sixteen HAMC milled samples, S_2, S_4, S_6, S_7, S_9, S_{12}, and S_{16} exhibited various peaks corresponding to diverse phases such as Al, SiC, Gr, Al_2O_3, SiO_2, and Fe_2O_3, which attributed to the homogeneous distribution of the tetra hybrid reinforcement throughout the base material. Furthermore, the presence of SiO_2 and Fe_2O_3 in HAMCs is strongly linked to the presence of SiO_2, Al_2O_3, and Fe_2O_3 in SCBA (Ikubanni et al., 2021b; Suresha et al., 2012). The diffraction peaks with the maximum intensity at angles of 2θ = 38.475˚, 44.723˚, 65.101˚, and 78.234˚, corresponds to the (111), (200), (220), and (311) crystallographic planes, indicating the presence of Al, a major component of HAMCs (JCPDS card number: *085-1327*) (Ravindran, Manisekar, Vinoth Kumar, et al., 2013).

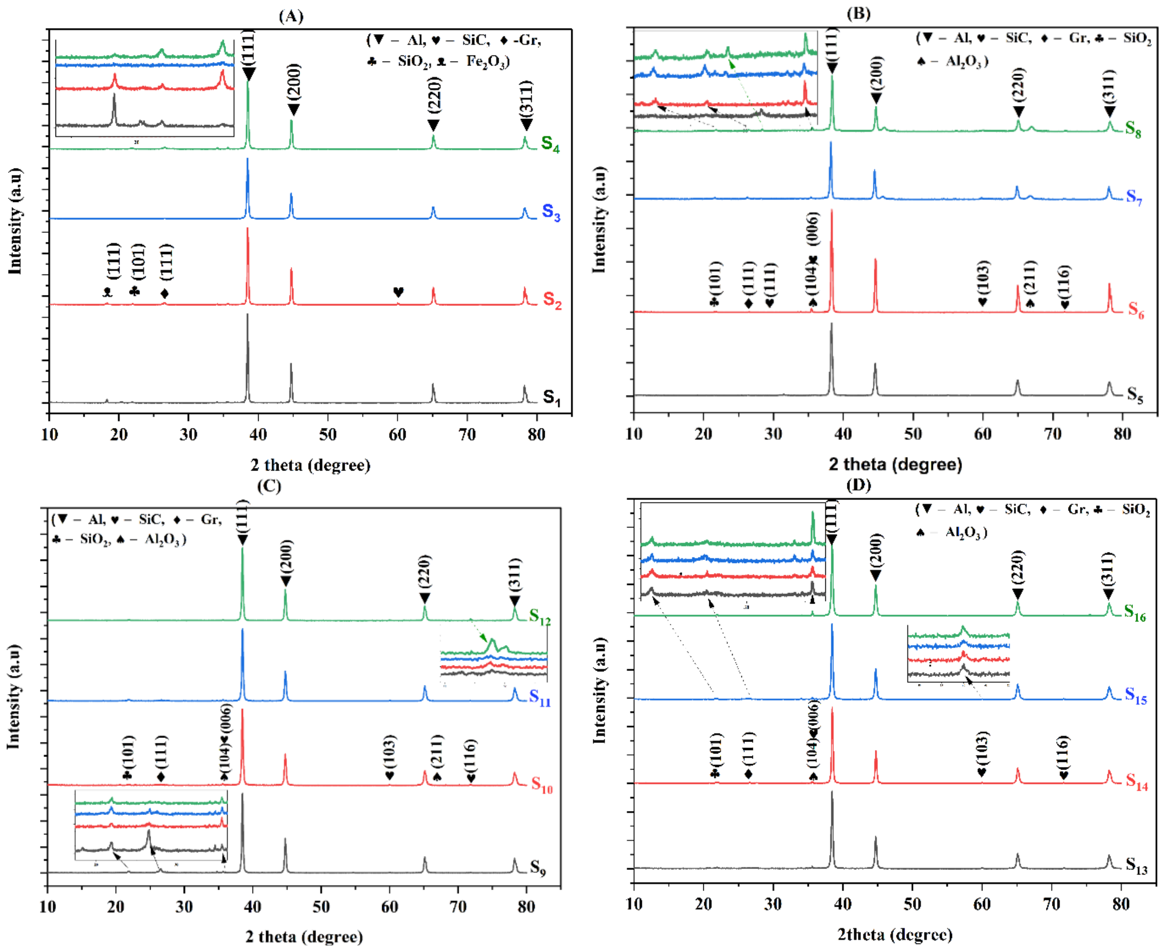

Figure 4.17 XRD results of as milled HAMC samples

The minor peak of Fe_2O_3 was shown at S_1 and S_2 at 2θ =18.062˚corresponding to the (111) crystallographic plane, but in other samples, this oxide is not further shown as it is dominated by the other oxides such as Al_2O_3 and SiO_2, which comes from SCBA. The minor peak of Gr was shown at angles 2θ =26.603˚corresponds to the (111), (JCPDS card number: 025-0284), and 21.895˚ corresponds to the (101) crystallographic plane of SiO_2 (JCPDS card number: 046-1045), The minor peaks at angles 2θ = 36.651˚, 60.034˚, and 71.772˚ correspond to the (006), (103), and (116) crystallographic planes, indicates the presence of SiC (JCPDS card number: 073-0603). The minor peaks Al_2O_3 were also shown at angles of 35.324˚, 45.790˚, and 66.763˚ (see S_7 and S_8) corresponding to (104), (111), and (211) crystallographic planes. The presence of more Al_2O_3 and SiO_2 ascribes to the presence of SCBA, which confirms that SCBA could be the promising material for the development of the tetra hybrid reinforced HAMC materials with Al as the matrix for the application of Aerospace and Automotive components.

4.3.2. Multi-Response Optimization of Process Parameters using GRA

4.3.2.1. Measured Responses Data

The following response data are measured for each of the HAMCs that were tested using the Taguchi method. Table 4.9 shows the responses of density and porosity, in which the quality characteristic feature must be minimized and the S/N ratio must be smaller to be better, whilst Table 4.10 shows the responses of Vickers hardness, compressive strength, and ultimate tensile strength, in which the quality characteristic feature must be maximized and, as a result, the S/N ratio of these responses must be larger to be better.

Table 4.9 Measured Responses data with smaller is the better-quality features

Exp. No.	ED-1	ED-2	ED-3	P-1	P-2	P-3
1.	2.5231	2.5531	2.5191	1.1649	1.1549	1.1745
2.	2.4956	2.5256	2.4916	1.3889	1.3789	1.3985
3.	2.3589	2.3889	2.3549	1.2033	1.1933	1.2129
4.	2.3172	2.3472	2.3132	3.0431	3.0331	3.0527
5.	2.2759	2.3059	2.2719	4.9367	4.9267	4.9463
6.	2.2782	2.3082	2.2742	3.8796	3.8696	3.8892
7.	2.4692	2.4992	2.4652	0.8731	0.8631	0.8827
8.	2.3281	2.3581	2.3241	2.0302	2.0202	2.0398
9.	2.2131	2.2431	2.2091	3.9312	3.9212	3.9408
10.	2.2828	2.3128	2.2788	3.4249	3.4149	3.4345
11.	2.2991	2.3291	2.2951	2.0272	2.0172	2.0368
12.	2.3033	2.3333	2.2993	0.9975	0.9875	1.0071
13.	2.3352	2.3652	2.3312	1.5437	1.5337	1.5533
14.	2.0546	2.0846	2.0506	4.2981	4.2881	4.3077
15.	2.0674	2.0974	2.0634	4.5079	4.4979	4.5175
16.	2.1996	2.2296	2.1956	2.2466	2.2366	2.2562

ED-1,2,3 Experimental density for three trials, P-1,2,3 porosity for three trials.

The ultimate tensile strength of HAMCs (as stated in section 3.3.8) could be estimated as follows; First, change the measured Vickers hardness number (HVN) into MPa using the following conversions (Annaz et al., 2020):

⇒ To convert HV to MPa, multiply it by 9.807

⇒ To convert HV to GPa, multiply it by 0.009807.

For instance; for S1 of first trial (HV-1);

HV-1 =155.900 HVN =155.900*9.807 = 1528.9113 MPa.

Table 4.10 Measured Responses data with Larger is the better-quality characteristic feature

Exp.No.	Vickers Hardness (HV) (MPa)			Compressive Strength (CS) (MPa)			Ultimate Tensile Strength (UTS) (MPa)		
	HV-1	HV-2	HV-3	CS-1	CS-2	CS-3	UTS-1	UTS-2	UTS-3
1.	1528.9113	1449.4746	1532.8341	311.0304	293.6851	301.2101	548.2992	519.8116	549.7060

2.	2175.6830	2216.8724	2260.0232	312.3364	294.9911	302.5161	780.2449	795.0163	810.4911
3.	2950.9263	3164.2286	3035.7569	262.3771	245.0318	252.5568	1058.2632	1134.7578	1088.6852
4.	1364.6441	1459.2816	1376.9028	272.9962	255.6509	263.1759	489.3896	523.3286	493.7858
5.	1838.3222	1872.1563	1967.7746	225.9245	208.5792	216.1042	659.2604	671.3940	705.6847
6.	1720.6382	1758.8855	1819.1985	345.5287	328.1834	335.7084	617.0564	630.7727	652.4022
7.	1995.7245	1841.7546	1850.0906	331.8357	314.4904	322.0154	715.7081	660.4913	663.4807
8.	1301.8793	1338.6555	1626.9813	324.1664	306.8211	314.3461	466.8808	480.0696	583.4692
9.	1709.8505	1726.5224	1827.0441	181.7716	164.4263	171.9513	613.1877	619.1666	655.2158
10.	1980.0333	2037.8946	1928.0562	225.2415	207.8962	215.4212	710.0809	730.8312	691.4408
11.	2732.7206	2820.0029	2818.0415	349.7826	332.4373	339.9623	980.0101	1011.3114	1010.6080
12.	2841.0879	2886.2001	2867.5668	311.1254	293.7801	301.3051	1018.8729	1035.0511	1028.3688
13.	1523.5175	1660.8155	1593.1472	327.2714	309.9261	317.4511	546.3649	595.6028	571.3355
14.	1804.4880	1863.8204	1818.2178	334.4439	317.0986	324.6236	647.1267	668.4045	652.0505
15.	2786.6591	2747.4311	2777.8328	327.3257	309.9804	317.5054	999.3536	985.2856	996.1883
16.	2395.8501	2369.8616	2308.0775	321.0304	303.6851	311.2101	859.2014	849.8814	827.7243

HV-1,2,3 Vickers hardness (MPa) for three trials, CS-1,2,3 compressive strength (MPa) for three trials, UTS-1,2,3 ultimate tensile strength (MPa) for three trials.

4.3.2.2. Multi-Response Optimization of Steps in GRA

In this analysis, the optimization of multiple performance characteristics can be converted into the optimization of a single grey relational grade (Haq et al., 2008). The following steps are considered for grey relational analysis.

Step 1: Using the relevant equations for the kind of quality characteristic feature, convert the original response data into S/N ratio (η). For each response, there are three replications. The data must now be translated into a S/N ratio. Because Vickers hardness (HV), compressive strength (CS), and Ultimate tensile strength (UTS) must all be maximized, the type of quality characteristic utilized is larger—the better. As a result, the S/N ratio for the larger—the better-quality characteristic feature is calculated using equation 4.6 given below:

$$\boldsymbol{S/N\,ratio(\eta) = -10\log\left[\frac{1}{n}\sum_{i=1}^{n}\frac{1}{y_i^2}\right]} \quad ------------------- \quad (\mathbf{4.6})$$

Where; n is the number of repetitions of the experiment, y_i is the observed response value

For instance, the first trial for HV is as follows;

$$S/N\,for\,HV = -10\log\frac{1}{3}\left[\frac{1}{(1528.9113)^2}+\frac{1}{(1449.4746)^2}+\frac{1}{(1532.8341)^2}\right] = 63.5347$$

The second performance measure (response) is smaller – the better type utilized for experimental density (ED) and porosity (P) and its S/N ratio is computed using equation 4.7, as follows:

$$S/N\,ratio(\eta) = -10\log\left[\frac{1}{n}\sum_{i=1}^{3} y_i^2\right] -----------------------(4.7)$$

For instance, the first trial for ED is as follows;

$$S/N\,ratio(\eta) for\ ED(1) = -10\log\frac{1}{3}[2.5231^2 + 2.5531^2 + 2.5191^2] = -8.0687$$

Similarly, the following S/N ratio for observed responses is calculated using the appropriate equations 4.6 and 4.7, you can normalize the S/N values in Table 4.11.

Table 4.11 The S/N ratio (η) for the measured responses

S/N ratio (η) for each response values					
Exp. No.	The smaller is the better		The larger is the better		
	ED	AP	HV	CS	UTS
1.	-8.0687	-1.3248	63.5347	49.5923	54.6275
2.	-7.9738	-2.8530	66.9142	49.6298	58.0069
3.	-7.4862	-1.6067	69.6762	48.0633	60.7689
4.	-7.3320	-9.6660	62.9128	48.4208	54.0055
5.	-7.1763	-13.8685	65.5311	46.7101	56.6239
6.	-7.1849	-11.7755	64.9342	50.5332	56.0269
7.	-7.8817	1.1794	65.5386	50.1719	56.6313
8.	-7.3726	-6.1504	62.9362	49.9627	54.0289
9.	-6.9343	-11.8903	64.8719	44.7248	55.9646
10.	-7.2026	-10.6927	65.9354	46.6826	57.0281
11.	-7.2641	-6.1374	68.9101	50.6425	60.0028
12.	-7.2800	0.0223	69.1418	49.5950	60.2345
13.	-7.3988	-3.7707	64.0254	50.0480	55.1181
14.	-6.2913	-12.6653	65.2410	50.2419	56.3338
15.	-6.3449	-13.0793	68.8511	50.0495	59.9438
16.	-6.8814	-7.0300	67.4474	49.8757	58.5401
Min	**-8.0687**	**-13.8685**	**62.9128**	**44.7248**	**54.0055**
Max	**-6.2913**	**1.1794**	**69.6762**	**50.6425**	**60.7689**

***Step* 2:** Normalize η_{ij} as Z_{ij} ($0 \leq Z_{ij} \leq 1$) by equations 4.8 and 4.9 to avoid the effect of using different units and to reduce variability. Normalization is a transformation performed on a single input to distribute the data evenly and scale it into an acceptable range for further analysis. The S/N ratios obtained by Taguchi's method are normalized in the range of 0 and 1, and this procedure is known as grey relational generating(Jailani et al., 2009). The calculation technique "higher the better" was used because maximizing the Vickers microhardness, compressive strength, and ultimate tensile strength of the HAMCs was intended, while for density and porosity "lower the better" was used because minimization of the density and porosity of the HAMCs was intended.

For the S/N ratio with Larger the better manner, normalization of S/N ratio is performed using equation 4.8.

$$Z_{ij} = \frac{(\eta_{ij}) - \min(\eta_{ij})}{\max(\eta_{ij}) - \min(\eta_{ij})} \quad \text{------------------------} 4.8$$

While for the S/N ratio with smaller the better manner, normalization is performed using equation 4.9 given below.

$$Z_{ij} = \frac{\max(\eta_{ij}) - (\eta_{ij})}{\max(\eta_{ij}) - \min(\eta_{ij})} \quad \text{------------------------} 4.9$$

where, Z_{ij} = Normalized value for i_{th} experiment for j_{th} dependent variable/response, η_{ij} are the S/N ratio value to be normalized, and max (η_{ij}) and min(η_{ij}) are the maximum and minimum values of η_{ij}, respectively. Larger normalized results correspond to better performance, according to Deng, and the best-normalized result should equal one (Julong, 1989). The grey relational coefficients are then computed to represent the link between the ideal (best) and actual experimental findings. For instance, the normalized S/N ratio (Z_{ij}) with larger the better-quality feature of the first trial for HV is as follows;

$$Z_{11}(HV) = \frac{63.5347 - 62.9128}{69.6762 - 62.9128} = \frac{0.6219}{6.7633} = 0.0920$$

The normalized S/N ratio (Z_{ij}) with smaller the better-quality feature of the first trial for ED is as follows;

$$Z_{11}(ED) = \frac{-6.2913 - (-8.0687)}{-6.2913 - (-8.0687)} = \frac{1.7774}{1.7774} = 1.0000$$

For the second experimental trial ED, it will be;

$$Z_{21}(ED) = \frac{-6.2913 - (-7.9738)}{-6.2913 - (-8.0687)} = \frac{1.6825}{1.7774} = 0.9466$$

Similarly, Table 4.12 displays the normalized S/N ratio values obtained from the S/N ratio in Table 4.11 using the above-mentioned equations 4.8 and 4.9.

Table 4.12 Normalized S/N ratios (η) of the measured responses

Exp. No.	Normalized S/N ratios (η) for smaller is the better		Normalized S/N ratios (η) for larger is the better		
	ED	**AP**	**HV**	**CS**	**UTS**
1.	1.0000	0.1664	0.0920	0.8225	0.0920
2.	0.9466	0.2680	0.5916	0.8289	0.5916
3.	0.6723	0.1851	1.0000	0.5641	1.0000
4.	0.5855	0.7207	0.0000	0.6246	0.0000
5.	0.4979	1.0000	0.3871	0.3355	0.3871
6.	0.5027	0.8609	0.2989	0.9815	0.2989
7.	0.8948	0.0000	0.3882	0.9205	0.3882
8.	0.6084	0.4871	0.0035	0.8851	0.0035
9.	0.3618	0.8685	0.2897	0.0000	0.2897
10.	0.5127	0.7890	0.4469	0.3308	0.4469
11.	0.5473	0.4862	0.8867	1.0000	0.8867
12.	0.5562	0.0769	0.9210	0.8230	0.9210
13.	0.6231	0.3290	0.1645	0.8995	0.1645
14.	0.0000	0.9200	0.3442	0.9323	0.3442
15.	0.0302	0.9476	0.8780	0.8998	0.8780
16.	0.3320	0.5456	0.6705	0.8704	0.6705
Min	**0.0000**	**0.0000**	**0.0000**	**0.0000**	**0.0000**
Max	**1.0000**	**1.0000**	**1.0000**	**1.0000**	**1.0000**

Step 3: Calculation of the deviation sequences(Δ_{ij}) in both quality features is similar, and the equation is as follows; Δ = absolute difference between Z_{ij}^0 and Z_{ij} which is a deviation from the target value and can be treated as a quality loss.

$$\boldsymbol{\Delta_{ij} = \left\| Z_{ij}^{0} - Z_{ij} \right\| ----------------------------- 4.10}$$

Where Δ_{ij} is the deviation sequence, and Z_{ij}^0 is usually equal to one ($Z_{ij}^0 = 1$).

For instance, Δ_{ij} of the given normalized data can be calculated as follows;

$$\Delta_{11} = \|1.0000 - 1.000\| = 0.0000$$

$$\Delta_{21} = \|1.0000 - 0.9466\| = 0.0534$$

Table 4.13 Deviation sequence with the respect to the normalized S/N ratios (η)

Exp. No.	Deviation Sequence (Δ_{ij} has the same formula for all)				
	ED	AP	HV	CS	UTS
1.	0.0000	0.8336	0.9080	0.1775	0.9080
2.	0.0534	0.7320	0.4084	0.1711	0.4084
3.	0.3277	0.8149	0.0000	0.4359	0.0000
4.	0.4145	0.2793	1.0000	0.3754	1.0000
5.	0.5021	0.0000	0.6129	0.6645	0.6129
6.	0.4973	0.1391	0.7011	0.0185	0.7011
7.	0.1052	1.0000	0.6118	0.0795	0.6118
8.	0.3916	0.5129	0.9965	0.1149	0.9965
9.	0.6382	0.1315	0.7103	1.0000	0.7103
10.	0.4873	0.2110	0.5531	0.6692	0.5531
11.	0.4527	0.5138	0.1133	0.0000	0.1133

12.	0.4438	0.9231	0.0790	0.1770	0.0790
13.	0.3769	0.6710	0.8355	0.1005	0.8355
14.	1.0000	0.0800	0.6558	0.0677	0.6558
15.	0.9698	0.0524	0.1220	0.1002	0.1220
16.	0.6680	0.4544	0.3295	0.1296	0.3295
Δ_{min}	**0.0000**	**0.0000**	**0.0000**	**0.0000**	**0.0000**
Δ_{max}	**1.0000**	**1.0000**	**1.0000**	**1.0000**	**1.0000**

Step 4: Calculation of the Grey relational coefficients (GRCs): Calculation of the grey relational co-efficient for the normalized S/N ratio values is based on the following equation

$$GRC_{ij} = \frac{\Delta_{min} + \lambda\Delta_{max}}{\Delta_{ij} + \lambda\Delta_{max}} \begin{cases} i = 1, 2, 3, \ldots, 16 \quad experiments \\ j = 1, 2, 3, 4, \text{ and } 5 \quad responses \end{cases} --------- 4.11$$

λ is the distinguishing coefficient, which is defined in the range 0 ≤λ ≤1 (the value may be changed depending on the system's actual needs). λ is also called the coefficient of identification, ranging between 0 and 1. According to (Acır et al., 2017; Agboola, 2021; Naqiuddin et al., 2018), λ =0.5 is commonly chosen for λ since using 0 or 1 does not affect the ranking order of the parameters.

For instance, GRC_{ij} of the first and second experimental trials of ED can be calculated as follows;

$$GRC_{11} = \frac{0.0000 + 0.5 \times 1.0000}{0.0000 + 0.5 \times 1.0000} = 1.0000$$

$$GRC_{21} = \frac{0.0000 + 0.5 \times 1.0000}{0.0534 + 0.5 \times 1.0000} = 0.9035$$

Similarly, Table 4.14 displays the GRC values obtained using equation 4.12 and in Table 4.13.

Step 5: Compute the grey relational grade (GRG_i): After calculating the GRC_{ij}, the GRG_i can be obtained as follows;

$$GRG_i = \frac{1}{m}\sum GRC_{ij} -------------------------- 4.12$$

where m is the number of responses (or the number of performance characteristics), and is equal to 5 since there are five responses, (namely; ED, P, HV, CS, and UTS).

For instance, GRG_i of the first and second (i.e., i =1,2) experimental trials of the five responses can be calculated as follows;

$$GRG_i = \frac{1}{m}\sum GRC_{ij} = \frac{1}{5}(1.0000 + 0.3749 + 0.3551 + 0.7380 + 0.3551) = 0.5646$$

$$GRG_i = \frac{1}{m}\sum GRC_{ij} = \frac{1}{5}(0.9035 + 0.4058 + 0.5504 + 0.7450 + 0.5504) = 0.6310$$

Similarly, for all the trials, the grey grade values are computed and are given in Table 4.8

Table 4.14 Grey relational coefficients (GRCs) and grey relational grades (GRGs)

Exp. No.	Grey Relational Coefficients (GRCs)					Grey Relational Grades (GRGs)	Rank
	ED	AP	HV	CS	UTS		
1.	1.0000	0.3749	0.3551	0.7380	0.3551	0.5646	11
2.	0.9035	0.4058	0.5504	0.7450	0.5504	0.6310	5
3.	0.6041	0.3803	1.0000	0.5343	1.0000	0.7037	3
4.	0.5468	0.6416	0.3333	0.5711	0.3333	0.4852	15
5.	0.4990	1.0000	0.4493	0.4294	0.4493	0.5654	10
6.	0.5014	0.7824	0.4163	0.9644	0.4163	0.6161	6
7.	0.8262	0.3333	0.4497	0.8628	0.4497	0.5843	9
8.	0.5608	0.4936	0.3341	0.8132	0.3341	0.5072	14
9.	0.4393	0.7918	0.4131	0.3333	0.4131	0.4781	16
10.	0.5064	0.7032	0.4748	0.4277	0.4748	0.5174	12
11.	0.5248	0.4932	0.8153	1.0000	0.8153	0.7297	2
12.	0.5298	0.3513	0.8635	0.7385	0.8635	0.6694	4
13.	0.5702	0.4270	0.3744	0.8327	0.3744	0.5157	13
14.	0.3333	0.8621	0.4326	0.8807	0.4326	0.5883	8
15.	0.3402	0.9051	0.8039	0.8330	0.8039	0.7372	1
16.	0.4281	0.5239	0.6027	0.7942	0.6027	0.5903	7

Step 5: Determine the optimal factor and its level combination. The higher grey relational grade implies a better product quality; therefore, based on the grey relational grade, the factor effect can be estimated and the optimal level for each controllable factor can also be determined (Haq et al., 2008). This can be done using two ways; (1) using Minitab software, it is possible to find out the optimal parameter settings, or (2) it can be computed by averaging the GRG values manually. The following is the process for determining the average grey relational grade (Jailani et al., 2009):

1. Grouping of the grey relational grades by factor level for each column in the orthogonal array
2. Taking the average of grey relational grades
3. Calculation of grade values for each experiment of the L_{16} orthogonal arrays

For example, consider the following exemplary calculations of the factor MT for levels 1 and 2 from Table 4.8;

$$MT_1 = \frac{1}{4}(0.5646 + 0.6310 + 0.7037 + 0.4852) = 0.5962$$

$$MT_2 = \frac{1}{4}(0.5654 + 0.6161 + 0.5843 + 0.5072) = 0.5683$$

To determine the effect of factor i, for example, we calculate the average of grade values (AGV) for each level j, represented as AGV_{ij}, and then the effect, E_i, is defined as:

$$E_i = \max(AGV_{ij}) - \min(AGV_{ij}) ---------------------- 4.13$$

If the factor i is controllable, the best level j* is determined by

$$j^* = \max(AGV_{ij}) ------------------------------ 4.14$$

Table 4.15 Response table of the average grey relational grade

Control Factors	Average grey relational grade by factor levels				Max-Min (E_i)	Rank
	1	2	3	4		
MT	0.5962	0.5683	0.5986	**0.6079**	0.0396	4
CP	0.5310	0.5882	**0.6887**	0.5630	0.1578	1
ST	0.6252	**0.6507**	0.5693	0.5257	0.1251	2
Gr	**0.6017**	0.5959	0.5942	0.5792	0.0225	5
SCBA	0.5816	0.5710	**0.6262**	0.5922	0.0553	3

Where MT is Milling time (hrs.), CP is compaction pressure (MPa), ST is sintering temperature (°C), Gr is graphite content (wt%), and SCBA is sugar cane bagasse ash content (wt%), and bolded results show optimal parameters setting values.

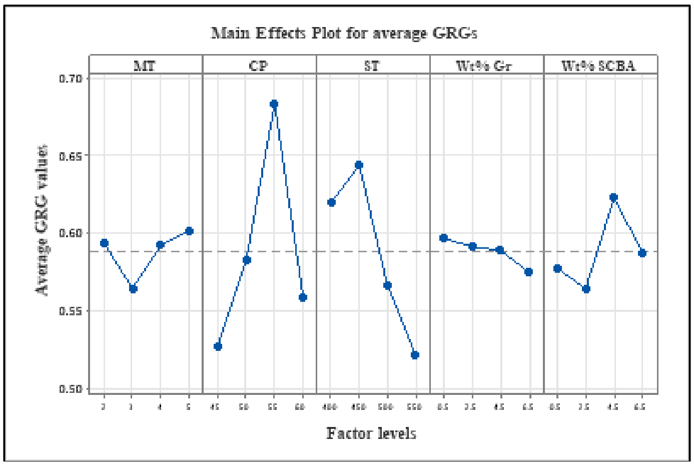

Figure 4.18 Response graphs for GRG showing the influence of processing parameters and reinforcement wt% on physicomechanical characteristics of HAMCs

Figure 4.18 shows a graph of the main effects of the influence of the various testing parameters on both the physical and mechanical properties of the HAMCs. In the main effect plot, if the line for a particular parameter is near horizontal, then the parameter has no significant effect. In contrast, a parameter for which the line has the highest inclination has the most significant effect. It was clear from the main effect plot that parameter CP (compaction pressure) was the most significant parameter, while parameters ST, SCBA, MT, and MT had relatively less influence. The increase in the compaction pressure caused less porosity and resulted in improved material behavior, which in turn led to the improved tribological and corrosion performance of the HAMC materials (Ravindran, Manisekar, Narayanasamy, et al., 2013).

As shown in Table 4.16, the values of the optimum parameters setting are milling time, (5 hrs.), compaction pressure, (55 MPa), sintering temperature, (450 °C), Gr content, (0.5 wt%), and SCBA content, (4.5 wt%). The difference between the maximum and the minimum value (Max-Min) of the grey relational grade is also indicated in Table 4.15. The maximum Max-Min value indicates that it is the most effective factor affecting the multi-performance characteristics (Jailani et al., 2009). The maximum of the Max-Min value in Table 4.15 is 0.1578, and the corresponding control factor, i.e., the compacting pressure, has the strongest effect on multi-performance characteristics. As shown in the rank given in Table 4.15, the order of importance of the controllable factors to the multi-performance characteristics in the overall HAMC fabrication process, in sequence, can be listed as: factor CP > ST > SCBA > MT > Gr, i.e., 0.1578 > 0.1251> 0.0553 > 0.0396 > 0.0225. Compaction pressure and sintering temperature are the most controllable factors in the creation of powder metallurgical HAMC for multiperformance features, and it is strongly correlated with previous studies (Kumar et al., 2021).

Table 4.16 Optimal parameter setting of HAMCs development

MT	CP	ST	Gr	SCBA
5 hrs.	55 MPa	450 °C	0.5 wt%	4.5 wt%

Table 4.16 indicates the optimum parameters (factors) which have been obtained from Table 4.15 for the confirmation test.

Step 6: Confirmation experiments

The confirmation test was carried out using the optimal parameter settings to check experimental density, porosity, in which the quality feature needed to be lower is the better, and Vickers hardness, compressive strength, and ultimate tensile strength, in which their quality features needed to be higher is the better. Based on their respective quality features, the following results have been recorded;

Table 4.17 Confirmation testing results

Sample	Avg. ED (g/cm^3)	Avg. P (%)	Avg. HV(MPa)	Avg. CS (MPa)	Avg. UTS (MPa)
OS	2.5118	0.8653	4228.45	343.33	1516.41

Where; Avg. ED is the average experimental density for three trials, Avg. P is average porosity (%) for three trials, Avg. HV Average Vickers hardness (MPa) for three trials, Avg. CS is the Average compressive strength of three trials, and Avg. UTS is the average ultimate tensile strength of three HV trials.

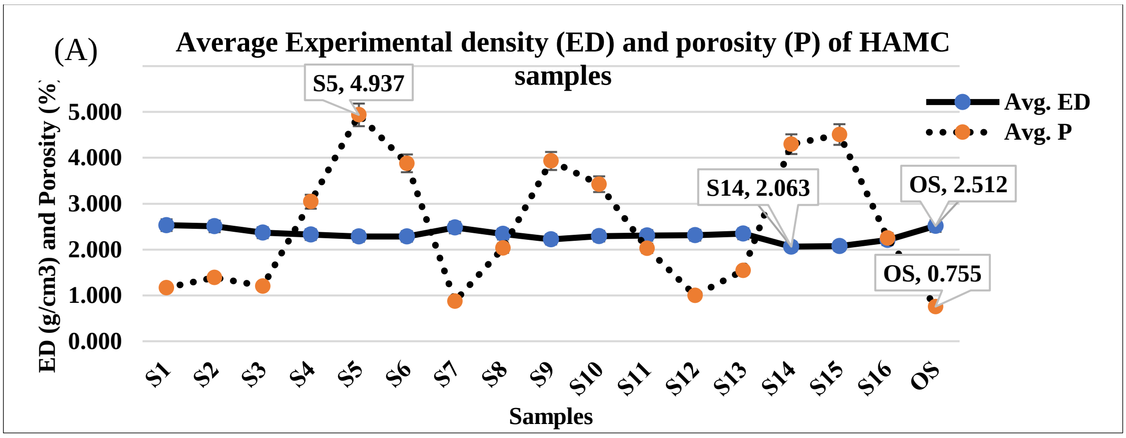

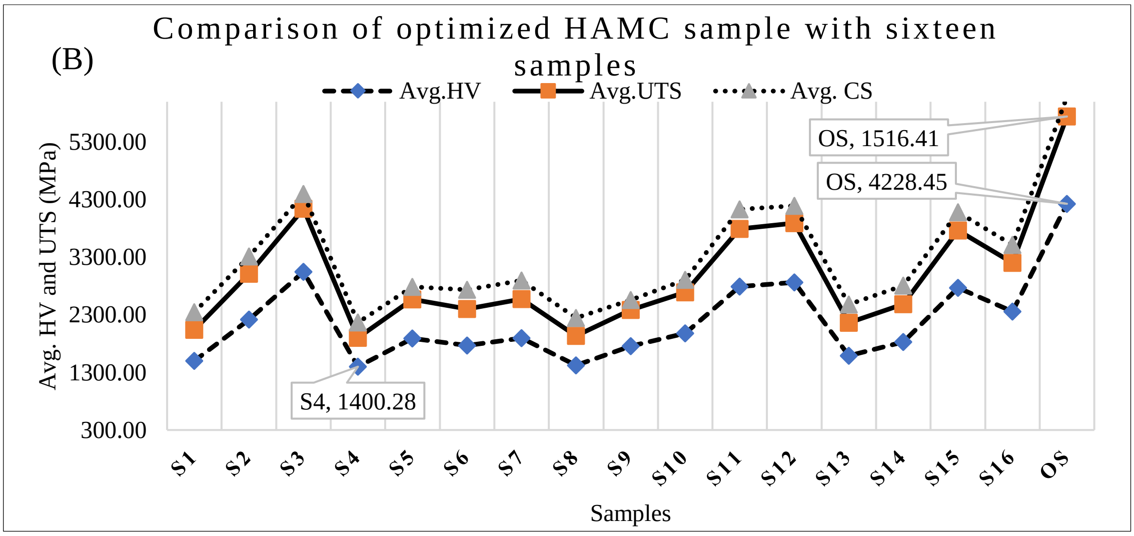

Figure 4.19 Comparison of OS and the L16 HAMC samples (A) for lower is better and (B) for higher is a better-quality feature in the multi-response optimization via GRA

As shown in Table 3.17 and Figure 4.19, the OS HAMC sample produced at optimum parameters outperforms the 16 HAMC samples in terms of property outcomes.

Based on the confirmation findings, it can be concluded that TGRA is a highly useful approach for doing multi-output optimization to anticipate physicomechanical characteristics for various applications in automotive and aerospace components.

5. CONCLUSIONS AND RECOMMENDATIONS

In the present study, a powder metallurgically synthesized tetra hybrid reinforced HAMCs has been studied. The main findings of this study can be summarized as follows:

⇒ The major peaks in the XRD findings are Al, while the hybrid reinforcements appear as minor peaks, indicating that HAMCs were effectively synthesized by the PM technique. The TGA-DTA results revealed that HAMCs have more thermal stability and a wider range of phase change temperatures than the base material (Al). The BET results revealed that the AS4 HAMC had smaller surface area and micropores than the AS1 HAMC. Decreased micropore sizes resulted in a lower surface area.

⇒ The density and porosity of the tetra hybrid reinforced HAMCs decreased slightly as the wt% of secondary reinforcements increased, but the hardness and compression strength of the HAMCs increased up to 9 wt% of secondary reinforcements (Gr and SCBA) and then reversed with further increases above 9 wt%. The Vickers hardness and compressive strength of AS4 were enhanced by 5.464 and 3.100 times, respectively, over the basis material (Al).

⇒ The wear loss and friction as well as corrosion resistance of the HAMCs increases with increasing of wt% of Gr and SCBA up to certain limit, after which it begins to decrease. The wear loss and COF increase linearly with the increase in normal load and sliding distance, with AS4 having the lowest wear loss of 60.27% of improvement. However, the HAMCs have a lower wear loss as compared to that observed in the Al-matrix, under dry sliding conditions. The corrosion inhibition efficacy (IE%) of the AS4 HAMC sample was enhanced by 99.691%.

⇒ According to the confirmation test results, the optimal HAMC sample outperforms all 16 experimental tests in all physicomechanical properties, indicating that the TGRA method is a promising technique for developing hybrid reinforced HAMCs via PM processing.

⇒ Compared to pure Al and double reinforced AMCs, the newly synthesized tetra hybrid reinforced HAMCs demonstrated superior physicomechanical, tribological, and corrosion properties. As a result, the tetra hybrid reinforced HAMC material could have potential applications in automotive, aerospace, defense, and a variety of other structural applications.

⇒ To reduce raw material costs, improve properties, and keep the environment clean, it is recommended to use various solid waste materials (Rice husk ash, filter cake, corn cob ash, and others) and solid lubricants (MoS_2, Gr) as secondary reinforcements in HAMCs with various matrix materials. Secondary processes such as forging and extrusion are also recommended in HAMC synthesis to reduce porosity and increase tailorability.

6. REFERENCES

Abbas shafqat, Q., et al. (2019). Mechanical, tribological, and electrochemical behavior of hybrid aluminum matrix composite containing boron carbide (B4C) and graphene nanoplatelets. *Journal of Materials Research*, *34*(18), 3116-3129. https://doi.org/10.1557/jmr.2019.242

Acır, A., et al. (2017). Parametric optimization of energy and exergy analyses of a novel solar air heater with grey relational analysis. *Applied Thermal Engineering*, *122*, 330-338.

Agboola, O. O. (2021). Optimization of the tribological properties of hybrid reinforced aluminium matrix composites using Taguchi and Grey's relational analysis. *Scientific African*, *12*, e00839.

Ahamad, N., et al. (2020). Wear characteristics of Al matrix reinforced with Al2O3-carbon hybrid metal matrix composites. *Materials Today: Proceedings*, *38*. https://doi.org/10.1016/j.matpr.2020.05.739

Akbar, H., et al. (2020). Investigation of Industrial and Agro Wastes for Aluminum Matrix Composite Reinforcement. *Procedia Structural Integrity*, *27*, 30-37. https://doi.org/10.1016/j.prostr.2020.07.005

Aktar Zahid Sohag, M., et al. (2020). Effect of ceramic reinforcement on the microstructural, mechanical and tribological behavior of Al-Cu alloy metal matrix composite. *Materials Today: Proceedings*, *21*, 1407-1411. https://doi.org/https://doi.org/10.1016/j.matpr.2019.08.179

Alam, M. A., et al. (2021). Modeling, Optimization and Performance Evaluation of TiC/Graphite Reinforced Al 7075 Hybrid Composites Using Response Surface Methodology. *Materials*, *14*(16). https://doi.org/10.3390/ma14164703

Alaneme, K. K., et al. (2014). Corrosion and wear behaviour of Al–Mg–Si alloy matrix hybrid composites reinforced with rice husk ash and silicon carbide. *Journal of Materials Research and Technology*, *3*(1), 9-16. https://doi.org/https://doi.org/10.1016/j.jmrt.2013.10.008

Alaneme, K. K., & Bodunrin, M. O. (2011). Corrosion behavior of alumina reinforced aluminium (6063) metal matrix composites. *Journal of Minerals and Materials Characterization and Engineering*, *10*(12), 1153-1165.

Alaneme, K. K., & Sanusi, K. O. (2015). Microstructural characteristics, mechanical and wear behaviour of aluminium matrix hybrid composites reinforced with alumina, rice husk ash and graphite. *Engineering Science and Technology, an International Journal*, *18*(3), 416-422. https://doi.org/https://doi.org/10.1016/j.jestch.2015.02.003

Allison, J. E., & Cole, G. S. (1993). Metal-matrix composites in the automotive industry: Opportunities and challenges. *JOM*, *45*(1), 19-24. https://doi.org/10.1007/BF03223361

Ankur, et al. (2021). A Re-investigation: Effect of various parameter on mechanical properties of copper matrix composite fabricated by powder metallurgy. *Materials Today: Proceedings*. https://doi.org/10.1016/j.matpr.2021.01.009

Annaz, A. A., et al. (2020). Comparative study of mechanical performance between Al–Graphite and Cu–Graphite self-lubricating composites reinforced by nano-Ag particles. *AIMS Materials Science*, *7*(5), 534-551.

Annigeri, U. K., & Veeresh Kumar, G. B. (2018). Effect of Reinforcement on Density, Hardness and Wear Behavior of Aluminum Metal Matrix Composites: A Review. *Materials Today: Proceedings*, *5*(5, Part 2), 11233-11237. https://doi.org/https://doi.org/10.1016/j.matpr.2018.02.002

Arjunan, T., et al. (2018). Latest Research Development in Aluminum Matrix with Particulate Reinforcement Composites – A Review. *Materials Today: Proceedings*, *5*, 1657-1665. https://doi.org/10.1016/j.matpr.2017.11.260

Arun, K. S., et al. (2015). Study on Mechanical Properties of Aluminium Based Metal Matrix Composites by Hybrid Reinforcement. *Applied Mechanics and Materials*, *813-814*, 116-120. https://doi.org/10.4028/www.scientific.net/AMM.813-814.116

Arunachalam, R., et al. (2019). A review on the production of metal matrix composites through stir casting – Furnace design, properties, challenges, and research opportunities. *Journal of Manufacturing Processes*, *42*, 213-245. https://doi.org/10.1016/j.jmapro.2019.04.017

Aynalem, G. F. (2020). Processing Methods and Mechanical Properties of Aluminium Matrix Composites. *Advances in Materials Science and Engineering*, *2020*, 3765791. https://doi.org/10.1155/2020/3765791

Bahl, S. (2021). Fiber reinforced metal matrix composites - a review. *Materials Today: Proceedings*, *39*, 317-323. https://doi.org/https://doi.org/10.1016/j.matpr.2020.07.423

Bahrami, A., et al. (2016). Development of metal-matrix composites from industrial/agricultural waste materials and their derivatives. *Critical Reviews in Environmental Science and Technology*, *46*(2), 143-208. https://doi.org/10.1080/10643389.2015.1077067

Baradeswaran, A., & Perumal, A. E. (2014). Study on mechanical and wear properties of Al 7075/Al2O3/graphite hybrid composites. *Composites Part B: Engineering*, *56*, 464-471.

Bhoi, N. K., et al. (2020). Developments in the aluminum metal matrix composites reinforced by micro/nano particles–a review. *Journal of Composite Materials*, *54*(6), 813-833.

Bodunrin, M., et al. (2015). Aluminium matrix hybrid composites: A review of reinforcement philosophies; mechanical, corrosion and tribological characteristics. *Journal of Materials Research and Technology*, *10*. https://doi.org/10.1016/j.jmrt.2015.05.003

Bodunrin, M. O., et al. (2015). Aluminium matrix hybrid composites: a review of reinforcement philosophies; mechanical, corrosion and tribological characteristics. *Journal of Materials Research and Technology*, *4*(4), 434-445.

Bolboacă, S. D., & Jäntschi, L. (2007). Design of experiments: Useful orthogonal arrays for number of experiments from 4 to 16. *Entropy*, *9*(4), 198-232.

Boyer, R. R., et al. (2015). Materials considerations for aerospace applications. *MRS Bulletin*, *40*(12), 1055-1066. https://doi.org/10.1557/mrs.2015.278

Callister, W. D., & Rethwisch, D. G. (2018). *Materials science and engineering an introduction* (10th edition. ed.). John Wiley & Sons, Inc.

Chakrapani, P., & Suryakumari, T. S. A. (2021). Mechanical properties of aluminium metal matrix composites-A review. *Materials Today: Proceedings*, *45*, 5960-5964. https://doi.org/https://doi.org/10.1016/j.matpr.2020.09.247

Chand, S., et al. (2020). Influence of Dispersoid Content on Compressibility, Sinterability and Mechanical Behaviour of B4C/BN Reinforced Al6061 Metal Matrix Hybrid Composites Fabricated via Mechanical Alloying. *Metals and Materials International*. https://doi.org/10.1007/s12540-020-00739-0

Chandel, R., et al. (2021a). A review on recent developments of aluminum-based hybrid composites for automotive applications. *Emergent Materials*. https://doi.org/10.1007/s42247-021-00186-6

Chandel, R., et al. (2021b). A review on recent developments of aluminum-based hybrid composites for automotive applications. *Emergent Materials*. https://doi.org/10.1007/s42247-021-00186-6

Chandra Kandpal, B., et al. (2018). Manufacturing and technological challenges in Stir casting of metal matrix composites– A Review. *Materials Today: Proceedings*, *5*(1, Part 1), 5-10. https://doi.org/https://doi.org/10.1016/j.matpr.2017.11.046

Chandradass, J., et al. (2021). Effect of silicon carbide and silicon carbide/alumina reinforced aluminum alloy (AA6061) metal matrix composite. *Materials Today: Proceedings*, *45*, 7147-7150. https://doi.org/https://doi.org/10.1016/j.matpr.2021.02.143

Charan Nayak, K., et al. (2020). Mechanical and physical characterization of powder metallurgy based aluminium metal matrix hybrid composite. *Materials Today: Proceedings*, *33*, 5408-5413. https://doi.org/https://doi.org/10.1016/j.matpr.2020.03.134

Chawla, K. K. (2012). Metal matrix composites. In *Composite materials* (pp. 197-248). Springer.

Dawoud, N., et al. (2020). A Review on Investigating the experimental process for partial replacement of cement with sugarcane bagasse in the construction industry.

Dev Srivyas, P., & Charoo, M. S. (2019). Application of Hybrid Aluminum Matrix Composite in Automotive Industry. *Materials Today: Proceedings*, *18*, 3189-3200. https://doi.org/https://doi.org/10.1016/j.matpr.2019.07.195

Dhanesh, S., et al. (2021). Recent developments in hybrid aluminium metal matrix composites: A review. *Materials Today: Proceedings*, *45*, 1376-1381. https://doi.org/https://doi.org/10.1016/j.matpr.2020.06.325

Dhanesh, S., et al. (2021). Aluminium metal matrix composites reinforced with non - conventional materials: A review. *Materials Today: Proceedings*, *45*, 1371-1375. https://doi.org/https://doi.org/10.1016/j.matpr.2020.06.324

Dixit, M., & Srivastava, R. K. (2018). Effect of compaction pressure on microstructure, density and hardness of Copper prepared by Powder Metallurgy route.

Dubey, A., et al. (2016). A Review on Role of Processing Parameter in Determining Properties of Silicon Carbide Reinforced Metal Matrix Nanocomposites. *Journal of Applied Science and Engineering*, *19*(3), 303-312. https://doi.org/10.6180/jase.2016.19.3.08

Elango M, A. K. (2019). Study on microstructure and EDAX analysis of Al/SiC/Gr hybrid metal matrix composites. *J. Surf. Sci. Technol. Journal of Surface Science and Technology*, *35*(1-2), 60-66.

Etemadi, R. (2014). *Effect of processing parameters and matrix shrinkage on porosity formation during synthesis of metal matrix composites with dual-scale fiber reinforcements using pressure infiltration process* [Theses and Dissertations, University of Wisconsin-Milwaukee]. https://dc.uwm.edu/etd/686

Evans, A., et al. (2003). *Metal Matrix Composites in Industry: An Introduction and a Survey* (1 ed.). Springer, Boston, MA. https://doi.org/https://doi.org/10.1007/978-1-4615-0405-4

Fanani, E. W., et al. (2021). Recent Progress in Hybrid Aluminum Composite: Manufacturing and Application. *Metals*, *11*(12). https://doi.org/10.3390/met11121919

Fayomi, J., et al. (2019). Corrosion performances and thermal behavior of AA8011 reinforced with hybrid-nano ZrB2 + Si3N4 particulates for automobile applications. *Materials Research Express*, *6*(11), 1150e1152. https://doi.org/10.1088/2053-1591/ab4fd0

Feng, L., et al. (2018). Anti-icing/frosting and self-cleaning performance of superhydrophobic aluminum alloys. *Applied Physics A*, *124*. https://doi.org/10.1007/s00339-017-1509-x

Fentahun, M. A., & Sava_, M. A. (2018). Materials Used in Automotive Manufacture and Material Selection Using Ashby Charts. *International Journal of Materials Engineering*, *8*, 40-54.

G, M., et al. (2019). Investigations on Mechanical Properties of Heat-treated Aluminum 7075/Graphite Powder/Bagasse ash Hybrid Metal Matrix Composites. *International Journal of Scientific Research in Science, Engineering and Technology*, 258-266. https://doi.org/10.32628/IJSRSET196351

Gadsden, J. A. (1975). *Infrared spectra of minerals and related inorganic c ompounds*.

Gaohui Wu, Z. K. (2020). Opportunities and Challenges for Metal Matrix Composites in the Context of Equipment Upgrading. *Strategic Study of Chinese Academy of Engineering*, *22*(2), 79-90. https://doi.org/10.15302/j-sscae-2020.02.012

Garg, P., et al. (2019). Advance research progresses in aluminium matrix composites: manufacturing & applications. *Journal of Materials Research and Technology*, *8*(5), 4924-4939. https://doi.org/https://doi.org/10.1016/j.jmrt.2019.06.028

Ghassemieh, E. (2011). Materials in Automotive Application, State of the Art and Prospects. In. IntechOpen.

Gloria, A., et al. (2019). Alloys for Aeronautic Applications: State of the Art and Perspectives. *Metals*, *9*(6). https://doi.org/10.3390/met9060662

Gupta, M. K., et al. (2019). Application of industrial waste in metal matrix composite. *J Polym Compos*, *4*(3), 27-34.

Gupta, R. (2013). Determination & experimental investigation of weight loss on Al/SiC/Gr -Metal Matrix Hybrid Composite by Taguchi method. *International Journal of Science, Engineering and Technology Research (IJSETR)*, *2*, 2038-2048.

Gupta, S., et al. (2017). Experimental investigation of mechanical properties of bagasse ash and SiC reinforced Al 7075 alloy matrix hybrid composites manufactured by stir casting method. *International Journal of Scientific and Engineering Research*, *8*.

Guttikonda, M., et al. (2018). *Fabrication of metal matrix composites by powder metallurgy: A review* (Vol. 1952). https://doi.org/10.1063/1.5032003

Guttikonda, M., et al. (2021). *Effect of Variations in Microwave Processing Temperatures on Microstructural and Mechanical Properties of AA7075/SiC/Graphite Hybrid Composite Fabricated by Powder Metallurgy Techniques*. https://doi.org/10.21203/rs.3.rs-901676/v1

Hadzima, B., & Arsic, D. (2018). Influence of load and reinforcement content on selected tribological properties of Al/SiC/Gr hybrid composites. *Production Engineering Archives*, *18*, 18-23. https://doi.org/10.30657/pea.2018.18.03

Han, Y.-M., & Chen, X. G. (2015). Electrochemical Behavior of Al-B4C Metal Matrix Composites in NaCl Solution. *Materials*, *8*(9). https://doi.org/10.3390/ma8095314

Haq, A. N., et al. (2008). Multi response optimization of machining parameters of drilling Al/SiC metal matrix composite using grey relational analysis in the Taguchi method. *The International Journal of Advanced Manufacturing Technology*, *37*(3), 250-255.

Hayajneh, M. T., et al. (2009). Artificial neural network modeling of the drilling process of self-lubricated aluminum/alumina/graphite hybrid composites synthesized by powder metallurgy technique. *Journal of Alloys and Compounds*, *478*(1), 559-565. https://doi.org/https://doi.org/10.1016/j.jallcom.2008.11.155

Hospodarova, V., et al. (2018). Characterization of cellulosic fibers by FTIR spectroscopy for their further implementation to building materials. *American journal of analytical chemistry*, *9*(6), 303-310.

Hussain, M. Z. i., et al. (2016). Fabrication and Microhardness Analysis of MWCNT/MnO2 Nanocomposite. *Journal of Materials*, *2016*, 6070468.

Iacob, G., et al. (2015). Studies on wear rate and micro-hardness of the Al/Al2O3/Gr hybrid composites produced via powder metallurgy. *Composites Part B: Engineering*, *69*, 603-611. https://doi.org/https://doi.org/10.1016/j.compositesb.2014.07.008

Ikubanni, P. P., et al. (2021a). Synthesis, physico-mechanical and microstructural characterization of Al6063/SiC/PKSA hybrid reinforced composites. *Scientific Reports*, *11*(1), 1-13.

Ikubanni, P. P., et al. (2021b). Synthesis, physico-mechanical and microstructural characterization of Al6063/SiC/PKSA hybrid reinforced composites. *Scientific Reports*, *11*(1), 14845. https://doi.org/10.1038/s41598-021-94420-0

Imran, M., et al. (2016). Study of hardness and tensile strength of Aluminium-7075 percentage varying reinforced with graphite and bagasse-ash composites. *Resource-Efficient Technologies*, *2*(2), 81-88. https://doi.org/https://doi.org/10.1016/j.reffit.2016.06.007

Jailani, H. S., et al. (2009). Multi-response optimisation of sintering parameters of Al–Si alloy/fly ash composite using Taguchi method and grey relational analysis. *The International Journal of Advanced Manufacturing Technology*, *45*(3), 362. https://doi.org/10.1007/s00170-009-1973-3

Jinfeng, L., et al. (2009). Effect of graphite particle reinforcement on dry sliding wear of SiC/Gr/Al composites. *Rare Metal Materials and Engineering*, *38*(11), 1894-1898.

Julong, D. (1989). Introduction to grey system theory. *The Journal of grey system*, *1*(1), 1-24.

Kammuluri.Baburaja, et al. (2016). Hybrid materials of aluminium. *Materials Today: Proceedings*, *3*(10, Part B), 4140-4145. https://doi.org/https://doi.org/10.1016/j.matpr.2016.11.087

Kanayo Alaneme, K., & Apata Olubambi, P. (2013). Corrosion and wear behaviour of rice husk ash—Alumina reinforced Al–Mg–Si alloy matrix hybrid composites. *Journal of Materials Research and Technology*, *2*(2), 188-194. https://doi.org/https://doi.org/10.1016/j.jmrt.2013.02.005

Katkar, V., et al. (2011). Effect of the reinforced boron carbide particulate content of AA6061 alloy on formation of the passive film in seawater. *Corrosion Science - CORROS SCI*, *53*, 2700-2712. https://doi.org/10.1016/j.corsci.2011.04.023

Khanna, V., et al. (2021). Mechanical properties of aluminium-graphene/carbon nanotubes (CNTs) metal matrix composites: Advancement, opportunities and perspective. *Materials Research Bulletin*, *138*, 111224. https://doi.org/https://doi.org/10.1016/j.materresbull.2021.111224

Kho, H. X., et al. (2014). Planetary ball mill process in aspect of milling energy. *Journal of Korean powder metallurgy institute*, *21*(2), 155-164.

Koli, D. K., et al. (2015). Advanced Aluminium Matrix Composites: The Critical Need of Automotive and Aerospace Engineering Fields. *Materials Today: Proceedings*, *2*(4), 3032-3041. https://doi.org/https://doi.org/10.1016/j.matpr.2015.07.290

Kúdela, S., et al. (2008). Application of FTIR spectra for evaluating interfacial reactions in metal matrix composites. *Analytical and Bioanalytical Chemistry*, *390*(6), 1477-1486. https://doi.org/10.1007/s00216-007-1820-z

Kulkarni, P., et al. (2019). A Survey on Effect of Agro Waste Ash as Reinforcement on Aluminium Base Metal Matrix Composites. *Open Journal of Composite Materials, 09*, 312-326. https://doi.org/10.4236/ojcm.2019.93019

Kumar, N., et al. (2021). A re-investigation: Effect of powder metallurgy parameters on the physical and mechanical properties of aluminium matrix composites. *Materials Today: Proceedings, 44*, 2188-2193. https://doi.org/https://doi.org/10.1016/j.matpr.2020.12.351

Lal, S., et al. (2018). Microstructure evaluation, thermal and mechanical characterization of hybrid metal matrix composite. *Science and Engineering of Composite Materials*, *25*(6), 1187-1196. https://doi.org/doi:10.1515/secm-2017-0210

Leon-Patino, C. A. (2001). *Infiltration processing of metal matrix composites using coated ceramic particulates* https://ui.adsabs.harvard.edu/abs/2001PhDT.......218L

Liu, Y. B., et al. (1994). Recent development in the fabrication of metal matrix-particulate composites using powder metallurgy techniques. *Journal of Materials Science, 29*(8), 1999-2007.

Mahdi, S. M., & Ghalib, L. (2021). Corrosion Behavior of Al/SiC Composite Prepared by Powder Metallurgy in Chloride Environments. *Journal of Bio- and Tribo-Corrosion*, *8*(1), 8. https://doi.org/10.1007/s40735-021-00612-6

Mallick, P. K. (2021). Chapter 6 - Thermoset matrix composites for lightweight automotive structures. In P. K. Mallick (Ed.), *Materials, Design and Manufacturing for Lightweight Vehicles (Second Edition)* (pp. 229-263). Woodhead Publishing. https://doi.org/https://doi.org/10.1016/B978-0-12-818712-8.00006-9

Manivannan, I., et al. (2018). Mechanical properties and tribological behavior of Al6061–SiC–Gr self-lubricating hybrid nanocomposites. *Transactions of the Indian Institute of Metals*, *71*(8), 1897-1911.

Manohar, G., et al. (2021). Effect of microwave sintering on the microstructure and mechanical properties of AA7075/B4C/ZrC hybrid nano composite fabricated by powder metallurgy techniques. *Ceramics International*. https://doi.org/https://doi.org/10.1016/j.ceramint.2021.08.156

Manohar, G., et al. (2021). Effect of compaction pressure on mechanical properties of AA7075/B4C/graphite hybrid composite fabricated by powder metallurgy techniques. *Materials Today: Proceedings, 38*, 2157-2161. https://doi.org/https://doi.org/10.1016/j.matpr.2020.05.194

Mavhungu, S. T., et al. (2017). Aluminum Matrix Composites for Industrial Use: Advances and Trends. *Procedia Manufacturing, 7*, 178-182. https://doi.org/https://doi.org/10.1016/j.promfg.2016.12.045

Mazen, A. A., & Ahmed, A. Y. (1998). Mechanical behavior of Al-Al2O3 MMC manufactured by PM techniques part I—scheme I processing parameters. *Journal of Materials Engineering and Performance, 7*(3), 393-401. https://doi.org/10.1361/105994998770347846

Menezes, P. L., et al. (2013). Self-Lubricating Behavior of Graphite-Reinforced Composites. In P. L. Menezes, M. Nosonovsky, S. P. Ingole, S. V. Kailas, & M. R. Lovell (Eds.), *Tribology for Scientists and Engineers: From Basics to Advanced Concepts* (pp. 341-389). Springer New York. https://doi.org/10.1007/978-1-4614-1945-7_11

Merabtene, M., et al. (2019). Elaboration of geopolymer binders from poor kaolin and dam sludge waste. *Heliyon*, *5*(6), e01938.

Miloradović, N., et al. (2020). Wear Behaviour of ZA27/SiC/Graphite Composites under Lubricated Sliding Conditions. *Materials (Basel, Switzerland)*, *13*(17), 3752. https://doi.org/10.3390/ma13173752

Miracle, D. B. (2005). Metal matrix composites–from science to technological significance. *Composites Science and Technology*, *65*(15-16), 2526-2540.
Mistry, J. M., & Gohil, P. P. (2018). Research review of diversified reinforcement on aluminum metal matrix composites: fabrication processes and mechanical characterization. *Science and Engineering of Composite Materials*, *25*(4), 633-647. https://doi.org/doi:10.1515/secm-2016-0278
Miyoshi, K. (2007). Solid Lubricants and Coatings for Extreme Environments: State-of-the-Art Survey [Technical Memorandum (TM)]. *NTRS - NASA Technical Reports Server*.
Mondal, S. (2021). Aluminum or Its Alloy Matrix Hybrid Nanocomposites. *Metals and Materials International*, *27*(7), 2188-2204. https://doi.org/10.1007/s12540-020-00750-5
Mosisa, M., et al. (2019). Extraction and Characterization of Bio-Silica from Sugar Cane Bagasse Ash of Wonji Sugar Industry, Ethiopia.
Muley, A. V., et al. (2015). Nano and hybrid aluminum based metal matrix composites: an overview [10.1051/mfreview/2015018]. *Manufacturing Rev.*, *2*. https://doi.org/10.1051/mfreview/2015018
Mussatto, A., et al. (2021). Advanced production routes for metal matrix composites. *Engineering Reports*, *3*. https://doi.org/10.1002/eng2.12330
Naim Shaikh, M. B. (2018). A Statistical Analysis of Wear Behaviour of Fly Ash Reinforced Al-Sic Hybrid Composites. *7*, 1000190. https://doi.org/10.4172/2168-9806.1000190
Naqiuddin, N. H., et al. (2018). Numerical investigation for optimizing segmented micro-channel heat sink by Taguchi-Grey method. *Applied Energy*, *222*, 437-450.
Natrayan, L., et al. (2019). Mechanical and Tribological Behaviour of Al2O3&SiC Reinforced Aluminium Composites Fabricated via Powder Metallurgy. *IOP Conference Series: Materials Science and Engineering*, *561*, 012038. https://doi.org/10.1088/1757-899x/561/1/012038
Omrani, E., et al. (2016). Influences of graphite reinforcement on the tribological properties of self-lubricating aluminum matrix composites for green tribology, sustainability, and energy efficiency—a review. *The International Journal of Advanced Manufacturing Technology*, *83*(1), 325-346. https://doi.org/10.1007/s00170-015-7528-x
Ononiwu, N., et al. (2020). A Concise Review of the Effects of Hybrid Particulate Reinforced Aluminium Metal Matrix Composites on the Microstructure, Density and Mechanical Properties. *Advances in Manufacturing Engineering*, 433-443.
Park, K., et al. (2019). Behavior of Intermetallic Compounds of Al-Ti Composite Manufactured by Spark Plasma Sintering. *Materials*, *12*(2). https://doi.org/10.3390/ma12020331
Parveen, A., et al. (2021). Influence of Process Parameters and Reinforcements on Aluminum Hybrid Composites Developed by Powder Metallurgy Process. *Physics of Metals and Metallography*, *122*(10), 1007-1013. https://doi.org/10.1134/S0031918X21100094
Pradeep Kumar, J., & Robinson Smart, D. S. (2021). Mechanical and wear characterization of LM13/SiC/Gr dispersed hybrid composites formed through stir casting. *Materials Today: Proceedings*, *46*, 8172-8179. https://doi.org/https://doi.org/10.1016/j.matpr.2021.03.117
Prakash, J. U., et al. (2021). Multi-objective drilling parameter optimization of hybrid metal matrix composites using grey relational analysis. *Materials Today: Proceedings*, *39*, 1345-1350.

Prasad, D. S., et al. (2014). Investigations on mechanical properties of aluminum hybrid composites. *Journal of Materials Research and Technology*, *3*(1), 79-85. https://doi.org/https://doi.org/10.1016/j.jmrt.2013.11.002
Prasad, S. V., & Asthana, R. (2004). Aluminum Metal-Matrix Composites for Automotive Applications: Tribological Considerations. *Tribology Letters*, *17*(3), 445-453. https://doi.org/10.1023/B:TRIL.0000044492.91991.f3
Radhika, N., et al. (2012). Dry sliding wear behaviour of aluminium/alumina/graphite hybrid metal matrix composites. *Industrial Lubrication and Tribology*, *64*, 359-366. https://doi.org/10.1108/00368791211262499
Radhika, N., & Subramaniam, R. (2013). Wear behaviour of aluminium/alumina/graphite hybrid metal matrix composites using Taguchi's techniques. *Industrial Lubrication and Tribology*.
Radhika, N., et al. (2012). Dry sliding wear behaviour of aluminium/alumina/graphite hybrid metal matrix composites. *Industrial Lubrication and Tribology*.
Radhika, N., et al. (2012). Dry sliding wear behaviour of aluminium/alumina/graphite hybrid metal matrix composites. *Industrial Lubrication and Tribology*, *64*(6), 359-366. https://doi.org/10.1108/00368791211262499
Raju, B., et al. (2014). Mechanical and tribological behaviour of aluminium metal matrix composites using powder metallurgy technique- A review.
Rao, R. N., & Das, S. (2010). Effect of matrix alloy and influence of SiC particle on the sliding wear characteristics of aluminium alloy composites. *Materials & Design*, *31*(3), 1200-1207.
Rathika, P. (2013). Tribological properties of powder metallurgy–Processed aluminium self lubricating hybrid composites with SiC additions. *Materials & Design*, *45*, 561-570.
Ravikumar, M., et al. (2021). Evaluation of corrosion properties of Al2O3 and SiC reinforced aluminium metal matrix composites using taguchi's techniques. *J. Sci. Res*, *65*, 253-259.
Ravikumar, M. M., et al. (2021). Evaluation of Corrosion Properties of Al2O3 and SiC Reinforced Aluminium Metal Matrix Composites Using Taguchi s Techniques. *Journal of Scientific Research*, *65*, 253-259.
Ravindran, P., et al. (2013). Tribological behaviour of powder metallurgy-processed aluminium hybrid composites with the addition of graphite solid lubricant. *Ceramics International*, *39*(2), 1169-1182. https://doi.org/https://doi.org/10.1016/j.ceramint.2012.07.041
Ravindran, P., et al. (2013). Investigation of microstructure and mechanical properties of aluminum hybrid nano-composites with the additions of solid lubricant. *Materials & Design*, *51*, 448-456. https://doi.org/https://doi.org/10.1016/j.matdes.2013.04.015
Reddy, P. V., et al. (2020). Mechanical and wear performances of aluminium-based metal matrix composites: a review. *Journal of Bio-and Tribo-Corrosion*, *6*(3), 1-16.
Reeves, C. J., et al. (2013). Tribology of Solid Lubricants. In P. L. Menezes, M. Nosonovsky, S. P. Ingole, S. V. Kailas, & M. R. Lovell (Eds.), *Tribology for Scientists and Engineers: From Basics to Advanced Concepts* (pp. 447-494). Springer New York. https://doi.org/10.1007/978-1-4614-1945-7_13
Sahu, M. K., & Sahu, R. K. (2020). Experimental Investigation, Modeling, and Optimization of Wear Parameters of B4C and Fly-Ash Reinforced Aluminum Hybrid Composite [Original Research]. *Frontiers in Physics*, *8*. https://www.frontiersin.org/article/10.3389/fphy.2020.00219

Sajan, S., & Selvaraj, D. P. (2021). A review on polymer matrix composite materials and their applications. *Materials Today: Proceedings*.

Seshappa, A., & Anjaneya Prasad, B. (2021). Characterization and Investigation of Mechanical Properties of Aluminium Hybrid Nano-composites: Novel Approach of Utilizing Silicon Carbide and Waste Particles to Reduce Cost of Material. *Silicon*, *13*(12), 4355-4369. https://doi.org/10.1007/s12633-020-00748-z

Shanmughasundaram, P., & Subramanian, R. (2013). Wear Behaviour of Eutectic Al-Si Alloy-Graphite Composites Fabricated by Combined Modified Two-Stage Stir Casting and Squeeze Casting Methods. *Advances in Materials Science and Engineering*, *2013*, 216536. https://doi.org/10.1155/2013/216536

Sharma, A. K., et al. (2020). Matrix materials used in composites: A comprehensive study. *Materials Today: Proceedings*, *21*, 1559-1562. https://doi.org/https://doi.org/10.1016/j.matpr.2019.11.086

Sharma, P., et al. (2014). Tribological and mechanical behavior of particulate aluminum matrix composites. *Journal of Reinforced Plastics and Composites*, *33*(23), 2192-2202.

Sherif, E.-S. M. (2014). A comparative study on the electrochemical corrosion behavior of iron and X-65 steel in 4.0 wt% sodium chloride solution after different exposure intervals. *Molecules*, *19*(7), 9962-9974.

Shukla, M., et al. (2018). Characteristic behaviour of aluminium metal matrix composites: A review. *Materials Today: Proceedings*, *5*(2, Part 1), 5830-5836. https://doi.org/https://doi.org/10.1016/j.matpr.2017.12.180

Singh, J. (2016). Fabrication characteristics and tribological behavior of Al/SiC/Gr hybrid aluminum matrix composites: A review. *Friction*, *4*(3), 191-207. https://doi.org/10.1007/s40544-016-0116-8

Singh, J., & Chauhan, A. (2014). A review on sliding wear behaviour of aluminium matrix composites with hybrid reinforcements for automotive applications. *Tribology online*, *9*(3), 121-134.

Singh, J., & Chauhan, A. (2016). Characterization of hybrid aluminum matrix composites for advanced applications – A review. *Journal of Materials Research and Technology*, *5*(2), 159-169. https://doi.org/https://doi.org/10.1016/j.jmrt.2015.05.004

Singh, K. M., & Chauhan, A. K. (2021). Fabrication, Characterization, and Impact of Heat Treatment on Sliding Wear Behaviour of Aluminium Metal Matrix Composites Reinforced with B₄C. *Advances in Materials Science and Engineering*, *2021*, 5554837. https://doi.org/10.1155/2021/5554837

Singh, V., et al. (2014). Enhancement of Wettability of Aluminum Based Silicon Carbide Reinforced Particulate Metal Matrix Composite. *High Temperature Materials and Processes*. https://doi.org/10.1515/htmp-2014-0043

Singla, M., et al. (2009). Development of aluminium based silicon carbide particulate metal matrix composite. *Journal of Minerals and Materials Characterization and Engineering*, *8*(06), 455.

Srivastava, A., et al. (2014). A Review on Fabrication & Characterization of Hybrid Aluminium Metal Matrix Composite. *International journal of Advance research and innovation*, *2*, 242-246.

Srivastava, A. K., et al. (2018). A review on the intensification of metal matrix composites and its nonconventional machining. *Science and Engineering of Composite Materials*, *25*(2), 213-228. https://doi.org/doi:10.1515/secm-2015-0287

Srivyas, P. D., & Charoo, M. S. (2018). Role of Reinforcements on the Mechanical and Tribological Behavior of Aluminum Metal Matrix Composites – A Review.

Materials Today: Proceedings, *5*(9, Part 3), 20041-20053. https://doi.org/https://doi.org/10.1016/j.matpr.2018.06.371

Stojanovic, B., & Ivanovic, L. (2015). Application of aluminium hybrid composites in automotive industry. *Tehnicki Vjesnik*, *22*, 247-251. https://doi.org/10.17559/TV-20130905094303

Sudindra, S., & Kumar, A. C. (2013). Studies on Al6061/Al2O3 and graphite hybrid metal matrix composites. *International journal of metallurgical & materials science and engineering*, *3*(3), 35-42.

Sultana, M., & Rahman, A. (2013). *Characterization of Calcined Sugarcane Bagasse Ash and Sugarcane Waste Ash for Industrial Use*.

Sunitha, N., et al. (2019). Study of SiC/graphite particulates on the corrosion behavior of Al 6065 MMCs using tafel polarization and impedance. *SN Applied Sciences*, *1*(9), 1024. https://doi.org/10.1007/s42452-019-1063-6

Suresh Kumar, R., et al. (2022). Investigation on Corrosion Behaviour of LM25-SiCp Composite Using Taguchi Method. *Advances in Materials Science and Engineering*, *2022*.

Suresh, R. (2020). Comparative study on dry sliding wear behavior of mono (Al2219/B4C) and hybrid (Al2219/B4C/Gr) metal matrix composites using statistical technique. *Journal of the Mechanical Behavior of Materials*, *29*(1), 57-68.

Suresha, S., & Sridhara, B. K. (2010). Effect of silicon carbide particulates on wear resistance of graphitic aluminium matrix composites. *Materials & Design*, *31*(9), 4470-4477. https://doi.org/https://doi.org/10.1016/j.matdes.2010.04.053

Suresha, S., & Sridhara, B. K. (2012). Friction characteristics of aluminium silicon carbide graphite hybrid composites. *Materials & Design*, *34*, 576-583. https://doi.org/https://doi.org/10.1016/j.matdes.2011.05.010

Sydow, Z., et al. (2021). Tribological performance of composites reinforced with the agricultural, industrial and post-consumer wastes: A review. *Materials*, *14*(8), 1863.

Tosun, N. (2006). Determination of optimum parameters for multi-performance characteristics in drilling by using grey relational analysis. *The International Journal of Advanced Manufacturing Technology*, *28*(5), 450-455. https://doi.org/10.1007/s00170-004-2386-y

Tsao, C. C. (2009). Grey–Taguchi method to optimize the milling parameters of aluminum alloy. *The International Journal of Advanced Manufacturing Technology*, *40*(1), 41-48. https://doi.org/10.1007/s00170-007-1314-3

Umair Zaki, M., & Hussain, S. (2021). Impact of addition of manganese and boron carbide on aluminium metal matrix composites using powder metallurgy process. *Materials Today: Proceedings*, *44*, 4364-4368. https://doi.org/https://doi.org/10.1016/j.matpr.2020.10.562

Vaziri, H. S., et al. (2020). Synthesis of WS2/CNT hybrid nanoparticles for fabrication of hybrid aluminum matrix nanocomposite. *Materials Research Express*, *7*(2), 025034.

Veličković Gajević, S., et al. (2018). Tribological characteristics of Al/SiC/Gr hybrid composites. *MATEC Web of Conferences*, *183*, 02001. https://doi.org/10.1051/matecconf/201818302001

Venkatesh, V. S. S., & Deoghare, A. B. (2021). Effect of Sintering Mechanisms on the Mechanical Behaviour of SiC and Kaoline Reinforced Hybrid Aluminium Metal Matrix Composite Fabricated through Powder Metallurgy Technique. *Silicon*. https://doi.org/10.1007/s12633-021-01333-8

Verma, A. S., et al. (2015). Corrosion Behavior of Aluminum Base Particulate Metal Matrix Composites: A Review. *Materials Today: Proceedings*, *2*(4), 2840-2851. https://doi.org/https://doi.org/10.1016/j.matpr.2015.07.299

Vijayakumar, S., & Karunamoorthy, L. (2013). Wear characterization of aluminium metal matrix composites. *Advanced Composites Letters*, *22*(4), 096369351302200401.

Viswanatha, B. M., et al. (2013). Mechanical property evaluation of A356/SICP/GR metal matrix composites. *Journal of Engineering Science and Technology*, *8*, 754-763.

Vyas, A. D., et al. (2013). Potential for Energy Efficiency Improvement Beyond the Light-Duty-Vehicle Sector.

Wolla, D. W., et al. (2014). Studies on the formability of powder metallurgical aluminum–copper composite. *Materials & Design*, *59*, 151-159.

Wu, S., et al. (2020). Carbon solid lubricants: role of different dimensions. *The International Journal of Advanced Manufacturing Technology*, *107*(9), 3875-3895. https://doi.org/10.1007/s00170-020-05297-8

Yashpal, et al. (2020). Effect of Particle Size Variation of Bagasse Ash on Mechanical Properties of Aluminium Hybrid Metal Matrix Composites. *Materials Today: Proceedings*, *21*, 2024-2029. https://doi.org/https://doi.org/10.1016/j.matpr.2020.01.319

Yemane, W. (2020). Design, Development And Performance Evaluation Of A Diesel Engine Driven Mechanical Sugarcane Harvester.

Yunus, M., et al. (2016). Taguchi-Grey relation analysis for assessing the optimal set of control factors of thermal barrier coatings for high-temperature applications. *Mechanics of Advanced Materials and Modern Processes*, *2*. https://doi.org/10.1186/s40759-016-0011-z

Zeren, A. (2015). Effect of the graphite content on the tribological properties of hybrid Al/SiC/Gr composites processed by powder metallurgy. *Industrial Lubrication and Tribology*, *67*(3), 262-268. https://doi.org/10.1108/ILT-07-2014-0066

Zhan, Y., & Zhang, G. (2003). Graphite and SiC hybrid particles reinforced copper composite and its tribological characteristic. *Journal of materials science letters*, *22*(15), 1087-1089.

Research Fund Acknowledgement

This research thesis was funded by Adama Science and Technology University under the grant number of ASTU/SM-R/470/22, Adama, Ethiopia